

DISSERTATION

DEVELOPMENT OF PAPER-BASED DEVICES FOR POINT-OF-NEED,  
BIOANALYTICAL APPLICATIONS

Submitted by

Eka Noviana

Department of Chemistry

In partial fulfillment of the requirements

For the Degree of Doctor of Philosophy

Colorado State University

Fort Collins, Colorado

Summer 2020

Doctoral Committee:

Advisor: Charles S. Henry

Melissa M. Reynolds

Jean Chung

Brian J. Geiss

Copyright by Eka Noviana 2020

All Rights Reserved

## ABSTRACT

### DEVELOPMENT OF PAPER-BASED DEVICES FOR POINT-OF-NEED, BIOANALYTICAL APPLICATIONS

The growing demand for reliable analytical tools to perform testing at the point-of-need has necessitated the development of novel sensors that are low cost (USD 1-10), portable, sensitive, selective, easy to use, and rapid (i.e. provide results within minutes or a few hours). Miniaturization of the sensors into microfluidic platforms has become a promising approach to achieve these sensors. However, traditional microfluidics often require relatively expensive and complicated pumping mechanisms that increase the cost and limit the portability of the sensors. From a material perspective, cellulosic paper is an attractive substrate for constructing point-of-need sensors due to its affordability, vast availability, self-pumping ability via capillary action, and easy fabrication using various printing and patterning techniques. My dissertation research has been focused on developing paper-based devices to address several key gaps that exist between the current technologies and the desired properties of point-of-need sensors.

Chapter 2 describes the development of a steady flow paper device that enabled a function similar to conventional flow injection analysis (FIA) without external pumps. Two-layer paper devices increased the attainable flow rate and reduced the analysis time to only a minute, compared with 10-20 min analysis time reported in previous paper-based FIA. Disposable Pt microwire electrodes were used as a detector in the electrochemical paper-based device (ePAD) and the proposed sensor has been used to detect the activity of  $\beta$ -galactosidase (a bacterial indicator for coliform detection and a common detection label in enzyme-linked immunosorbent assay). Similar enzyme kinetics to those reported in the literature was obtained using the proposed sensor, showing a great promise for semi-automation in bioanalysis.

Implementing a similar flow ePAD, the goal has now expanded toward improving the detection sensitivity as well as reducing the cost of the sensors. In Chapter 3, low-cost (~1 USD) and reusable thermoplastic electrodes (TPEs) were fabricated by mixing carbon and a plastic binder and pressing the

material into an acrylic mold. These TPEs showed an improved electrochemical activity over conventional carbon paste electrodes typically used in ePADs. In addition, electrode arrays can also be fabricated using the technique to improve detection sensitivity via a generation-collection experiment, where the first electrode in the array oxidizes the analyte, the second reduces it, and the process is repeated across the entire array to provide an enhanced cumulative signal. Nanomolar detection limits were achieved using TPEs in both single detector and detector arrays configurations. A 5× improved sensitivity was obtained by employing electrode arrays over the single detector.

In Chapter 4, the dissertation shifts focus to a more specific application, detecting nucleic acid, an important biological analyte that has been largely targeted to diagnose various diseases including genetic disorders, cancer, neurodegenerative, and infectious diseases. This chapter describes the integration of nuclease protection assay (NPA), a highly specific hybridization-based technique, with a reader-free colorimetric detection via lateral flow assay (LFA). In NPA, the hybridization of an antisense probe to the target sequence is followed by single-strand nuclease digestion. The protected double-stranded target-probe hybrids are then captured on the LFA device, followed by the addition of a colorimetric enzyme-substrate pair for signal visualization. The proposed paper-based NPA can detect sub-femtomole ( $\sim 10^8$  copies) of target DNA with high specificity.

While the paper-based NPA can serve a good screening tool for several types of chronic infection in which large copies of pathogen DNA is present in the samples, the high detection limit hinders the application of this method for early disease diagnosis and detecting pathogens in environmental samples. In Chapter 5, polymerase chain reaction (PCR), a nucleic acid amplification technique, was coupled to the colorimetric LFA to improve the detection limit and enable the detection of antimicrobial-resistant (AMR) genes and bacteria in environmental samples. Six orders of magnitude lower detection limit (i.e.  $10^2$  plasmid DNA copies) was achieved by the PCR-LFA. The proposed method can be applied for rapid detection (less than 3 h) of AMR bacteria in environmental samples.

Several works presented in this dissertation provided different approaches to achieve viable paper-based sensors for point-of-need applications. Progress has been made in improving both analytical figures

of merit (i.e. sensitivity and detection limit) and practical specifications of the paper sensors (i.e. reduced sensor cost, semi-automation via an external pump-free flow-based system, instrument-free colorimetric readout, and improved assay time).

## ACKNOWLEDGMENTS

All praise to Allah SWT, the Almighty, for giving me the blessing, strength, and patience during my PhD journey. I am forever indebted to my advisor and one of my role models, Dr. Chuck Henry, for all the help, guidance, wisdom, and patience he has given me for my scientific and personal development throughout the years. Pursuing grad school is definitely not an easy path but with Chuck as a mentor I have never felt discouraged. I would also like to thank my committee members for their valuable time and feedback and collaborating PIs, Dr. Brian Geiss and Dr. David Dandy for their guidance and support.

I am really grateful to have been a part of the Henry group for the last five years and working with great people around the world. I would like to thank Jaclyn Adkins who had helped me get started with research; Rob Channon and Kevin Klunder for providing suggestions and feedback on some of the electrochemistry work; Sid Jain who had been a great partner in the LFA projects; Kyle Howe who had assisted me with some of the projects; coauthors of my review papers: Shirley, Mike, Cynthia, Kaylee, Ilhoon, Daniel, and Rima; and all members of the group, past and present, for the support and friendship. I also would like to acknowledge my former mentors, Dr. Abdul Rohman who has been providing continuous support since my undergraduate year and Dr. Craig Aspinwall who had advised me during my Master's degree and suggested me to apply to CSU.

Lastly, I would like to acknowledge family and friends for their outpouring of love and support. Thanks to my Dad, Mom, and brother for their love, pray, and continuous support; my travel and eating buddies: Neil, Dhira, and Owen; kind sisters: Isnief, Hesti, and Yati who have treated me with lots of great food and driven me around; members of PERMIAS past and present; and friends in Fort Collins, Pengajian Colorado, Arcinda, and other places whose names I cannot mention one by one. I am truly grateful to have you around.

## TABLE OF CONTENTS

ABSTRACT .....	ii
ACKNOWLEDGMENTS .....	v
LIST OF FIGURES .....	ix
<b>CHAPTER 1: INTRODUCTION TO PAPER-BASED DEVICES FOR BIOANALYTICAL</b>	
<b>APPLICATIONS .....</b>	<b>1</b>
Microfluidic paper-based analytical devices.....	1
Fabrication of $\mu$ PADs .....	2
Detection in $\mu$ PADs.....	5
Colorimetry.....	5
Electrochemistry .....	6
Lateral flow assays.....	8
Paper-based nucleic acid detection .....	11
REFERENCES .....	15
<b>CHAPTER 2: QUASI-STEADY FLOW ELECTROCHEMICAL PAPER-BASED DEVICES</b>	
<b>FOR FLOW INJECTION ANALYSIS .....</b>	<b>23</b>
Chapter Overview .....	23
Introduction.....	24
Experimental Section .....	25
Chemicals and materials .....	25
Fabrication of flow ePADs .....	26
Characterization of flow ePADs.....	27
Enzyme kinetics detection .....	28
Results and Discussion.....	28
Characterization of flow ePADs .....	28
Enzyme kinetics study .....	32
Conclusions.....	34
REFERENCES .....	36
<b>CHAPTER 3: THERMOPLASTIC ELECTRODE ARRAYS IN FLOW-BASED</b>	
<b>ELECTROCHEMICAL PAPER DEVICES .....</b>	<b>38</b>

Chapter Overview .....	38
Introduction .....	38
Experimental Section .....	41
Chemicals and materials .....	41
Fabrication of TPE-ePADs .....	41
Characterization of TPEs .....	43
Characterization of flow ePADs .....	43
Results and Discussion.....	44
Characterization of TPEs .....	44
Morphology of the electrodes.....	44
Electrochemical behavior .....	46
Electrochemical detection in flow ePADs.....	48
Signal generation in TPE arrays .....	50
Modification of ePADs and GC performance .....	52
Comparison of detection limit and sensitivity .....	54
Conclusions.....	55
REFERENCES .....	57
<b>CHAPTER 4: PAPER-BASED NUCLEASE PROTECTION ASSAY FOR NUCLEIC ACID</b>	
DETECTION .....	60
Chapter Overview .....	60
Introduction .....	60
Experimental Section .....	63
Chemicals and materials .....	63
Device fabrication.....	64
Paper-based nuclease protection assay .....	64
On-chip sample pretreatment using chitosan-modified paper .....	65
Image analysis.....	65
Results and Discussion.....	66
Nucleic acid detection.....	66
Nuclease protection assay (NPA) .....	66
Assay specificity .....	70
Sample pretreatment with chitosan-modified paper .....	72
Conclusions.....	74

REFERENCES .....	76
CHAPTER 5: POLYMERASE CHAIN REACTION-LATERAL FLOW ASSAY FOR DETECTION OF ANTIMICROBIAL RESISTANCE BACTERIA .....	78
Chapter Overview .....	78
Introduction .....	78
Experimental Section .....	82
Chemicals and materials .....	82
Fabrication of lateral flow strips .....	82
PCR-LFA .....	83
Sample pretreatment using chitosan-modified paper.....	84
Gel electrophoresis .....	84
Testing bacterial cultures .....	84
Image analysis.....	85
Results and Discussion.....	85
PCR-LFA for $\beta$ -lactamase gene detection .....	85
Detection of AMR bacteria.....	88
Conclusions.....	91
REFERENCES .....	93
CHAPTER 6: CONCLUSIONS AND FUTURE DIRECTIONS.....	95
REFERENCES .....	98
APPENDIX. SUPPLEMENTARY INFORMATION FOR CHAPTER 3 .....	99

## LIST OF FIGURES

<b>Figure 1:</b> Schematic representation of a colorimetric lateral flow assay.....	8
<b>Figure 2.1:</b> Fabrication schematic of the quasi-steady flow ePAD showing: (A) multiple layers for device assembly, (B) top view of the fabricated device with the packing tape on the back of the device slightly moved to the side for visualization, (C) a finished device connected to electrode leads .....	27
<b>Figure 2.2:</b> Amperometric detection with quasi-steady flow ePADs: (A) flow-current profile with the top left inset showing the blown up profile from the 2 mM injection, (B) calibration obtained from oxidation and reduction of $K_4Fe(CN)_6/K_3Fe(CN)_6$ in 0.5 M KCl at 0.6 V and -0.6 V vs Pt, respectively. Error bars represent standard deviations of measurements in 3 separate devices .....	30
<b>Figure 2.3:</b> Oxidation of $K_4Fe(CN)_6/K_3Fe(CN)_6$ in 0.5 M KCl at Pt microwires (0.6 V vs Pt): (A) a schematic depiction of the ePADs, (B) resulting calibration at each device,(C) plot from B were normalized to 5 mM $K_4Fe(CN)_6/K_3Fe(CN)_6$ injection at the end of each device measurement. Error bars represent standard deviations of measurements in 3 separate devices .....	31
<b>Figure 2.4:</b> Detection PAP in the presence of PAPG: (A) an enzymatic conversion of PAPG by $\beta$ -galactosidase into PAP. (B) Cyclic voltammograms of 1 mM PAP and PAPG in PBS pH 7.4 obtained in separate saturated ePADs. (C) Plateau current as a function of applied potential obtained from amperometric detection of 1 mM PAP and PAPG on the flow ePADs. (D) Calibration curve of PAP detection at 0.3 V vs Pt. Error bars represent standard deviation in 3 separate device measurements .....	32
<b>Figure 2.5:</b> Enzyme kinetics determination by measuring PAPG conversion into PAP by $\beta$ -galactosidase shown in Michaelis-Menten (A) and Lineweaver-Burk (B) plots. Error bars represent standard deviation in 3 separate device measurements .....	34
<b>Figure 3.1:</b> Schematic illustration of TPE fabrication (A) and assembly into an electrochemical PAD (B). The finished device is shown in C.....	41
<b>Figure 3.2:</b> Surface morphology of the TPE bands imaged using: (A) light microscopy, (B) profilometry and (C) scanning electron microscopy. The electrodes were fabricated using 3:1 graphite-COC ( $w/w$ ).....	45
<b>Figure 3.3:</b> TPE electrochemical characterization: (A) through-plane conductivity ( $n = 4$ ) and (B) dependence of solvent window on electrode composition, (C) cyclic voltammograms of 5 mM $FcTMA^+$ , $Fe(CN)_6^{3-}/Fe(CN)_6^{4+}$ , dopamine and ascorbic acid in 0.5 M KCl, collected at 0.1 V/s on a $0.15 \times 3.5$ mm TPE and (D) scan rate study using 5 mM $FcTMA^+$ with the resulting Randles-Sevcik plot shown in the bottom right inset.....	47
<b>Figure 3.4:</b> (A) Hydrodynamic amperogram obtained by injecting 5-25 $\mu$ L of 1 mM $FcTMA^+$ onto an ePAD (channel width ( $w$ ) = 4 mm, TPE band width ( $x_c$ ) = 160 $\mu$ m). Inset shows the integrated current for each injection plotted against the solution volume. (B) ePAD channel cross section during flow of a dyed solution .....	49

<b>Figure 3.5:</b> TPE arrays flow-ePAD under GG mode: (A) Schematic illustration of the device and redox reaction that is taking place, (B) current signals simultaneously monitored at 8 individually addressable electrodes (E1 was the closest to the inlet (upstream), $w = 3$ mm) from the injection of 10 $\mu\text{L}$ of 1 mM FcTMA <sup>+</sup> , and (C) plateau currents in B plotted against the electrode number and predicted values based on Levich and sequential regime approximation (Eq. 5).....	51
<b>Figure 3.6:</b> TPE arrays operated within flow-ePAD under GC mode experiment: schematic illustration of redox reaction that is taking place between generator ( $g_1$ ) and collector ( $c_2$ ) in the device (A), and conversion and collection efficiency for different number of Whatman 1 paper layer (B) and types of paper substrate (C). All these were tested using 10 $\mu\text{L}$ of 1 mM FcTMA <sup>+</sup> ( $n = 4$ devices). .....	52
<b>Figure 3.7:</b> Signal improvement with TPE arrays: (A) total charges measured from ePAD operated with increasing number of electrodes in GG and GC modes using 1 mM FcTMA <sup>+</sup> ( $n = 4$ injections), (B) calibration curves of FcTMA <sup>+</sup> using single electrode ( $y = 0.24x + 0.04$ ) and electrode arrays operated in GG ( $y = 0.63x + 0.54$ ) and GC ( $y = 1.20x + 0.36$ ) modes ( $n = 4$ devices). Experiments were performed using 1-layer Whatman 1, $w = 4$ mm .....	54
<b>Figure 4.1:</b> Schematic representation of paper-based Nuclease Protection Assay.....	62
<b>Figure 4.2:</b> Dose response of varying amounts of digoxigenin/biotin-labeled oligo probes. Error bars indicate standard deviations ( $n = 4$ devices). .....	66
<b>Figure 4.3:</b> Effect of formamide concentration on : (A) The detection of labeled probe in lateral flow devices and (B) nuclease protection assay.. .....	67
<b>Figure 4.4:</b> Optimization of nuclease digestion. (A) Comparison between S1 and P1 nuclease activity in degrading 10 pmol single-stranded oligo probe at 37°C for 30 min. (B) Effect of P1 nuclease quantity/activity and digestion time (right top inset) in degrading 10 pmol oligo probe. Digestion was carried out for 30 min in experiment shown in the main graph. Error bars indicate standard deviations ( $n = 4$ devices).....	68
<b>Figure 4.5:</b> Dose response of varying amounts of target complementary oligos. Error bars indicate standard deviations ( $n = 4$ devices).....	70
<b>Figure 4.6:</b> (A) Colorimetric signals for NPA with complementary, mismatch and random sequences. 1 U P1 nuclease was used for the digestion. Error bars indicate standard deviations ( $n = 4$ devices). (B) NPA signal for complementary and 1-base mismatch at different activities of P1 nuclease. Error bars indicate standard deviations ( $n = 3$ devices) .....	71
<b>Figure 4.7:</b> On-chip sample pretreatment device made of chitosan-modified filter paper affixed to a PMMA template: DNA from nuclease digested samples is captured in the chitosan layer at an acidic pH (pH $\sim 5$ ). The chitosan layer is then washed with a wash buffer (MES pH 5.0), followed by elution of the DNA directly onto the lateral flow device using an alkaline pH buffer (Tris pH 8.6).....	72

<b>Figure 4.8:</b> Colorimetric signals obtained for samples run with chitosan sample pretreatment (blue circle) and untreated controls (red diamond). Error bars indicate standard deviations (n = 3 devices).....	73
<b>Figure 5.1:</b> Schematic representations of: <b>(A)</b> PCR cycles with biotin-labeled and digoxigenin-labeled primers to amplify a fragment of beta-lactamase gene in pUC19 <b>(B)</b> lateral flow assay to detect PCR amplicons.....	81
<b>Figure 5.2:</b> Image of Gel Red-stained PCR products at different amounts of pUC19 after gel electrophoresis at 120 V for 30 min on 1% agarose.....	86
<b>Figure 5.3:</b> <b>(A)</b> LFA detection of non-treated and chitosan-treated PCR products <b>(B)</b> PCR-LFA at various amounts of pUC19 plasmid. Error bars indicate standard deviation of triplicate experiments. LOD = limit of detection (blank average + 3x standard deviation) .....	87
<b>Figure 5.4:</b> <b>(A)</b> PCR-LFA detection of ampicillin-resistant ( <b>Amp</b> ) and chloramphenicol-resistant ( <b>Chlor</b> ) <i>E. coli</i> at various bacteria concentrations. Error bars indicate standard deviation of triplicate experiments. LOD = limit of detection (blank average + 3x standard deviation). <b>(B)</b> Image of Gel Red-stained PCR products after gel electrophoresis at 120 V for 30 min on 1% agarose .....	89
<b>Figure 5.5:</b> Image of Gel Red-stained PCR products from 2300 CFU of ampicillin-resistant <i>E. coli</i> at different concentrations of LB medium: 1 $\mu$ L 1:100 diluted LB medium in water ( <b>1:100</b> ), 1 $\mu$ L 1:10 diluted LB medium in water ( <b>1:10</b> ), 1 $\mu$ L undiluted LB medium ( <b>1:1</b> ), and 10 $\mu$ L undiluted LB medium ( <b>10:1</b> ).....	90
<b>Figure 5.6:</b> Sequential reagent delivery device made of transparency film and double-sided adhesive (a courtesy of Ilhoon Jang) coupled to an LFA, tested with a sample containing 280 femtomoles biotin/digoxigenin-labeled oligonucleotide. A result of manual pipetting comparable amounts of sample and reagents to the lateral flow device is also shown for comparison.....	91

## CHAPTER 1: INTRODUCTION TO PAPER-BASED DEVICES FOR BIOANALYTICAL APPLICATIONS

The focus of my dissertation is on paper-based analytical devices and their application to different sensing needs. This chapter contains a review of the state-of-the-art in the field and where key gaps exist that I helped fill. The first two works (Chapters 2 and 3) describe the integration of multilayered paper devices (the first was assembled with two layers of paper, the second one was in form of paper stacked on a plastic substrate) to create rapid (i.e. 1-2 min analysis time), steady flow devices to perform a function similar to flow injection analysis without the need of external pumps. The second work (Chapter 3) also investigated the feasibility of low-cost carbon-based detector arrays (~ USD 1) to increase detection sensitivity in electrochemical paper-based devices. The next two works (Chapters 4 and 5) describe the integration of external reader-free lateral flow assays into two nucleic acid testing methods, nuclease protection assay and polymerase chain reaction (PCR). These two methods are typically performed in the laboratory as they require a benchtop fluorescence, absorbance, or electrochemical reader and often involve some laborious DNA clean-up procedures that limit the applicability of the methods outside the laboratory.

### **Microfluidic paper-based analytical devices\***

\*Contents of this section are based on a series of published review articles,<sup>1-3</sup> in which I was listed as an author, with modifications and edits for this document.

Miniaturizing analytical systems using microfluidics offer several advantages over traditional instrumental approaches such as relatively low cost (~ USD 1-100 depending on fabrication techniques), rapid analysis (typically in a few minute), low consumption of reagents and samples (nL to  $\mu$ L), high throughput analysis, portability, and automation.<sup>4-6</sup> A key consideration for microfluidic device is the substrate material. Various substrates have been used for fabricating microfluidic devices. Initially, glass and silicon were the main substances used to construct microfluidics.<sup>7</sup> Polymers such as polymethylmethacrylate, polycarbonate, and polydimethylsiloxane were introduced later as more versatile

and less expensive substrates.<sup>8</sup> More recently, the use of paper and other hydrophilic porous materials as substrates for microfluidic devices has gained significant interest due to the low cost, wide availability, straightforward fabrication, self-pumping abilities via capillary action, and easy disposal relative to traditional materials.<sup>9-11</sup> Since its introduction in 2007 by the Whitesides group,<sup>12</sup> microfluidic paper-based analytical devices ( $\mu$ PADs) have been used for numerous applications such as diagnostics, environmental testing, and analysis of food, pharmaceutical, and clinical samples.<sup>13-17</sup> Numerous reviews have been published covering the field both broadly and for specific aspects including detection, fabrication methods, and specific applications.<sup>1-3,10,18-21</sup>

### ***Fabrication of $\mu$ PADs***

Various types of hydrophilic porous materials have been used for the construction of  $\mu$ PADs. Cellulose-based materials such as Whatman filter papers are commonly used due to their low-cost and wide availability.<sup>21,22</sup> Filter papers vary based on their physical properties, which include thickness, porosity, and wicking speed.<sup>23</sup> Several grades of Whatman filter paper, such as Whatman Grade/No. 1, 3, 4 and 6, have been used in the fabrication of paper-based sensors.<sup>22,24-27</sup> Filter paper with a smaller pore size has been shown to improve assay sensitivity possibly due to the relatively slower flow rate, allowing for increased reaction efficiency and improved rehydration as well as the release of reagents that were previously dried onto the paper substrate.<sup>28</sup> Whatman No. 1 chromatography paper has similar properties to the Whatman No. 1 filter paper including the thickness and particle retention.<sup>22</sup> However, chromatography paper contains no strengthening or whitening agents which reduces the possibility of interference, making the paper a popular substrate to construct  $\mu$ PADs.<sup>29,30</sup> This substrate has also been used to perform analyte separations within  $\mu$ PADs.<sup>31,32</sup> Other substrates that have been reported useful to perform separation include Whatman Grade 3 MM chromatography paper, Whatman P81, Whatman SG81, VWR 413 filter paper, and glass fiber.<sup>3</sup> The use of low-cost office copy paper has also been reported in paper devices.<sup>33,34</sup> The presence of additives in this material, however, should be taken into consideration when choosing copy paper as a  $\mu$ PAD substrate since the substance may interfere with the chemical measurements.<sup>35</sup>

To define a fluidic path within the  $\mu$ PADs, a hydrophobic barrier is often created on the hydrophilic paper substrates to contain the solution and prevent leakage to the surroundings.<sup>10</sup> Numerous fabrication techniques have been reported to pattern fluidic channels in  $\mu$ PADs including wax printing,<sup>36-38</sup> screen printing,<sup>39</sup> ink-jet printing,<sup>40,41</sup> flexographic printing,<sup>42</sup> wax dipping,<sup>43</sup> and manual drawing of the barriers using wax pen,<sup>44</sup> permanent marker,<sup>45</sup> and correction pen.<sup>46</sup> Early fabrication techniques such as photolithography<sup>47</sup> and plasma treatment<sup>48</sup> require more specialized equipment that significantly increase the cost of device fabrication. Wax patterning is the most commonly used technique to fabricate  $\mu$ PADs due to its low-cost fabrication. However, some organic solvents can dissolve the wax, and thus materials such as silicon resin and hydrophobic sol-gel derived methyl silsesquioxane may be useful to construct paper devices for organic solvent-based applications.<sup>49,50</sup> Another fabrication strategy that can be applied for the organic solvent-based application is by cutting using a laser or craft cutter to create a free-standing  $\mu$ PAD.<sup>20</sup>

There are several ways of depositing reagents on  $\mu$ PADs ranging from manual pipetting to more controlled deposition using printing techniques. The manual addition of reagents to the paper can be done by drop-casting reagent to a designated zone within the  $\mu$ PAD.<sup>51</sup> While this technique is very simple and requires no specialized equipment (outside of a pipettor), the reagent deposition is often non-uniform, thus introducing irreproducibility within the measurements. A phenomenon called the “coffee ring effect” is also frequently observed in  $\mu$ PADs employing drop-casting.<sup>52,53</sup> This phenomenon occurs due to evaporation of sessile droplets containing non-volatile solutes dispersed in a volatile solvent, leaving ring-like solid stains behind. To improve uniformity in reagent deposition on paper via drop-casting, modifiers such as poly(ethylene oxide), poly(vinyl alcohol), poly(vinylpyrrolidone), chitosan, and polyelectrolytes have been utilized.<sup>54-56</sup> Printing techniques provide a more uniform deposition of assay reagents, thereby can significantly improve reproducibility of the fabricated devices, allow for construction of complicated paper sensors with high precision, and facilitate large scale production of  $\mu$ PADs.<sup>57</sup>

Multilayered or three-dimensional (3D) paper devices are often assembled to allow the generation of vertical flows and provide a convenient control on assays that involve multistep reactions and/or reagent additions. Two methods are often applied to construct 3D  $\mu$ PADs: stacking<sup>58,59</sup> and folding/origami.<sup>60,61</sup> To stack multiple layers of substrate (including paper) for constructing 3D  $\mu$ PADs, adhesive materials (one-sided adhesive film or double-sided adhesive) are often employed.<sup>62,63</sup> The use of a 3D-printed holder and paper-based holder to hold the stacked device has also been demonstrated.<sup>64,65</sup> While the 3D-printed holder costs more than the adhesive material, the holder is typically reusable and can be designed to help align the multi-layered device more precisely. Alternatively, the folding/origami technique provides easy fabrication of a 3D  $\mu$ PAD on a single sheet of paper and eliminates the need for manual alignment.<sup>60</sup>

Controls over fluid transport within  $\mu$ PADs have also been demonstrated. By adjusting the geometrical shape of the paper substrate, fluid transport within the  $\mu$ PAD can be programmed precisely. For example, Elizalde et al. described several paper strip designs with decaying width and thickness to achieve constant fluid velocity.<sup>66</sup> Besides altering the shape of the paper microfluidic channel, a constant fluid velocity can also be achieved by employing gravity-driven flow<sup>67</sup> and/or integrating a downstream pumping mechanism using a sorbent pad as the outlet reservoir.<sup>68-70</sup> However, the relatively slow flow rates within these reported fluidic devices employing a single layer of paper resulted in around 10-20 min analysis time for a single sample. Flow rates within  $\mu$ PADs can be tuned by selecting paper substrates with a certain pore size and thickness, modification of the paper substrate (e.g. laser etching), and the use of multilayer paper devices.<sup>71-75</sup> Chapters 2 and 3 in this dissertation described the use of two-layer devices (i.e. paper and paper in Chapter 2; paper and an acrylic plate in Chapter 2) which allowed for a gap to exist at the interface, generating much faster flow compared with the single-layer paper devices. Using these multilayered devices, analysis time was significantly reduced to 1-2 min per sample. The use of several types of filter paper with different pore sizes within the multilayered device and how this variable affects flow rates and the detector response was also investigated (Chapter 3 and Appendix).

To meter or control the fluid movement within the  $\mu$ PADs, various types of valve mechanisms have also been reported by using multilayered devices, dissolvable bridges, and absorbent pad; adjusting the geometry of the paper channels; and integration of magnetic, pressure- and temperature-sensitive switches.<sup>11</sup> With the programmable flow rates and various easy-to-integrate fluidic controls, paper is promising for constructing a low-cost semi-automated analytical tool.

### ***Detection in $\mu$ PADs***

Various detection methods have been reported in  $\mu$ PADs including colorimetry,<sup>12,60,76</sup> electrochemistry,<sup>77-79</sup> luminescence (fluorescence, chemiluminescence, and electrochemiluminescence),<sup>80-82</sup> Raman spectroscopy,<sup>83,84</sup> and mass spectrometry.<sup>85,86</sup>

### ***Colorimetry***

Colorimetric detection is the most commonly employed detection method in  $\mu$ PADs because it provides easy readout of the chemical signals, opening the door for equipment-free measurements. Qualitative assays on  $\mu$ PADs are commonly done without any external instrumentation as they give yes/no results that can be readily determined by visual inspection on the color signal.<sup>87</sup> Semi-quantitative analysis can involve the use of a color chart for estimating relative analyte amount based on a pre-established calibration curve.<sup>88</sup> Instrument-free distance-based detection that relies on reading a visual signal length linearly corresponding to analyte concentration has also been demonstrated for semiquantitative analysis.<sup>89-93</sup> Colored bands can be generated as analyte flows along a channel due to capillary force and reacts with pre-deposited reagents to form colored products that remain on the paper substrate,<sup>93,94</sup> or based on the flow stopping resulting from channel constriction as molecular binding to surface receptors occurs.<sup>91,92</sup> More rigorous and carefully controlled measurements are required for quantitative analyses on  $\mu$ PADs in order to obtain accurate and precise analyte levels. These measurements are typically performed by employing instruments to acquire images and image-processing software to quantify the color signal intensities and/or hues.<sup>95,96</sup> Detectors such as charge-coupled devices (CCD) and complementary metal-oxide sensors (CMOS) embedded in phone cameras or flatbed scanners are often employed.<sup>95-97</sup> Measurements using

cameras and scanners are based on light reflectance whereby a light source is used to illuminate a sample and the subsequent light reflected from the surface of the sample is then captured by a photodetector. Transmittance-based measurements such as those in traditional absorbance spectroscopy have also been utilized to provide more sensitive analyte quantification on  $\mu$ PADs.<sup>98,99</sup>

Colorimetric  $\mu$ PADs typically work on the principle that visible colors result from the reaction between analyte and chromogenic reagents.<sup>87,94</sup> The chromogenic reagents are chosen to selectively react with the analyte with minimal to no interference from other substances. Colored products can also be generated upon enzymatic conversion of substrates.<sup>54,100,101</sup> The ability of enzyme to act as a catalyst for the colorimetric reaction provides signal amplification, thus improving detection sensitivity. Metal nanoparticles (NPs) have high extinction coefficients, making them attractive as colorimetric labels.<sup>102</sup> The optical response of metal NPs is also tunable by controlling nanoparticle composition, morphology, size, and solution environment.<sup>103</sup> Due to their unique surface plasmon properties, metal NPs such as AuNPs and AgNPs, are widely utilized for colorimetric detection of ionic species such as metal cations, anionic organic compounds (e.g. ascorbic acid) and proteins.<sup>104-106</sup> Depending on size and charge of the ionic species, the surface charge of the NPs can be either stabilized or destabilized, maintaining particle segregation or causing aggregation, respectively. NP aggregation causes a shift in color due to changes in the plasmon resonance. In addition, aggregation of metal NPs can be induced by antigen-antibody binding.<sup>107</sup>

### *Electrochemistry*

Electrochemical detection offers improved sensitivity and selectivity over colorimetric detection through the selection of electrode materials, detection schemes, and measurement techniques. Miniaturization of electronic components allow measurements in electrochemical  $\mu$ PADs (ePADs) to be kept portable yet still high performance.<sup>2,108-110</sup> For example, the use of inexpensive, commercial glucometers with ePADs has been reported for the detection of disease biomarkers.<sup>111,112</sup> In addition, affordable potentiostats that can be built in-house for USD ~10-120 have been demonstrated as promising alternatives to the more expensive commercial portable potentiostats that typically cost thousands of

dollars.<sup>108,113-117</sup> Due to the flexible nature of paper, electrodes can be easily patterned or printed on the paper substrate for the low-cost detection. Various fabrication techniques to incorporate electrodes onto ePADs have been presented in the literature such as stencil printing,<sup>62,118-121</sup> inkjet printing,<sup>122-127</sup> microwire placement,<sup>79,128</sup> laser scribing,<sup>129</sup> using carbon tape,<sup>130</sup> pencil drawing,<sup>131,132</sup> spray and spin coating,<sup>133</sup> and sputtering.<sup>134-136</sup> Carbon-based electrodes are common in ePADs due to the low cost.<sup>34,62,137,138</sup> However, these electrodes can suffer from poor electrochemical activity. To overcome this issue, modifiers such as metal NPs, nanocomposites and/or graphene have been reportedly used to enhance catalytic activity and improve the sensitivity of the detection.<sup>138-140</sup> However, electrode modification can often be time-consuming. In Chapter 3, the integration of thermoplastic electrodes (TPEs), which were fabricated via a simple solvent-assisted method using carbon and a plastic binder, into an ePAD was described. Unlike conventional carbon-paste electrodes used in ePADs, these TPEs exhibited an improved electrochemical activity comparable to those of glassy carbon and metal electrodes.<sup>141</sup> The versatile fabrication method for TPEs also enabled the construction of electrode arrays to improve detection sensitivity in the ePAD.

Direct detection is the simplest detection motif in ePADs where the measured electrochemical signal comes from the analyte of interest. This detection motif is typically employed to quantify analytes that are redox-active. Direct detection with chronoamperometry and various voltammetry techniques have been used for the determination of metals,<sup>136,142,143</sup> redox-active small biomolecules,<sup>118</sup> and redox-active drug analytes.<sup>131,144</sup> To detect non redox-active analytes, labels such as enzymes, metal NPs, or redox-active organic molecules are often used.<sup>78,145-147</sup> For example, in enzyme-based detection, analytes can be quantified based on their ability to modulate enzyme activity<sup>148</sup> or enzyme inhibition.<sup>6,149</sup> Affinity-based detection of non-redox active analytes is based on the binding of target analytes to their biorecognition elements on the electrode which results in a change in measurable electrochemical signal. The use of antibodies and aptamers as recognition elements is common.<sup>150-154</sup> Molecularly imprinted polymers (MIPs) are other alternatives for more stable and less expensive recognition elements.<sup>155-158</sup> Enzymes and metal NPs are often used as labels in the affinity-based detection to generate the electrochemical signal.<sup>78,145,146</sup>

Label-free detection of non-redox active analytes has also been demonstrated for relatively larger analytes such as proteins, viruses, and bacteria.<sup>79,159,160</sup> The binding of these large analytes to their recognition elements at the electrode surface is quantified through the increase in charge transfer resistance of the surface to a redox mediator, commonly ferricyanide/ferrocyanide ( $[\text{Fe}(\text{CN})_6]^{3-/4-}$ ).<sup>161,162</sup> The label-free assays frequently use electrochemical impedance spectroscopy as it is highly sensitive to changes in electrode surface conditions.<sup>79</sup> The use of enzymes and affinity-based recognition elements in ePADs improves detection selectivity and thus allows for sensitive detection of analytes in complex matrices.<sup>2</sup>

### Lateral flow assays

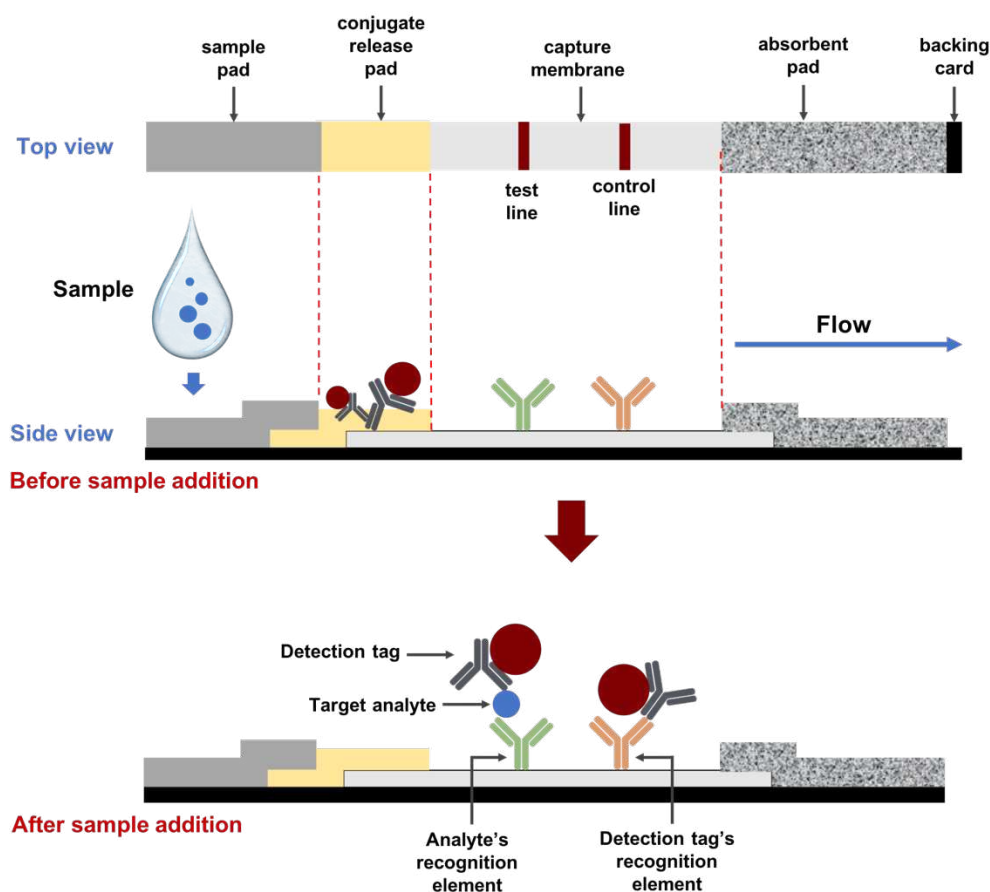


**Figure 1:** Schematic representation of a colorimetric lateral flow assay

Lateral flow assays (LFA), also known as “dipstick tests”, are the most established form of paper-based device and have been widely used for rapid diagnostics.<sup>163</sup> LFAs can produce results within 5-30 min and have been used to detect a wide range of analytes including biomarkers,<sup>164,165</sup> pathogens,<sup>166,167</sup> drugs,<sup>168,169</sup> and contaminants in food and environmental samples.<sup>166,170</sup> The basic principle of the assay is the movement of a liquid sample containing a target analyte along a strip of polymeric material(s) where the analyte interacts with pre-deposited detection molecules or particles to form a complex which is later captured at the detection zone/test line to produce a signal (Figure 1). A typical LFA device consists of: a sample pad where the sample is dropped, a conjugate release pad where detection tags/labels are pre-stored and can be released upon sample addition, a membrane with immobilized recognition elements to the target analyte, and an absorbent pad to maintain the flow rate; assembled on a backing card. A control line, at which a capture/recognition element to the detection label is immobilized, is usually placed next to the test line to confirm that the assay works properly.

The capture membrane is a very important component of the test system as it dictates the binding capacity (from the surface coverage of immobilized recognition elements) as well as the binding efficiency (based on the flow rate at which the sample is transported along the membrane). Nitrocellulose is the most commonly used membrane material for LFAs.<sup>171</sup> Proteins can bind to this membrane via direct adsorption<sup>172</sup> and the membrane is available in various pore sizes varying from 0.05  $\mu\text{m}$  to 12  $\mu\text{m}$ ,<sup>171</sup> allowing the flow rate to be easily tuned for the desired detection sensitivity. Other types of membrane materials that have been used as a capture membrane in LFAs include nylon,<sup>173</sup> polyethersulfone,<sup>174</sup> polyethylene,<sup>175</sup> and fused silica (e.g. Fusion 5).<sup>176</sup> One of the major functions of a sample pad is promoting a controlled distribution of the sample to the conjugate pad. Some modifiers such as proteins, detergents, viscosity enhancers, and/or buffer salts can be deposited onto the sample pad to increase the sample viscosity and reaction time, reduce non-specific binding, or chemically modify the sample prior to binding at the test line.<sup>171</sup> Low protein binding cellulose membranes or glass fiber are commonly used as materials for the sample pad.<sup>177</sup> Another function of the sample pad is for removing coarse materials or other assay interferences, for example,

removing red blood cells from whole blood samples. For this specific application, membranes with blood separation capabilities such as LF1, MF1, and VF2 can be utilized.<sup>177</sup> Two important requirements of a conjugate release pad are rapid wetting and low protein binding such that the stored reagents can be efficiently released upon sample addition. Glass fiber and surface-modified polyester are often used for the release pads.<sup>177,178</sup> It is also important to select a suitable drying buffer for the stored reagents to ensure long-term stability and activity of the detection tags within the release pads. As for the absorbent pad, cellulose membranes are commonly used due to the high liquid hold-up capacity of the materials.<sup>171,178</sup>

Recognition/capture elements used in LFAs can be antibodies<sup>164</sup> or aptamers<sup>179</sup> to the target analytes, antigens<sup>180</sup> to the target antibodies, complementary oligonucleotide probes to the target nucleic acids,<sup>181</sup> or proteins that are specific to the ligand labels.<sup>182</sup> Sandwich or competitive assay is often used in lateral flow immunoassay. In a sandwich immunoassay (Figure 1), the target analyte is sandwiched between a capture antibody and a labeled reporter antibody, and the signal intensity is proportional to the concentration of the target analyte.<sup>164</sup> On the other hand, a competitive immunoassay is based on the competitive binding between target analytes present in the sample and immobilized antigens on the capture membrane, to the labeled antibodies. The more analytes are present in the sample, the less labeled antibodies will be available to bind to the immobilized antigens and thus, the measured signal is inversely proportional to the concentration of the analyte in the sample. Competitive immunoassays are commonly used to detect small molecules as the molecules rarely have multiple epitopes (i.e. the part of antigen molecule at which antibody attaches itself) required for the sandwich immunoassays.<sup>183,184</sup> Similarly, sandwich and competitive immunoassays can also be performed using aptamers as recognition elements and/or detection tags.<sup>179</sup> Several assay formats have been reported for the detection of nucleic acid targets including direct hybridization of labeled targets to the immobilized capture probes,<sup>181</sup> a sandwich assay through the hybridization of the target with both capture and reporter probes,<sup>185</sup> and a sandwich assay through the binding of the ligand- or antigen-labeled target to a protein or an antibody capture element and detection reporter.<sup>186</sup>

Colorimetric LFAs, where the presence of analyte is indicated by the appearance of a colored line, are popular due to the simplicity of the readout and assay interpretation. Colloidal AuNPs are the most extensively used colorimetric reporters/labels for LFA. 5-100 nm Au nanospheres give an intense red color (~700 nm) resulting from the surface plasmon resonance after absorption in the blue-green region of the light (515-580 nm).<sup>187</sup> AuNPs with different shapes/morphologies (in addition to sizes) exhibit different colors depending on their localized SPR (LSPR) peaks. For example, Au nanoprisms with 80-170 nm edge lengths have LSPR peaks around 590-792 nm and give grey to brown color.<sup>188,189</sup> Enzyme-substrate pairs have also been used as colorimetric reporters. The use of horseradish peroxidase (HRP) - 3,3',5,5'-tetramethylbenzidine (TMB)/H<sub>2</sub>O<sub>2</sub> pair is common, giving an intense blue color on the LFA test lines.<sup>190-192</sup> Other chromogenic substrates to HRP such as 3-amino-9-ethylcarbazole (EAC) and 3,3'-diaminobenzidine tetrahydrochloride (DAB) have also been used in lateral flow devices.<sup>193,194</sup> Other detection methods including fluorescence,<sup>165,195</sup> chemiluminescence,<sup>196,197</sup> electrochemistry,<sup>198-200</sup> and surface-enhanced Raman spectroscopy (SERS)<sup>164,201</sup> have also been explored to improve detection sensitivity in LFA. These methods, however, require external equipment for the readout.

### **Paper-based nucleic acid detection**

Nucleic acids are important biological analytes in laboratory diagnostics. Nucleic acid detection has been widely used to diagnose various diseases such as cancer,<sup>202,203</sup> neurodegenerative,<sup>204,205</sup> and infectious diseases.<sup>206,207</sup> Nucleic acid testing (NAT) techniques interrogate nucleic acid (DNA or RNA) sequences directly and thus allow further clinically relevant information to be rapidly obtained from either patient or pathogen. Low cost, portable NAT for point-of-care or field-based diagnostics especially, are greatly desired to cater to bioanalytical needs in resource-limited settings and geographically isolated areas, as well as to reduce both personal health impact of the diseases and public health burden. Recent advances in paper fabrication and modification technologies have made it possible to integrate key steps of NAT (i.e. sample preparation, amplification, and detection) in a single device,<sup>208</sup> making paper-based NAT a promising tool for rapid diagnostics in resource-limited settings.

Nucleic acid hybridization is the basis of many NAT methods, including those implemented on paper devices. For example, Teengam et al. reported a colorimetric paper device based on charge-induced NPs aggregation to detect viral oligonucleotides using positively charged peptide nucleic acid (PNA) probes.<sup>209</sup> In the absence of target oligonucleotides, the positively charged probes destabilized citrate-stabilized AgNPs, causing particle aggregation that gave off a reddish-brown color. The hybridization of target oligos to the probes reduced the aggregation of the particles and the subsequent color signal. Another paper-based nucleic acid-induced NPs aggregation was demonstrated by Tsai et al using AuNPs and single-stranded DNA (ssDNA) probes for detecting tuberculosis DNA.<sup>210</sup> Fluorescence resonance energy transfer (FRET) based on DNA hybridization on paper devices was reported by Noor and Krull.<sup>210</sup> Green-emitting quantum dots (QD)-conjugated probe was immobilized on paper substrate. Upon hybridization of the target nucleic acid to the probe and a Cy3 (i.e. red-emitting dye)-labeled oligo reporter to the target, energy transfer occurred from the QD to the dye, increasing and reducing red and green light emission, respectively. A fluorescence paper-based competitive assay was reported by Scida et al. using a quencher-labeled ssDNA that competed with the target ssDNA to hybridize to the immobilized fluorophore-labeled ssDNA.<sup>211</sup> In electrochemical paper devices, the hybridization of target nucleic acids to their complementary immobilized probes on the electrodes has been measured with and without detection labels. Label-free electrochemical detection of DNA hybrids is based on steric hindrance or electrostatic repulsion/attraction exerted by the negatively-charged DNA on the electrode surface which affects electron transfer between redox mediators and the electrode.<sup>212,213</sup> Redox-active molecules (e.g. methylene blue),<sup>214</sup> metal NPs,<sup>215</sup> and enzyme-substrate pairs<sup>216</sup> been used as reporters in the labeled electrochemical paper-based detection. While DNA hybridization provides high selectivity for target analyte detection, the formation of secondary structures or partial hybridization of the probes to non-target sequences present in the samples can increase the background signal, adversely affect the detection limit, and potentially lead to false-positive results. In chapter 4, a specific NAT method called nuclease protection assay (NPA) was integrated into a simple colorimetric LFA detection. NPA uses a nuclease to selectively degrade single-stranded oligomers present

in unhybridized probes, interfering single-stranded oligonucleotides in the sample, and oligo hybrids that bind partially, reducing the non-specific background signal.

Nucleic acid amplification is often mandatory in NAT when the amount of extracted target nucleic acid from the samples is too low. In fact, polymerase chain reaction (PCR), a nucleic acid amplification method, is the most established and widely used method to detect nucleic acids.<sup>217</sup> Amplification allows for up to millions of copies of detectable amplicons (i.e. products of nucleic acid amplification) to be generated from low copies of target nucleic acids. Due to the complexity of temperature requirements in PCR (i.e. PCR requires three precisely controlled temperatures for the operation), isothermal amplification methods which necessitate only a single reaction temperature are more common in paper-based devices.<sup>208</sup> Primers (i.e. short nucleic acid sequences that provide a starting point for nucleic acid synthesis) for these single-temperature amplification methods, however, are more difficult to design.<sup>218</sup> Although conventional PCR methods rely on expensive instruments that cost thousands to ten thousands USD and are used exclusively in centralized laboratories, affordable thermocyclers (USD ~100) using off-the-shelf electronics have been reported,<sup>219,220</sup> showing a great promise for expanding PCR application to point-of-care or field-based use. In chapter 5, PCR was coupled with a colorimetric LFA to provide an alternative tool to rapidly (i.e. less than 3 h) detect antimicrobial-resistant bacteria in the field.

Single-temperature amplification techniques such as loop-mediated isothermal amplification (LAMP),<sup>221-224</sup> helicase-dependent amplification (HDA),<sup>225,226</sup> rolling circle amplification (RCA),<sup>227</sup> and recombinase polymerase amplification (RPA)<sup>228</sup> have been demonstrated in paper devices. RCA in particular can be performed at room temperature, further simplifying the assay.<sup>227</sup> Reagents for the amplification reaction can be dried on the paper substrate and rehydrated upon sample addition to start the reaction. To detect the amplicons, various strategies can be applied such as the addition of nucleic acid staining dyes,<sup>229</sup> detecting labeled amplicons via LFA,<sup>228,230,231</sup> and other previously mentioned hybridization-based methods. In addition to nucleic acid amplification, preconcentration techniques can be employed to detect nucleic acid at low concentrations. Several methods have been demonstrated to

preconcentrate/stack DNA using paper devices including ion concentration polarization<sup>232</sup> and isotachopheresis.<sup>233,234</sup>

Besides being used as a substrate for nucleic acid detection and amplification, paper can also be used to fabricate low-cost, portable devices for nucleic acid extraction. Conventional nucleic acid extraction kits typically require a microcentrifuge or a vacuum pump to operate, limiting their applicability outside the laboratory. A cellulose paper-based origami device was reported by Govindarajan et al. to extract DNA from viscous biological samples.<sup>235</sup> The device consisted of multiple layers of paper for sample addition, lysis buffer storage, DNA entrapment, and collection of cell lysis waste. A single layer Fusion 5 membrane has been used by Jangam et al. to entrap leukocytes and erythrocytes from a whole blood sample, followed by the addition of NaOH solution to the disk to lyse the cells and release cellular DNA from the cells.<sup>236</sup> The DNA stayed entrapped in the membrane while cell debris was washed away. Similar strategy using Fusion 5 was also reported by Gan et al. to extract DNA from various samples including whole blood, dried blood on Whatman 903 paper and FTA<sup>TM</sup> cards, buccal swabs, saliva, and cigarette butts, and coupled the extraction step to a downstream DNA amplification process using a fluidic device.<sup>237</sup> Another potential material for nucleic acid extraction and clean-up is chitosan. Chitosan (pKa ~6.4) is a polycationic polymer that exhibits a pH-dependent affinity for the negatively charged backbone of nucleic acids.<sup>238</sup> At low pH (below the pKa) chitosan is positively-charged, allowing the nucleic acid to be captured by the polymer and later eluted by adding an alkaline pH buffer. Preliminary studies on using chitosan-modified filter paper for DNA clean-up are provided in Chapters 4 and 5. This chitosan-based pretreatment device can be easily integrated into the LFA and only takes approximately 10 min to extract DNA, remove assay interferents from the sample, and elute the DNA directly onto the LFA device.

## REFERENCES

- (1) Yang, Y.; Noviana, E.; Nguyen, M. P.; Geiss, B. J.; Dandy, D. S.; Henry, C. S. *Analytical Chemistry* **2016**, *89*, 71-91.
- (2) Noviana, E.; McCord, C. P.; Clark, K. M.; Jang, I.; Henry, C. S. *Lab on A Chip* **2019**, *20*, 9-34.
- (3) Noviana, E.; Carrão, D. B.; Pratiwi, R.; Henry, C. S. *Analytica Chimica Acta* **2020**.
- (4) Sackmann, E. K.; Fulton, A. L.; Beebe, D. J. *Nature* **2014**, *507*, 181.
- (5) Malbec, R.; Cacheux, J.; Cordelier, P.; Leichle, T.; Joseph, P.; Bancaud, A. *Micro and Nano Engineering* **2018**, *1*, 25-32.
- (6) Jenkins, G.; Wang, Y.; Xie, Y. L.; Wu, Q.; Huang, W.; Wang, L.; Yang, X. *Microfluidics and Nanofluidics* **2015**, *19*, 251-261.
- (7) Convery, N.; Gadegaard, N. *Micro and Nano Engineering* **2019**.
- (8) Luo, G.; Du, L.; Wang, Y.; Wang, K. *Particuology* **2019**.
- (9) Fu, L.-M.; Wang, Y.-N. *TrAC Trends in Analytical Chemistry* **2018**, *107*, 196-211.
- (10) Cate, D. M.; Adkins, J. A.; Mettakoonpitak, J.; Henry, C. S. *Analytical Chemistry* **2014**, *87*, 19-41.
- (11) Akyazi, T.; Basabe-Desmonts, L.; Benito-Lopez, F. *Analytica Chimica Acta* **2018**, *1001*, 1-17.
- (12) Martinez, A. W.; Phillips, S. T.; Butte, M. J.; Whitesides, G. M. *Angewandte Chemie - International Edition* **2007**, *46*, 1318-1320.
- (13) Hu, J.; Wang, S.; Wang, L.; Li, F.; Pingguan-Murphy, B.; Lu, T. J.; Xu, F. *Biosensors and Bioelectronics* **2014**, *54*, 585-597.
- (14) Sriram, G.; Bhat, M. P.; Patil, P.; Uthappa, U. T.; Jung, H.-Y.; Altalhi, T.; Kumeria, T.; Aminabhavi, T. M.; Pai, R. K.; Kurkuri, M. D. *TrAC Trends in Analytical Chemistry* **2017**, *93*, 212-227.
- (15) Sharma, N.; Barstis, T.; Giri, B. *European Journal of Pharmaceutical Sciences* **2018**, *111*, 46-56.
- (16) Almeida, M. I. G.; Jayawardane, B. M.; Kolev, S. D.; McKelvie, I. D. *Talanta* **2018**, *177*, 176-190.
- (17) Li, F.; You, M.; Li, S.; Hu, J.; Liu, C.; Gong, Y.; Yang, H.; Xu, F. *Biotechnology Advances* **2019**, 107442.
- (18) Xia, Y.; Si, J.; Li, Z. *Biosensors and Bioelectronics* **2016**, *77*, 774-789.
- (19) Yetisen, A. K.; Akram, M. S.; Lowe, C. R. *Lab on A Chip* **2013**, *13*, 2210-2251.
- (20) Yamada, K.; Shibata, H.; Suzuki, K.; Citterio, D. *Lab on A Chip* **2017**, *17*, 1206-1249.
- (21) Paschoalino, W. J.; Kogikoski Jr, S.; Barragan, J. T.; Giarola, J. F.; Cantelli, L.; Rabelo, T. M.; Pessanha, T. M.; Kubota, L. T. *ChemElectroChem* **2019**, *6*, 10-30.
- (22) Evans, E.; Gabriel, E. F. M.; Coltro, W. K. T.; Garcia, C. D. *Analyst* **2014**, *139*, 2127-2132.
- (23) GE-Healthcare. *Back to Basics Part I: A Guide to Types of Whatman Filter Paper Grades*, <https://www.gelifesciences.com/en/us/solutions/lab-filtration/knowledge-center/a-guide-to-whatman-filter-paper-grades>, Accessed on 12 April 2020
- (24) Dungchai, W.; Chailapakul, O.; Henry, C. S. *Analytica Chimica Acta* **2010**, *674*, 227-233.
- (25) Weaver, A. A.; Halweg, S.; Joyce, M.; Lieberman, M.; Goodson, H. V. *Analytical and Bioanalytical Chemistry* **2015**, *407*, 615-619.
- (26) Pratiwi, R.; Septyani, R. N.; Febriany, R.; Saputri, F. A.; Nuwarda, R. F. *International Journal of Analytical Chemistry* **2019**, *2019*, 4682839.
- (27) Manmana, Y.; Chutvirasakul, B.; Suntornsuk, L.; Nuchtavorn, N. *Pharmaceutical Science Asia* **2019**, *46*, 270-277.
- (28) Boehle, K. E.; Carrell, C. S.; Caraway, J.; Henry, C. S. *ACS Sensors* **2018**, *3*, 1299-1307.
- (29) Bracher, P. J.; Gupta, M.; Whitesides, G. M. *Advanced Materials* **2009**, *21*, 445-450.
- (30) Bracher, P. J.; Gupta, M.; Whitesides, G. M. *Soft Matter* **2010**, *6*, 4303-4309.
- (31) Shiroma, L. Y.; Santhiago, M.; Gobbi, A. L.; Kubota, L. T. *Analytica Chimica Acta* **2012**, *725*, 44-50.
- (32) Luo, L.; Li, X.; Crooks, R. M. *Analytical Chemistry* **2014**, *86*, 12390-12397.
- (33) da Silva, G. O.; de Araujo, W. R.; Paixão, T. R. *Talanta* **2018**, *176*, 674-678.

- (34) Petroni, J. M.; Lucca, B. G.; da Silva Júnior, L. C.; Barbosa Alves, D. C.; Souza Ferreira, V. *Electroanalysis* **2017**, *29*, 2628-2637.
- (35) Nery, E. W.; Kubota, L. T. *Analytical and Bioanalytical Chemistry* **2013**, *405*, 7573-7595.
- (36) Dungchai, W.; Chailapakul, O.; Henry, C. S. *Analyst* **2011**, *136*, 77-82.
- (37) Carrilho, E.; Martinez, A. W.; Whitesides, G. M. *Analytical Chemistry* **2009**, *81*, 7091-7095.
- (38) Lu, Y.; Shi, W.; Qin, J.; Lin, B. *Analytical Chemistry* **2009**, *82*, 329-335.
- (39) Sameenoi, Y.; Nongkai, P. N.; Nouanthavong, S.; Henry, C. S.; Nacapricha, D. *Analyst* **2014**, *139*, 6580-6588.
- (40) Abe, K.; Kotera, K.; Suzuki, K.; Citterio, D. *Analytical and Bioanalytical Chemistry* **2010**, *398*, 885-893.
- (41) Abe, K.; Suzuki, K.; Citterio, D. *Analytical Chemistry* **2008**, *80*, 6928-6934.
- (42) Olkkonen, J.; Lehtinen, K.; Erho, T. *Analytical Chemistry* **2010**, *82*, 10246-10250.
- (43) Songjaroen, T.; Dungchai, W.; Chailapakul, O.; Laiwattanapaisal, W. *Talanta* **2011**, *85*, 2587-2593.
- (44) Lu, Y.; Shi, W.; Jiang, L.; Qin, J.; Lin, B. *Electrophoresis* **2009**, *30*, 1497-1500.
- (45) Nie, J.; Zhang, Y.; Lin, L.; Zhou, C.; Li, S.; Zhang, L.; Li, J. *Analytical Chemistry* **2012**, *84*, 6331-6335.
- (46) Mani, N. K.; Prabhu, A.; Biswas, S. K.; Chakraborty, S. *Scientific reports* **2019**, *9*, 1752.
- (47) Cheng, C. M.; Martinez, A. W.; Gong, J.; Mace, C. R.; Phillips, S. T.; Carrilho, E.; Mirica, K. A.; Whitesides, G. M. *Angewandte Chemie International Edition* **2010**, *49*, 4771-4774.
- (48) Li, X.; Tian, J.; Nguyen, T.; Shen, W. *Analytical Chemistry* **2008**, *80*, 9131-9134.
- (49) Wang, J.; Monton, M. R. N.; Zhang, X.; Filipe, C. D.; Pelton, R.; Brennan, J. D. *Lab on a Chip* **2014**, *14*, 691-695.
- (50) Rajendra, V.; Sicard, C.; Brennan, J. D.; Brook, M. A. *Analyst* **2014**, *139*, 6361-6365.
- (51) Cate, D. M.; Dungchai, W.; Cunningham, J. C.; Volckens, J.; Henry, C. S. *Lab on A Chip* **2013**, *13*, 2397-2404.
- (52) Sun, P.; Ma, R.; Wang, K.; Zhong, M.; Wei, J.; Wu, D.; Sasaki, T.; Zhu, H. *Nanotechnology* **2013**, *24*, 075601.
- (53) Eng, A. Y. S.; Chua, C. K.; Pumera, M. *Electrochemistry Communications* **2015**, *59*, 86-90.
- (54) Gabriel, E. F. M.; Garcia, P. T.; Cardoso, T. M. G.; Lopes, F. M.; Martins, F. T.; Coltro, W. K. T. *The Analyst* **2016**, *141*, 4749-4756.
- (55) de Freitas, S. V.; de Souza, F. c. R.; Rodrigues Neto, J. C.; Vasconcelos, G. A.; Abdelnur, P. c. V.; Vaz, B. G.; Henry, C. S.; Coltro, W. K. *Analytical Chemistry* **2018**, *90*, 11949-11954.
- (56) Li, F.; Hu, Y.; Li, Z.; Liu, J.; Guo, L.; He, J. *Analytical and Bioanalytical Chemistry* **2019**, 1-12.
- (57) Yamada, K.; Henares, T. G.; Suzuki, K.; Citterio, D. *Angewandte Chemie International Edition* **2015**, *54*, 5294-5310.
- (58) Martinez, A. W.; Phillips, S. T.; Whitesides, G. M. *Proceedings of the National Academy of Sciences* **2008**, *105*, 19606-19611.
- (59) Cheng, C.-M.; Mazzeo, A. D.; Gong, J.; Martinez, A. W.; Phillips, S. T.; Jain, N.; Whitesides, G. M. *Lab on A Chip* **2010**, *10*, 3201-3205.
- (60) Liu, H.; Crooks, R. M. *Journal of the American Chemical Society* **2011**, *133*, 17564-17566.
- (61) Ge, L.; Wang, S.; Song, X.; Ge, S.; Yu, J. *Lab on A Chip* **2012**, *12*, 3150-3158.
- (62) Nantaphol, S.; Kava, A. A.; Channon, R. B.; Kondo, T.; Siangproh, W.; Chailapakul, O.; Henry, C. S. *Analytica Chimica Acta* **2019**, *1056*, 88-95.
- (63) Lee, S. H.; Lee, J. H.; Tran, V.-K.; Ko, E.; Park, C. H.; Chung, W. S.; Seong, G. H. *Sensors and Actuators B: Chemical* **2016**, *232*, 514-522.
- (64) Primpray, V.; Chailapakul, O.; Tokeshi, M.; Rojanarata, T.; Laiwattanapaisal, W. *Analytica Chimica Acta* **2019**.
- (65) Nilghaz, A.; Lu, X. *Analytica Chimica Acta* **2019**, *1046*, 163-169.
- (66) Elizalde, E.; Urteaga, R.; Berli, C. L. *Lab on A Chip* **2015**, *15*, 2173-2180.

- (67) Lankelma, J.; Nie, Z.; Carrilho, E.; Whitesides, G. M. *Analytical Chemistry* **2012**, *84*, 4147-4152.
- (68) WitkowskaNery, E.; Santhiago, M.; Kubota, L. T. *Electroanalysis* **2016**, *28*, 2245-2252.
- (69) Dossi, N.; Toniolo, R.; Pizzariello, A.; Impellizzieri, F.; Piccin, E.; Bontempelli, G. *Electrophoresis* **2013**, *34*, 2085-2091.
- (70) Granica, M.; Fiedoruk-Pogrebniak, M.; Koncki, R.; Tymecki, Ł. *Sensors and Actuators B: Chemical* **2018**, *257*, 16-22.
- (71) Noviana, E.; Klunder, K. J.; Channon, R. B.; Henry, C. S. *Analytical Chemistry* **2019**, *91*, 2431-2438.
- (72) Adkins, J. A.; Noviana, E.; Henry, C. S. *Analytical Chemistry* **2016**, *88*, 10639-10647.
- (73) Xu, Y.; Enomae, T. *RSC Advances* **2014**, *4*, 12867-12872.
- (74) Camplisson, C. K.; Schilling, K. M.; Pedrotti, W. L.; Stone, H. A.; Martinez, A. W. *Lab Chip* **2015**, *15*, 4461-4466.
- (75) Channon, R. B.; Nguyen, M.; Scorzelli, A.; Henry, E.; Volckens, J.; Dandy, D.; Henry, C. *Lab on A Chip* **2018**, *18*, 793-802.
- (76) Cate, D. M.; Dungchai, W.; Cunningham, J. C.; Volckens, J.; Henry, C. S. *Lab on A Chip* **2013**, *13*, 2397-2404.
- (77) Dungchai, W.; Chailapakul, O.; Henry, C. S. *Analytical Chemistry* **2009**, *81*, 5821-5826.
- (78) Zang, D.; Ge, L.; Yan, M.; Song, X.; Yu, J. *Chemical Communications* **2012**, *48*, 4683-4685.
- (79) Channon, R. B.; Yang, Y.; Feibelman, K. M.; Geiss, B. J.; Dandy, D. S.; Henry, C. S. *Analytical Chemistry* **2018**, *90*, 7777-7783.
- (80) Sun, X. E.; Li, B. W.; Tian, C. Y.; Yu, F. B.; Zhou, N.; Zhan, Y. H.; Chen, L. X. *Analytica Chimica Acta* **2018**, *1007*, 33-39.
- (81) Yamada, K.; Henares, T. G.; Suzuki, K.; Citterio, D. *ACS Applied Materials and Interfaces* **2015**, *7*, 24864-24875.
- (82) Delaney, J. L.; Hogan, C. F.; Tian, J. F.; Shen, W. *Analytical Chemistry* **2011**, *83*, 1300-1306.
- (83) Berger, A. G.; Restaino, S. M.; White, I. M. *Analytica Chimica Acta* **2017**, *949*, 59-66.
- (84) Restaino, S. M.; Berger, A.; White, I. M. In *Biosensors and Biodetection*; Springer, 2017, pp 525-540.
- (85) Manicke, N. E.; Abu-Rabie, P.; Spooner, N.; Ouyang, Z.; Cooks, R. G. *Journal of the American Society for Mass Spectrometry* **2011**, *22*, 1501-1507.
- (86) Espy, R. D.; Teunissen, S. F.; Manicke, N. E.; Ren, Y.; Ouyang, Z.; van Asten, A.; Cooks, R. G. *Analytical Chemistry* **2014**, *86*, 7712-7718.
- (87) Li, M.; Cao, R.; Nilghaz, A.; Guan, L.; Zhang, X.; Shen, W. *Analytical Chemistry* **2015**, *87*, 2555-2559.
- (88) Lin, T.; Li, Z.; Song, Z.; Chen, H.; Guo, L.; Fu, F.; Wu, Z. *Talanta* **2016**, *148*, 62-68.
- (89) Berry, S. B.; Fernandes, S. C.; Rajaratnam, A.; DeChiara, N. S.; Mace, C. R. *Lab on A Chip* **2016**, *16*, 3689-3694.
- (90) Chen, Y. T.; Yang, J. T. *Biomedical Microdevices* **2015**, *17*, 52-52.
- (91) Wei, X.; Tian, T.; Jia, S.; Zhu, Z.; Ma, Y.; Sun, J.; Lin, Z.; Yang, C. J. *Analytical Chemistry* **2016**, *88*, 2345-2352.
- (92) Wei, X.; Tian, T.; Jia, S.; Zhu, Z.; Ma, Y.; Sun, J.; Lin, Z.; Yang, C. J. *Analytical Chemistry* **2015**, *87*, 4275-4282.
- (93) Zhang, Y.; Gao, D.; Fan, J.; Nie, J.; Le, S.; Zhu, W.; Yang, J.; Li, J. *Biosensors and Bioelectronics* **2016**, *78*, 538-546.
- (94) Cate, D. M.; Noblitt, S. D.; Volckens, J.; Henry, C. S. *Lab on A Chip* **2015**, *15*, 2808-2818.
- (95) Alkasir, R. S. J.; Rossner, A.; Andreescu, S. *Environmental Science and Technology* **2015**, *49*, 9889-9897.
- (96) Ismail, A.; Araújo, M. O.; Chagas, C. L. S.; Griveau, S.; D'Orlyé, F.; Varenne, A.; Bedioui, F.; Coltro, W. K. T. *Analyst* **2016**, *141*, 6314-6320.

- (97) Jain, S.; Rajasingham, R.; Noubary, F.; Coonahan, E.; Schoepflein, R.; Baden, R.; Curry, M.; Afdhal, N.; Kumar, S.; Pollock, N. R. *PLoS One* **2015**, *10*, 1-15.
- (98) Ellerbee, A. K.; Phillips, S. T.; Siegel, A. C.; Mirica, K. A.; Martinez, A. W.; Striehl, P.; Jain, N.; Prentiss, M.; Whitesides, G. M. *Analytical Chemistry* **2009**, *81*, 8447-8452.
- (99) Swanson, C.; Lee, S.; Aranyosi, A. J.; Tien, B.; Chan, C.; Wong, M.; Lowe, J.; Jain, S.; Ghaffari, R. *Sensing and Bio-Sensing Research* **2015**, *5*, 55-61.
- (100) Talalak, K.; Noiphung, J.; Songjaroen, T.; Chailapakul, O.; Laiwattanapaisal, W. *Talanta* **2015**, *144*, 915-921.
- (101) Robinson, R.; Wong, L.; Monnat, R. J.; Fu, E. *Micromachines* **2016**, *7*, 2-11.
- (102) Jain, P. K.; Lee, K. S.; El-Sayed, I. H.; El-Sayed, M. A. *The Journal of Physical Chemistry B* **2006**, *110*, 7238-7248.
- (103) Noguez, C. *The Journal of Physical Chemistry C* **2007**, *111*, 3806-3819.
- (104) Apilux, A.; Siangproh, W.; Praphairaksit, N.; Chailapakul, O. *Talanta* **2012**, *97*, 388-394.
- (105) Lai, T. S.; Chang, T. C.; Wang, S. C. *Sensors and Actuators, B: Chemical* **2017**, *239*, 9-16.
- (106) Ferreira, D. C. M.; Giordano, G. F.; Soares, C. C. D. S. P.; De Oliveira, J. F. A.; Mendes, R. K.; Piazzetta, M. H.; Gobbi, A. L.; Cardoso, M. B. *Talanta* **2015**, *141*, 188-194.
- (107) Khan, S. A.; DeGrasse, J. A.; Yakes, B. J.; Croley, T. R. *Analytica Chimica Acta* **2015**, *892*, 167-174.
- (108) Ainla, A.; Mousavi, M. P.; Tsaloglou, M.-N.; Redston, J.; Bell, J. G.; Fernández-Abedul, M. T.; Whitesides, G. M. *Analytical Chemistry* **2018**, *90*, 6240-6246.
- (109) Pal, A.; Cuellar, H. E.; Kuang, R.; Caurin, H. F.; Goswami, D.; Martinez, R. V. *Advanced Materials Technologies* **2017**, *2*, 1700130.
- (110) Beni, V.; Nilsson, D.; Arven, P.; Norberg, P.; Gustafsson, G.; Turner, A. P. *ECS Journal of Solid State Science and Technology* **2015**, *4*, S3001-S3005.
- (111) Nie, Z.; Deiss, F.; Liu, X.; Akbulut, O.; Whitesides, G. M. *Lab on A Chip* **2010**, *10*, 3163-3169.
- (112) Wang, C.-C.; Hennek, J. W.; Ainla, A.; Kumar, A. A.; Lan, W.-J.; Im, J.; Smith, B. S.; Zhao, M.; Whitesides, G. M. *Analytical chemistry* **2016**, *88*, 6326-6333.
- (113) Zhao, C.; Thuo, M. M.; Liu, X. *Science and Technology of Advanced Materials* **2013**, *14*, 54402-54402.
- (114) Giordano, G. F.; Vicentini, M. B.; Murer, R. C.; Augusto, F.; Ferrão, M. F.; Helfer, G. A.; da Costa, A. B.; Gobbi, A. L.; Hantao, L. W.; Lima, R. S. *Electrochimica Acta* **2016**, *219*, 170-177.
- (115) Rowe, A. A.; Bonham, A. J.; White, R. J.; Zimmer, M. P.; Yadgar, R. J.; Hobza, T. M.; Honea, J. W.; Ben-Yaacov, I.; Plaxco, K. W. *PloS One* **2011**, *6*, e23783.
- (116) Dryden, M. D.; Wheeler, A. R. *PloS One* **2015**, *10*, e0140349.
- (117) Lopin, P.; Lopin, K. V. *PloS One* **2018**, *13*, e0201353.
- (118) Cincotto, F. H.; Fava, E. L.; Moraes, F. C.; Fatibello-Filho, O.; Faria, R. C. *Talanta* **2019**, *195*, 62-68.
- (119) Devarakonda, S.; Singh, R.; Bhardwaj, J.; Jang, J. *Sensors* **2017**, *17*, 2597.
- (120) Nantaphol, S.; Channon, R. B.; Kondo, T.; Siangproh, W.; Chailapakul, O.; Henry, C. S. *Analytical Chemistry* **2017**, *89*, 4100-4107.
- (121) de Oliveira, T. R.; Fonseca, W. T.; Setti, G. D.; Faria, R. C. *Talanta* **2019**, *195*, 480-489.
- (122) Cinti, S.; Colozza, N.; Cacciotti, I.; Moscone, D.; Polomoshnov, M.; Sowade, E.; Baumann, R. R.; Arduini, F. *Sensors and Actuators B: Chemical* **2018**, *265*, 155-160.
- (123) Kit-Anan, W.; Olarnwanich, A.; Sriprachuabwong, C.; Karuwan, C.; Tuantranont, A.; Wisitsoraat, A.; Srituravanich, W.; Pimpin, A. *Journal of Electroanalytical Chemistry* **2012**, *685*, 72-78.
- (124) Ruecha, N.; Chailapakul, O.; Suzuki, K.; Citterio, D. *Analytical Chemistry* **2017**, *89*, 10608-10616.
- (125) Tortorich, R. P.; Shamkhalichenar, H.; Choi, J. W. *Applied Sciences-Basel* **2018**, *8*.
- (126) Shamkhalichenar, H.; Choi, J.-W. *Journal of Electrochemical Society* **2017**, *164*, B3101-B3106.

- (127) da Costa, T. H.; Song, E.; Tortorich, R. P.; Choi, J. W. *Ecs Journal of Solid State Science and Technology* **2015**, *4*, S3044-S3047.
- (128) Channon, R. B.; Nguyen, M. P.; Scorzelli, A. G.; Henry, E. M.; Volckens, J.; Dandy, D. S.; Henry, C. S. *Lab on A Chip* **2018**, *18*, 793-802.
- (129) de Araujo, W. R.; Frasson, C. M.; Ameku, W. A.; Silva, J. R.; Angnes, L.; Paixão, T. R. *Angewandte Chemie International Edition* **2017**, *56*, 15113-15117.
- (130) Gomez, F. J. V.; Reed, P. A.; Gonzalez Casamachin, D.; Rivera de la Rosa, J.; Chumanov, G.; Silva, M. F.; Garcia, C. D. *Analytical Methods* **2018**, *10*, 4020-4027.
- (131) Dias, A. A.; Cardoso, T. M. G.; Chagas, C. L. S.; Oliveira, V. X. G.; Munoz, R. A. A.; Henry, C. S.; Santana, M. H. P.; Paixao, T.; Coltro, W. K. T. *Electroanalysis* **2018**, *30*, 2250-2257.
- (132) Oliveira, V. X. G.; Dias, A. A.; Carvalho, L. L.; Cardoso, T. M. G.; Colmati, F.; Coltro, W. K. T. *Analytical Sciences* **2018**, *34*, 91-95.
- (133) Carvalhal, R. F.; Simão Kfourri, M.; de Oliveira Piazetta, M. H.; Gobbi, A. L.; Kubota, L. T. *Analytical Chemistry* **2010**, *82*, 1162-1165.
- (134) Parrilla, M.; Canovas, R.; Andrade, F. J. *Biosensors & Bioelectronics* **2017**, *90*, 110-116.
- (135) Núñez-Bajo, E.; Blanco-López, M. C.; Costa-García, A.; Fernández-Abedul, M. T. *Talanta* **2018**, *178*, 160-165.
- (136) Kokkinos, C.; Economou, A.; Giokas, D. *Sensors and Actuators B: Chemical* **2018**, *260*, 223-226.
- (137) Costa-Rama, E.; Nouws, H.; Delerue-Matos, C.; Blanco-López, M.; Fernández-Abedul, M. *Analytica Chimica Acta* **2019**, *1074*, 89-97.
- (138) Narang, J.; Singhal, C.; Khanuja, M.; Mathur, A.; Jain, A.; Pundir, C. *Artificial Cells, Nanomedicine, and Biotechnology* **2018**, *46*, 1586-1593.
- (139) Narang, J.; Malhotra, N.; Singhal, C.; Mathur, A.; PN, A. K.; Pundir, C. *Materials Science and Engineering: C* **2017**, *80*, 728-735.
- (140) Narang, J.; Malhotra, N.; Singhal, C.; Mathur, A.; Chakraborty, D.; Anil, A.; Ingle, A.; Pundir, C. S. *Biosensors and Bioelectronics* **2017**, *88*, 249-257.
- (141) Klunder, K. J.; Nilsson, Z.; Sambur, J. B.; Henry, C. S. *Journal of the American Chemical Society* **2017**, *139*, 12623-12631.
- (142) Pungjunun, K.; Chaiyo, S.; Jantrahong, I.; Nantaphol, S.; Siangproh, W.; Chailapakul, O. *Microchim. Acta* **2018**, *185*.
- (143) Sanchez-Calvo, A.; Fernandez-Abedul, M. T.; Blanco-Lopez, M. C.; Costa-Garcia, A. *Sensor and Actuator B-Chemistry*. **2019**, *290*, 87-92.
- (144) Petroni, J. M.; Lucca, B. G.; da Silva, L. C.; Alves, D. C. B.; Ferreira, V. S. *Electroanalysis* **2017**, *29*, 2628-2637.
- (145) Ma, C.; Li, W.; Kong, Q.; Yang, H.; Bian, Z.; Song, X.; Yu, J.; Yan, M. *Biosensors and Bioelectronics* **2015**, *63*, 7-13.
- (146) Li, W.; Li, L.; Li, M.; Yu, J.; Ge, S.; Yan, M.; Song, X. *Chemical Communications* **2013**, *49*, 9540-9542.
- (147) Li, L.; Li, W.; Yang, H.; Ma, C.; Yu, J.; Yan, M.; Song, X. *Electrochimica Acta* **2014**, *120*, 102-109.
- (148) Scordo, G.; Moscone, D.; Palleschi, G.; Arduini, F. *Sensor and Actuator B-Chemistry*. **2018**, *258*, 1015-1021.
- (149) Cinti, S.; Minotti, C.; Moscone, D.; Palleschi, G.; Arduini, F. *Biosensors and Bioelectronics* **2017**, *93*, 46-51.
- (150) Sun, X.; Li, B.; Tian, C.; Yu, F.; Zhou, N.; Zhan, Y.; Chen, L. *Analytica Chimica Acta* **2018**, *1007*, 33-39.
- (151) Liu, H.; Xiang, Y.; Lu, Y.; Crooks, R. M. *Angewandte Chemie International Edition* **2012**, *51*, 6925-6928.
- (152) Wei, B.; Mao, K.; Liu, N.; Zhang, M.; Yang, Z. *Biosensors and Bioelectronics* **2018**, *121*, 41-46.

- (153) Boonkaew, S.; Chaiyo, S.; Jampasa, S.; Rengpipat, S.; Siangproh, W.; Chailapakul, O. *Microchimica Acta* **2019**, *186*, 153.
- (154) Scala-Benuzzi, M. L.; Raba, J.; Soler-Illia, G.; Schneider, R. J.; Messina, G. A. *Analytical Chemistry* **2018**, *90*, 4104-4111.
- (155) Sun, X.; Jian, Y.; Wang, H.; Ge, S.; Yan, M.; Yu, J. *ACS Applied Materials and Interfaces* **2019**, *11*, 16198-16206.
- (156) Ge, L.; Wang, S.; Yu, J.; Li, N.; Ge, S.; Yan, M. *Advanced Functional Materials* **2013**, *23*, 3115-3123.
- (157) Amatongchai, M.; Sitanurak, J.; Sroysee, W.; Sodanat, S.; Chairam, S.; Jarujamrus, P.; Nacapricha, D.; Lieberzeit, P. A. *Analytica Chimica Acta* **2019**.
- (158) Fang, M.; Zhou, L.; Zhang, H.; Liu, L.; Gong, Z.-Y. *Food Chemistry* **2019**, *274*, 156-161.
- (159) Boonyasit, Y.; Chailapakul, O.; Laiwattanapaisal, W. *Analytica Chimica Acta* **2016**, *936*, 1-11.
- (160) Bhardwaj, J.; Devarakonda, S.; Kumar, S.; Jang, J. *Sensors and Actuators B: Chemical* **2017**, *253*, 115-123.
- (161) Boonyasit, Y.; Chailapakul, O.; Laiwattanapaisal, W. *Biosensors and Bioelectronics* **2019**, *130*, 389-396.
- (162) Ruecha, N.; Shin, K.; Chailapakul, O.; Rodthongkum, N. *Sensors and Actuators B: Chemical* **2019**, *279*, 298-304.
- (163) Bahadır, E. B.; Sezgintürk, M. K. *TrAC Trends in Analytical Chemistry* **2016**, *82*, 286-306.
- (164) Zhang, D.; Huang, L.; Liu, B.; Ni, H.; Sun, L.; Su, E.; Chen, H.; Gu, Z.; Zhao, X. *Biosensors and Bioelectronics* **2018**, *106*, 204-211.
- (165) Li, Z.; Wang, Y.; Wang, J.; Tang, Z.; Pounds, J. G.; Lin, Y. *Analytical chemistry* **2010**, *82*, 7008-7014.
- (166) Ngom, B.; Guo, Y.; Wang, X.; Bi, D. *Analytical and Bioanalytical Chemistry* **2010**, *397*, 1113-1135.
- (167) Wu, W.; Zhao, S.; Mao, Y.; Fang, Z.; Lu, X.; Zeng, L. *Analytica Chimica Acta* **2015**, *861*, 62-68.
- (168) Carrio, A.; Sampedro, C.; Sanchez-Lopez, J. L.; Pimienta, M.; Campoy, P. *Sensors* **2015**, *15*, 29569-29593.
- (169) Teerinen, T.; Lappalainen, T.; Erho, T. *Analytical and Bioanalytical Chemistry* **2014**, *406*, 5955-5965.
- (170) Raaisosadati, M. J.; Danesh, N. M.; Borna, F.; Gholamzad, M.; Ramezani, M.; Abnous, K.; Taghdisi, S. M. *Biosensors and Bioelectronics* **2016**, *86*, 235-246.
- (171) Posthuma-Trumpie, G. A.; Korf, J.; van Amerongen, A. *Analytical and Bioanalytical Chemistry* **2009**, *393*, 569-582.
- (172) Holstein, C. A.; Chevalier, A.; Bennett, S.; Anderson, C. E.; Keniston, K.; Olsen, C.; Li, B.; Bales, B.; Moore, D. R.; Fu, E. *Analytical and Bioanalytical Chemistry* **2016**, *408*, 1335-1346.
- (173) Buechler, K. F.; Moi, S.; Noar, B.; McGrath, D.; Villela, J.; Clancy, M.; Shenhav, A.; Colleymore, A.; Valkirs, G.; Lee, T. *Clinical Chemistry* **1992**, *38*, 1678-1684.
- (174) Kalogianni, D. P.; Goura, S.; Aletras, A. J.; Christopoulos, T. K.; Chanos, M. G.; Christofidou, M.; Skoutelis, A.; Ioannou, P. C.; Panagiotopoulos, E. *Analytical Biochemistry* **2007**, *361*, 169-175.
- (175) Fernández-Sánchez, C.; McNeil, C. J.; Rawson, K.; Nilsson, O.; Leung, H. Y.; Gnanapragasam, V. *Journal of Immunological Methods* **2005**, *307*, 1-12.
- (176) Jones, K. In *Lateral Flow Immunoassay*; Springer, 2009, pp 1-15.
- (177) GE-Healthcare. 2016. *Helping you build a smarter diagnostic assay*, <https://cdn.gelifesciences.com/dmm3bwsv3/AssetStream.aspx?mediaformatid=10061&destinationid=10016&assetid=16472>, Accessed on 8 May 2020
- (178) Chan, C. P.; Sum, K. W.; Cheung, K. Y.; Glatz, J. F.; Sanderson, J. E.; Hempel, A.; Lehmann, M.; Renneberg, I.; Renneberg, R. *Journal of Immunological Methods* **2003**, *279*, 91-100.
- (179) Jauset-Rubio, M.; El-Shahawi, M. S.; Bashammakh, A. S.; Alyoubi, A. O.; Ciara, K. *TrAC Trends in Analytical Chemistry* **2017**, *97*, 385-398.

- (180) Corstjens, P. L.; Claudia, J.; van der Ploeg-van, J. J.; Wiesmeijer, K. C.; Riuttamäki, T.; van Meijgaarden, K. E.; Spencer, J. S.; Tanke, H. J.; Ottenhoff, T. H.; Geluk, A. *Clinical Biochemistry* **2011**, *44*, 1241-1246.
- (181) Mao, X.; Ma, Y.; Zhang, A.; Zhang, L.; Zeng, L.; Liu, G. *Analytical Chemistry* **2009**, *81*, 1660-1668.
- (182) Liu, J.; Mazumdar, D.; Lu, Y. *Angewandte Chemie International Edition* **2006**, *45*, 7955-7959.
- (183) Pratt, G. W.; Fan, A.; Melakeberhan, B.; Klapperich, C. M. *Analytica Chimica Acta* **2018**, *1017*, 34-40.
- (184) Posthuma-Trumpie, G. A.; Korf, J.; van Amerongen, A. *Analytical and Bioanalytical Chemistry* **2008**, *392*, 1215-1223.
- (185) Seal, J.; Braven, H.; Wallace, P. *IVD Technology* **2006**, *12*, 41-51.
- (186) Noviana, E.; Jain, S.; Hofstetter, J.; Geiss, B. J.; Dandy, D. S.; Henry, C. S. *Analytical and Bioanalytical Chemistry* **2020**, 1-11.
- (187) Soh, J. H.; Chan, H.-M.; Ying, J. Y. *Nano Today* **2020**, 100831.
- (188) Kuttner, C.; Mayer, M.; Dulle, M.; Moscoso, A.; López-Romero, J. M.; Förster, S.; Fery, A.; Pérez-Juste, J.; Contreras-Cáceres, R. *ACS Applied Materials and Interfaces* **2018**, *10*, 11152-11163.
- (189) Liu, B.; Xie, J.; Lee, J.; Ting, Y.; Chen, J. P. *The Journal of Physical Chemistry B* **2005**, *109*, 15256-15263.
- (190) Zhang, C.; Zhang, Y.; Wang, S. *Journal of Agricultural and Food Chemistry* **2006**, *54*, 2502-2507.
- (191) Gao, X.; Xu, L.-P.; Wu, T.; Wen, Y.; Ma, X.; Zhang, X. *Talanta* **2016**, *146*, 648-654.
- (192) Adhikari, M.; Dhamane, S.; Hagström, A. E.; Garvey, G.; Chen, W.-H.; Kourentzi, K.; Strych, U.; Willson, R. C. *Analyst* **2013**, *138*, 5584-5587.
- (193) Özalp, V. C.; Zeydanlı, U. S.; Lunding, A.; Kavruk, M.; Öz, M. T.; Eyidoğan, F.; Olsen, L. F.; Öktem, H. A. *Analyst* **2013**, *138*, 4255-4259.
- (194) Parolo, C.; de la Escosura-Muñiz, A.; Merkoçi, A. *Biosensors and Bioelectronics* **2013**, *40*, 412-416.
- (195) Xu, Y.; Liu, Y.; Wu, Y.; Xia, X.; Liao, Y.; Li, Q. *Analytical Chemistry* **2014**, *86*, 5611-5614.
- (196) Joung, H.-A.; Oh, Y. K.; Kim, M.-G. *Biosensors and Bioelectronics* **2014**, *53*, 330-335.
- (197) Zangheri, M.; Cevenini, L.; Anfossi, L.; Baggiani, C.; Simoni, P.; Di Nardo, F.; Roda, A. *Biosensors and Bioelectronics* **2015**, *64*, 63-68.
- (198) Akanda, M. R.; Joung, H.-A.; Tamilaivan, V.; Park, S.; Kim, S.; Hyun, M. H.; Kim, M.-G.; Yang, H. *Analyst* **2014**, *139*, 1420-1425.
- (199) Sinawang, Prima D.; Rai, V.; Ionescu, R. E.; Marks, R. S. *Biosensors and Bioelectronics* **2016**, *77*, 400-408.
- (200) Du, D.; Wang, J.; Wang, L.; Lu, D.; Lin, Y. *Analytical Chemistry* **2012**, *84*, 1380-1385.
- (201) Fu, X.; Cheng, Z.; Yu, J.; Choo, P.; Chen, L.; Choo, J. *Biosensors and Bioelectronics* **2016**, *78*, 530-537.
- (202) Johnson, P. J.; Lo, Y. D. *Clinical Chemistry* **2002**, *48*, 1186-1193.
- (203) Sidransky, D. *Science* **1997**, *278*, 1054-1058.
- (204) Gaylord, B. S.; Massie, M. R.; Feinstein, S. C.; Bazan, G. C. *Proceedings of the National Academy of Sciences* **2005**, *102*, 34-39.
- (205) Chakravarthy, M.; Chen, S.; Dodd, P. R.; Veedu, R. N. *Theranostics* **2017**, *7*, 3933.
- (206) Niemz, A.; Ferguson, T. M.; Boyle, D. S. *Trends in Biotechnology* **2011**, *29*, 240-250.
- (207) Ivnitski, D.; O'Neil, D. J.; Gattuso, A.; Schlicht, R.; Calidonna, M.; Fisher, R. *Biotechniques* **2003**, *35*, 862-869.
- (208) Choi, J. R.; Yong, K. W.; Tang, R.; Gong, Y.; Wen, T.; Li, F.; Pingguan-Murphy, B.; Bai, D.; Xu, F. *TrAC Trends in Analytical Chemistry* **2017**, *93*, 37-50.
- (209) Teengam, P.; Siangproh, W.; Tuantranont, A.; Vilaivan, T.; Chailapakul, O.; Henry, C. S. *Analytical Chemistry* **2017**, *89*, 5428-5435.
- (210) Noor, M. O.; Krull, U. J. *Analytical Chemistry* **2014**, *86*, 10331-10339.
- (211) Scida, K.; Li, B.; Ellington, A. D.; Crooks, R. M. *Analytical Chemistry* **2013**, *85*, 9713-9720.

- (212) Teengam, P.; Siangproh, W.; Tuantranont, A.; Henry, C. S.; Vilaivan, T.; Chailapakul, O. *Analytica Chimica Acta* **2017**, *952*, 32-40.
- (213) Teengam, P.; Siangproh, W.; Tuantranont, A.; Vilaivan, T.; Chailapakul, O.; Henry, C. S. *Analytica Chimica Acta* **2018**, *1044*, 102-109.
- (214) Cunningham, J. C.; Brenes, N. J.; Crooks, R. M. *Analytical Chemistry* **2014**, *86*, 6166-6170.
- (215) Li, X.; Scida, K.; Crooks, R. M. *Analytical Chemistry* **2015**, *87*, 9009-9015.
- (216) Ye, D.; Li, L.; Li, Z.; Zhang, Y.; Li, M.; Shi, J.; Wang, L.; Fan, C.; Yu, J.; Zuo, X. *Nano Letters* **2018**, *19*, 369-374.
- (217) Kralik, P.; Ricchi, M. *Frontiers in Microbiology* **2017**, *8*, 108.
- (218) Kimura, Y.; de Hoon, M. J.; Aoki, S.; Ishizu, Y.; Kawai, Y.; Kogo, Y.; Daub, C. O.; Lezhava, A.; Arner, E.; Hayashizaki, Y. *Nucleic Acids Research* **2011**, *39*, e59-e59.
- (219) Mendoza-Gallegos, R. A.; Rios, A.; Garcia-Cordero, J. L. *Analytical Chemistry* **2018**, *90*, 5563-5568.
- (220) Wong, G.; Wong, I.; Chan, K.; Hsieh, Y.; Wong, S. *PLoS One* **2015**, *10*.
- (221) Seok, Y.; Joung, H.-A.; Byun, J.-Y.; Jeon, H.-S.; Shin, S. J.; Kim, S.; Shin, Y.-B.; Han, H. S.; Kim, M.-G. *Theranostics* **2017**, *7*, 2220.
- (222) Fang, X.; Guan, M.; Kong, J. *RSC Advances* **2015**, *5*, 64614-64616.
- (223) Choi, J.-S.; Kim, J.-S.; Joe, C.-O.; Kim, S.; Ha, K.-S.; Park, Y.-M. *Experimental and Molecular Medicine* **1999**, *31*, 20-24.
- (224) Connelly, J. T.; Rolland, J. P.; Whitesides, G. M. *Analytical Chemistry* **2015**, *87*, 7595-7601.
- (225) Tang, R.; Yang, H.; Gong, Y.; You, M.; Liu, Z.; Choi, J. R.; Wen, T.; Qu, Z.; Mei, Q.; Xu, F. *Lab on A Chip* **2017**, *17*, 1270-1279.
- (226) Shetty, P.; Ghosh, D.; Singh, M.; Tripathi, A.; Paul, D. *RSC Advances* **2016**, *6*, 56205-56212.
- (227) Liu, M.; Hui, C. Y.; Zhang, Q.; Gu, J.; Kannan, B.; Jahanshahi-Anbuhi, S.; Filipe, C. D. M.; Brennan, J. D.; Li, Y. *Angewandte Chemie - International Edition* **2016**, *55*, 2709-2713.
- (228) Rohrman, B. A.; Richards-Kortum, R. R. *Lab on A chip* **2012**, *12*, 3082-3088.
- (229) Roy, S.; Mohd-Naim, N. F.; Safavi, M.; Ahmed, M. U. *ACS Sensors* **2017**, *2*, 1713-1720.
- (230) Kim, T.-H.; Park, J.; Kim, C.-J.; Cho, Y.-K. *Analytical Chemistry* **2014**, *86*, 3841-3848.
- (231) Kersting, S.; Rausch, V.; Bier, F. F.; von Nickisch-Rosenegk, M. *Malaria Journal* **2014**, *13*, 99.
- (232) Gong, M. M.; Nosrati, R.; San Gabriel, M. C.; Zini, A.; Sinton, D. *Journal of the American Chemical Society* **2015**, *137*, 13913-13919.
- (233) Li, X.; Luo, L.; Crooks, R. M. *Lab on A Chip* **2015**, *15*, 4090-4098.
- (234) Rosenfeld, T.; Bercovici, M. *Lab on A Chip* **2018**, *18*, 861-868.
- (235) Govindarajan, A.; Ramachandran, S.; Vigil, G.; Yager, P.; Böhringer, K. *Lab on a Chip* **2012**, *12*, 174-181.
- (236) Jangam, S. R.; Yamada, D. H.; McFall, S. M.; Kelso, D. M. *Journal of Clinical Microbiology* **2009**, *47*, 2363-2368.
- (237) Gan, W.; Zhuang, B.; Zhang, P.; Han, J.; Li, C.-X.; Liu, P. *Lab on A chip* **2014**, *14*, 3719-3728.
- (238) Shahidi, F.; Abuzaytoun, R. *Advances in Food and Nutrition Research* **2005**, *49*, 93-137.

## CHAPTER 2: QUASI-STEADY FLOW ELECTROCHEMICAL PAPER-BASED DEVICES FOR FLOW INJECTION ANALYSIS

### Chapter Overview

Flow injection analysis (FIA) is a widely implemented technique to automate sample analysis. However, the size, complexity, and cost of infrastructure required to perform FIA have limited the applicability of this technique mainly to tests carried out in centralized laboratories. Herein, a quasi-steady flow generated in an electrochemical paper-based device (ePAD) is described. This device enables a function similar to FIA to be performed without the need for expensive external pumps. The paper device implements a fan-shaped geometry connected to an analysis channel whereby the solution is pulled from an inlet, through a channel, and into the steadily increasing capillary network of the fan-shaped paper. Microwire electrodes were embedded between two paper layers within the analysis channel, such that solution flow occurred on the whole perimeter of the wire electrodes. The ePAD provided a detection limit of 31  $\mu\text{M}$  for *p*-aminophenol using Pt electrodes and was also used to detect enzyme activity for the reaction of  $\beta$ -galactosidase with *p*-aminophenyl-galactopyranoside. Measured enzyme kinetics provided a similar Michaelis-Menten constant ( $K_m = 0.36 \text{ mM}$ ) as those found in the literature. The developed sensor is promising for performing multiple injection analysis with steady-flow and online detection that would normally require an external pump to perform. This work was published in *Analytical Chemistry*.<sup>1</sup> Jaclyn Adkins (1<sup>st</sup> author) performed the initial work of prototyping the device and studied the electrochemical behavior in flow devices made of one- and two-layer of paper (data are mostly not shown here). The results shown in this chapter are based on the experiments I performed as part of this project. More recent work on the next generation of the flow ePAD has been published in *ACS Sensors*,<sup>2</sup> using low-cost thermoplastic electrodes (more details on this type of electrodes will be described later in Chapter 3). This new flow ePAD has incorporated an upstream buffer reservoir and a sample injection inlet to produce a flow profile similar to that in conventional FIA.

## Introduction

Flow injection analysis (FIA) has been widely used over the last few decades since first being proposed by Ruzicka and Hansen.<sup>3</sup> With developments in pumping, flow programming, valve control, and hyphenating the platform with different detection methods, FIA has been used for clinical diagnostics, environmental monitoring, and food analysis.<sup>4,5</sup> While the platform can automate routine analysis in laboratory settings, the size, and complexity of instrumentation limit the application of FIA for on-site monitoring. Miniaturizing the platform using microfluidic devices can improve portability, reduce sample consumption and improve analysis time,<sup>6</sup> but typically requires peristaltic, syringe, and/or vacuum pumps to precisely and reliably control fluid flow.<sup>7</sup> Unfortunately, the pump size and power requirements limit the portability of the system for field analysis. Piezoelectric, electrostatic, and magnetic pumps have been introduced that significantly reduce the overall size of the fluidic platforms.<sup>8-10</sup> These pumps, however, can be expensive, require external power, and are not disposable making them less than ideal for portable and field-based applications.

Passive pumping without external power has been of interest for creating inexpensive and portable fluidic systems. Both silicon-based materials and cellulosic paper have been used to construct such capillary-driven fluidic systems.<sup>11-15</sup> Paper substrates, in particular, are low-cost, widely available in various pore sizes and thicknesses, disposable, and flexible, allowing for convenient engineering of the fluidic systems using established printing and patterning techniques.<sup>14,16</sup> Capillary-driven flow within a microfluidic paper-based analytical device ( $\mu$ PAD) with a constant cross-section, however, does not exhibit steady-state flow due to the increasing viscous drag as the solution moves further down the paper substrate.<sup>17</sup> This non-steady flow rate behavior is undesirable in FIA as it may affect both signal and reproducibility, reducing accuracy and limiting utility. FIA in paper devices has been previously demonstrated by employing gravity-driven flow<sup>18</sup> and a combination of an upstream fluid reservoir and a downstream sorbent pad<sup>19,20</sup> to afford continuous flow rates within the paper devices. However, the slow flow rate in the microfluidic channel made of a single paper layer resulted in around 10-20 min analysis

time for a single injection. Higher flow rates have been reported in multi-layer paper devices which can potentially reduce the analysis time.<sup>21,22</sup>

Among the available FIA detection methods, electrochemistry has been widely used due to the simple construction of the flow-through detectors, sensitive detection, and easy miniaturization of electrodes and instruments.<sup>5</sup> Various ways to incorporate electrodes into  $\mu$ PADs are available to create electrochemical PADs (ePADs).<sup>23</sup> Screen or stencil printing carbon as well as metal inks onto paper substrate are the most common approaches.<sup>24-26</sup> Conductive carbon is popular in ePADs due to its low cost, wide potential window, and widespread availability, whereas metal electrodes provide benefits of high conductivity and catalytic activity.<sup>27</sup> Metal electrodes can be patterned onto paper using thin film deposition, nanoparticle growth, and inkjet printing.<sup>28,29</sup> Another simple method to incorporate metal electrodes is by using prefabricated microwires. Previous work has revealed an increase in the flux of species to the electrode surface with the use of metal microwires in contact with the paper, exhibiting improved detection performance over stencil-printed carbon electrodes.<sup>30</sup> These prefabricated microwires can also be cleaned and modified prior to incorporation into ePAD without damaging the paper substrate. While previously reported microwire electrode-based ePAD were employed in quiescent solutions,<sup>30</sup> this work describes the integration of microwire electrodes into a paper-based flow-through device. The addition of flow to the ePAD provides an increase in the flux of species to the electrode via convection to enhance the signal. Moreover, the use of a previously reported 270° fan-shaped device allows for generation of quasi-steady flow on ePADs to provide semi-automation in analyte measurements.<sup>31</sup> As a proof-of-concept, an enzyme kinetics study was performed on the devices using  $\beta$ -galactosidase and *p*-aminophenyl-galactopyranoside (PAPG) as the enzyme and substrate, respectively.

## **Experimental Section**

### ***Chemicals and materials***

Potassium chloride (KCl), potassium hydroxide (KOH), potassium ferricyanide ( $K_3Fe(CN)_6$ ), 30% hydrogen peroxide ( $H_2O_2$ ), and Whatman # 1 filter paper were purchased from Fisher Scientific (New

Jersey, USA). *p*-aminophenol (PAP) was purchased from and EMD Millipore (Massachusetts, USA), respectively.  $\beta$ -galactosidase enzyme and *p*-aminophenyl-galactopyranoside (PAPG) substrate were purchased from Sigma-Aldrich. Both enzyme and substrate stock solution aliquots were stored at  $-20\text{ }^{\circ}\text{C}$  prior to use. Fresh aliquots were thawed prior to use daily. Potassium ferrocyanide ( $\text{K}_4\text{Fe}(\text{CN})_6$ ) was purchased from Mallinckrodt Chemical Works (Missouri, USA). High purity silver ink was purchased from SPI Supplies (Philadelphia, USA). Platinum (Pt)  $30\text{ }\mu\text{m}$ -diameter microwires were purchased from California Fine Wire Company (California, USA). All reagents were used as received without further purification. 2-inch-wide Scotch® transparent packaging tape was purchased from 3 M (Minnesota, USA).

### ***Fabrication of flow ePADs***

The ePAD was designed using CorelDRAW (Corel, Ontario, Canada) and fabricated on Whatman #1 filter paper (Figure 2.1A). To contain the fluid flow, a hydrophobic barrier was created by printing 4-pt line thick wax on the filter paper using a Xerox ColorCube 8870 wax printer (Connecticut, USA), followed by wax melting on a hot plate at  $120\text{ }^{\circ}\text{C}$  for 90 s. Packing tape was used to seal the bottom of the device to prevent leaking. Pt microwires were placed 1 mm apart on the top of the paper as the reference, working, and counter electrodes (RE, WE, and CE) using printed alignment marks as a guide. Prior to ePAD fabrication, the Pt microwires were cleaned by immersing the wires in 0.05 M KOH/25%  $\text{H}_2\text{O}_2$  solution for 5 min, followed by washing in water and drying at ambient temperature. After placing the microwires on the wax-patterned paper, the device was then covered with a laser-cut Whatman paper wicking layer and packing tape cover, prepared using a 30 W Epilog Zing laser cutter (Colorado, USA). The ePAD inlet used a 4.1 mm inner diameter wax-printed well connected to an 11 mm x 5 mm channel. The channel flows into the center of a 27.8 mm inner diameter circle with  $\frac{1}{4}$  of the section removed to form a  $270^{\circ}$  wicking fan. The laser-cut wicking layer has the same dimension as the paper region within the wax barrier. The laser-cut tape cover consists of a 9 mm x 7 mm rectangle connected 8 mm into a 34 mm diameter circle. The sample inlet was left uncovered for sample addition (Figure 2.1B). Silver paint was added to the wire ends to create contact pads that can be connected to the potentiostat (Figure 2.1C).

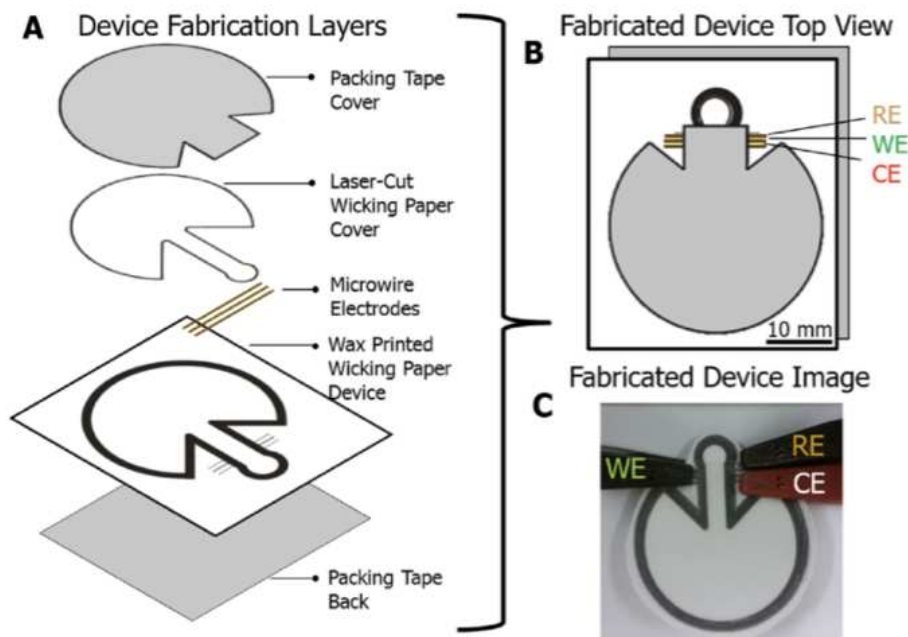


**Figure 2.1:** Fabrication schematic of the quasi-steady flow ePAD showing: **(A)** multiple layers for device assembly, **(B)** top view of the fabricated device with the packing tape on the back of the device slightly moved to the side for visualization, **(C)** a finished device connected to electrode leads.

### Characterization of flow ePADs

All electrochemical measurements were done using a CHI 660B potentiostat (Texas, USA). Characterization was performed via amperometry by injecting 10  $\mu\text{L}$   $\text{K}_4\text{Fe}(\text{CN})_6/\text{K}_3\text{Fe}(\text{CN})_6$  solution in 0.5 M KCl onto the sample inlet. A -0.6 V or 0.6 V vs Pt overpotential was applied for reducing or oxidizing the species, respectively. To enhance the current response, two working and counter Pt microwire electrodes were also tested in addition to the above-mentioned single-microwire device. To calibrate the ePADs, 10  $\mu\text{L}$  of 0–5.0 mM  $\text{K}_4\text{Fe}(\text{CN})_6/\text{K}_3\text{Fe}(\text{CN})_6$  in 0.5 M KCl were injected onto the devices to determine the plateau currents. Plateau currents were then normalized to a standard 5.0 mM  $\text{K}_4\text{Fe}(\text{CN})_6/\text{K}_3\text{Fe}(\text{CN})_6$  in 0.5 M KCl solution added at the end of each device use. Measurements were done in triplicates using separate devices and the plateau currents were averaged.

### ***Enzyme kinetics detection***

A kinetic study on  $\beta$ -galactosidase activity using PAPG as the substrate was performed in the flow ePADs. The product of this enzymatic reaction, PAP, is an electrochemically active molecule. Cyclic voltammograms (CVs) of 1 mM PAPG and 1 mM PAP in phosphate-buffered saline (PBS) pH 7.4 were obtained at 0.1 V/s from 0.2 to 0.7 V vs Pt and from -0.1 to 0.4 V vs Pt, respectively. The optimal applied overpotential for PAP detection in the presence of PAPG background current was determined by measuring the plateau current with discrete flow containing 1 mM PAP or PAPG solution in PBS pH 7.4 using amperometry at 0.1, 0.2, 0.3, and 0.4 V vs. Pt. A 0.3 V overpotential vs Pt was then determined as the optimum potential and applied for PAP detection during kinetics measurement. A PAP calibration curve was established by measuring 0–1.0 mM PAP solutions in PBS pH 7.4 in the ePADs. To determine the rate of the enzymatic reaction, 50  $\mu$ L of 0.2-10 mM PAPG solutions were mixed with an equal volume of 10 U/mL  $\beta$ -galactosidase solution (both in PBS pH 7.4) and 5  $\mu$ L aliquots of the mixture were added to the device every 30-100 s. At least five time points during the initial linear enzymatic response were collected for each substrate concentration to calculate rates of the reaction. The rates of reaction were calculated from the change in PAP concentration with time based on the measured currents. Measurements were carried out in three separate devices and the measured rates were averaged. A Lineweaver-Burk plot (i.e.  $1/[\text{substrate}]$  vs  $1/\text{rate}$  plot) was established and Michaelis-Menten constant ( $K_m$ ) was extracted from the plot.<sup>32</sup>

## **Results and Discussion**

### ***Characterization of flow ePADs***

Capillary-driven flow on paper substrate potentially enables sample processing automation such as that in FIA. However, the velocity of fluid flow on a paper strip with a constant cross-section decreases with time due to an increase in viscous drag force as the wetted area increases, as described by the Lucas-Washburn equation:<sup>33</sup>

(1)

$$l(t) = \sqrt{\frac{\gamma r \cos \theta t}{2\mu}}$$

where the distance of the fluid front with time,  $l(t)$ , is proportional to the square root of solution surface tension ( $\gamma$ ), the mean capillary pore radius of the paper ( $r$ ), the solution contact angle with paper ( $\theta$ ), and time ( $t$ ); as well as inversely proportional to the square root of the viscosity ( $\mu$ ). As the detector response in a flow channel depends on the solution volumetric flow rate according to Levich,<sup>34</sup> this decay can change the response with time. One way to overcome this flow rate decay was proposed by Mendez et al. by creating a 270° fan attached to the channel exit, provide a steady increase in the capillary pressure to counterbalance to the increased viscous drag.<sup>31</sup> The flow rate resulting from this fan-shaped device has been characterized visually by the group. A quasi-steady flow was observed within the paper device as long as the fan region is not fully saturated with the solution. There was an increase in flow rate by 273% in a device with two layers of paper (i.e. device described here) compared to a single layer device generally used in  $\mu$ PADs.<sup>1</sup> This increase in flow rate resulted from the presence of a gap between the two layers of paper, reducing the overall resistance to the fluid flow.

Figure 2.2A shows the amperometric response of the ePAD with no flow and the subsequent spike and plateau of current from the flow of the solution across the electrodes as droplets were added onto the inlet. A small spike can be observed immediately after the droplet addition due to the high initial velocity of the flow from small resistance encountered when displacing air with the solution. The spike decays as the flow rate stabilizes, giving a plateau at which current was recorded for the measurements. The plateau is then followed by a decay of signal back to the baseline as the flow stops due to liquid depletion at the inlet. Due to the enhanced flow rate within the two-layer paper device, single analyte injection took only about 1 min which is significantly faster than the previously reported paper-based FIA.<sup>18-20</sup> Calibration curves for both cathodic (reduction) and anodic (oxidation) detection of  $K_4Fe(CN)_6/K_3Fe(CN)_6$  are shown in Figure 2.2B where there is an overall lower current from the anodic injections. This lower anodic current could possibly due to some interaction between the electrode and the cellulose matrix. Cellulose is a

polysaccharide comprised of glucose and intermediates from glucose oxidation is known to adsorb on Pt electrode.<sup>35,36</sup>

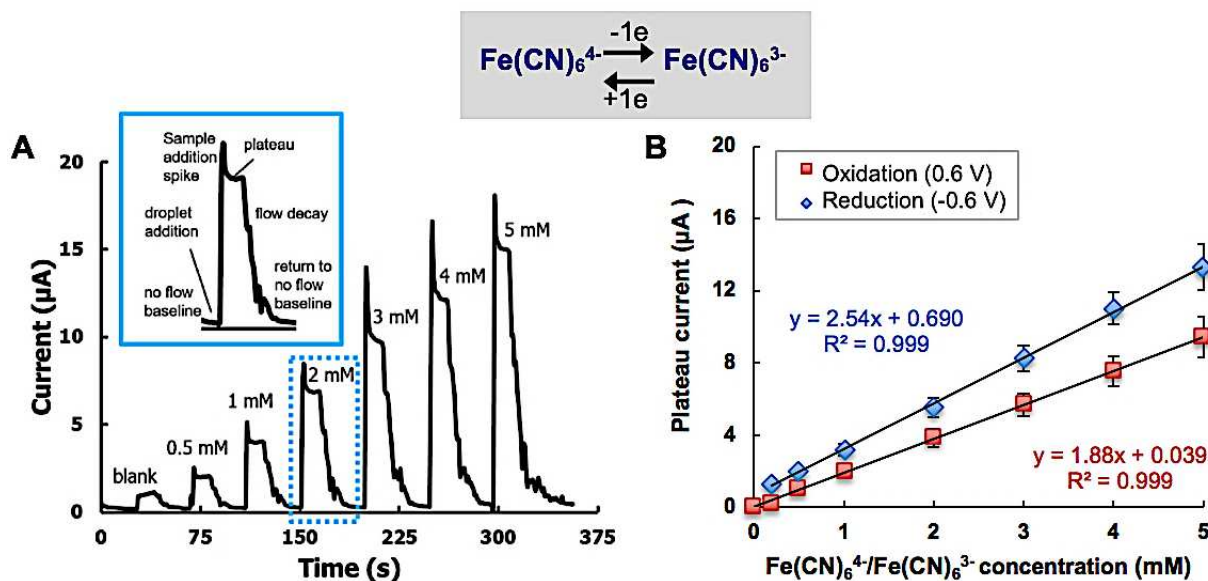


**Figure 2.2:** Amperometric detection with quasi-steady flow ePADs: (A) flow-current profile with the top left inset showing the blown up profile from the 2 mM injection, (B) calibration obtained from oxidation and reduction of  $\text{K}_4\text{Fe(CN)}_6/\text{K}_3\text{Fe(CN)}_6$  in 0.5 M KCl at 0.6 V and -0.6 V vs Pt, respectively. Error bars represent standard deviations of measurements in 3 separate devices.

To increase the sensitivity of the ePAD, the use of double Pt microwires was compared to a single microwire (Figure 2.3A). According to the Levich equation, the limiting current generated by a channel electrode is related to the number of electrons involved in the redox ( $n$ ), Faraday constant ( $F = 96,485$  C/mol), bulk concentration of the redox species ( $C_\infty$ ), width of the channel or electrode ( $w$ ), diffusion coefficient of the species in solution ( $D$ ), length of the electrode ( $x_e$ ), volumetric flow rate of the solution ( $V_f$ ), and height of the channel ( $2h$ ):<sup>34</sup>

$$i_{\text{lim}} = 0.925nFC_\infty w^{2/3} D^{2/3} x_e^{2/3} V_f^{1/3} h^{-2/3} \quad (2)$$

The circular perimeter of the microwire ( $2\pi r$ ) represents the electrode length in this flow system as the microwire electrodes were sandwiched between two layers of paper where the solution was flowing

through. Expanding the cross-sectional area of the electrode by doubling the number of microwires increased the sensitivity to  $2.95 \mu\text{A}/\text{mM}$  from  $1.88 \mu\text{A}/\text{mM}$  in the single-wire device (Figure 2.3B). This is approximately 1.57 times signal increase which is close to that predicted based on the Levich eq. (i.e.  $2^{2/3}$  or 1.59 times from original) as  $x_e$  was doubled. The slight difference between the experimental and predicted signal enhancement might be due to the droplet addition used in this ePAD system, instead of continuous flow where the volumetric flow rate remains constant at all times.

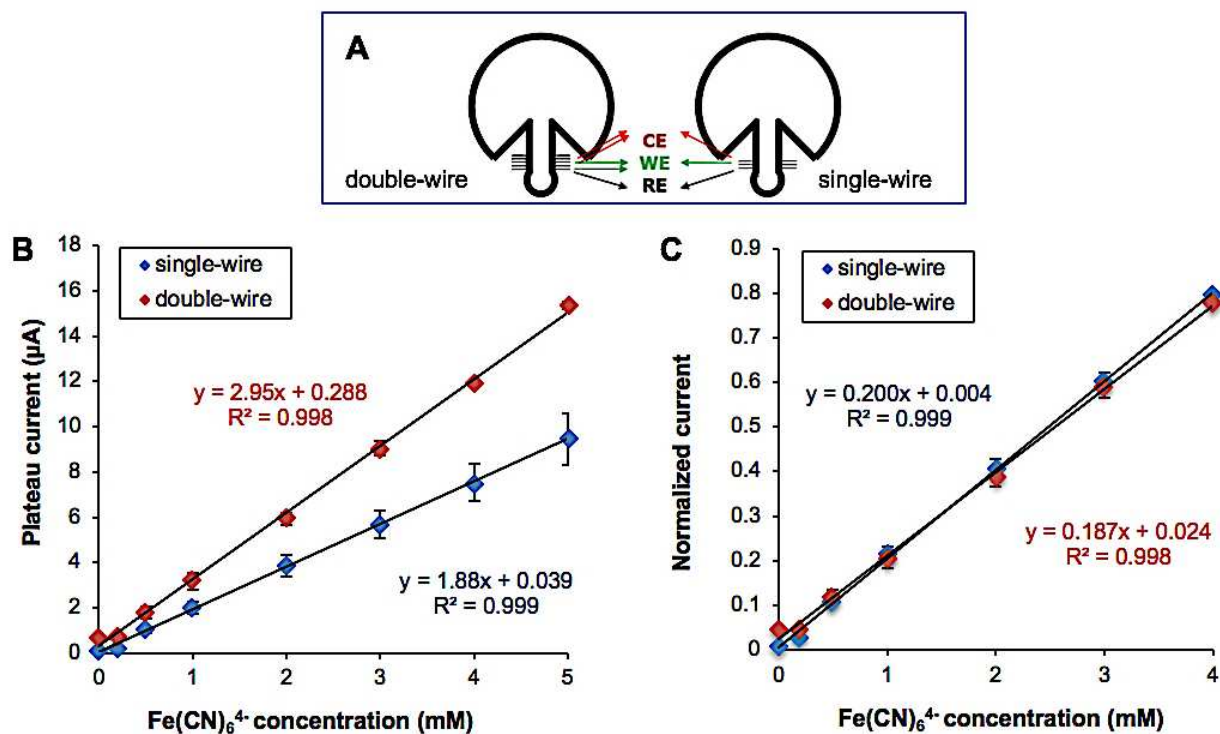


**Figure 2.3:** Oxidation of  $\text{K}_4\text{Fe}(\text{CN})_6/\text{K}_3\text{Fe}(\text{CN})_6$  in 0.5 M KCl at Pt microwires (0.6 V vs Pt): (A) a schematic depiction of the ePADs, (B) resulting calibration at each device, (C) plots from B were normalized to 5 mM  $\text{K}_4\text{Fe}(\text{CN})_6/\text{K}_3\text{Fe}(\text{CN})_6$  injection at the end of each device measurement. Error bars represent standard deviations of measurements in 3 separate devices.

With droplet addition, the quasi-steady flow is only achieved within a certain period of time before the solution is depleted from the inlet and the flow rate starts to decay. Depending on how far the two working electrodes were spaced apart and the injection volume, the farther electrode might experience a lower flux of species due to decay in the flow rate, which contributes to the lower current response.

Average measurements among devices produced relative standard deviation (RSD = standard deviation / average) of 10-12% with the single-wire devices. Normalization of the current response to a standard solution injected at the end of device measurements was able to lower the RSD to less than 5% (Figure 2.3C). The higher inter-device RSD prior to normalization was attributed to variations in device alignment and/or the amount of pressure used to seal the device as the ePADs were assembled by hand.

### Enzymatic kinetics study

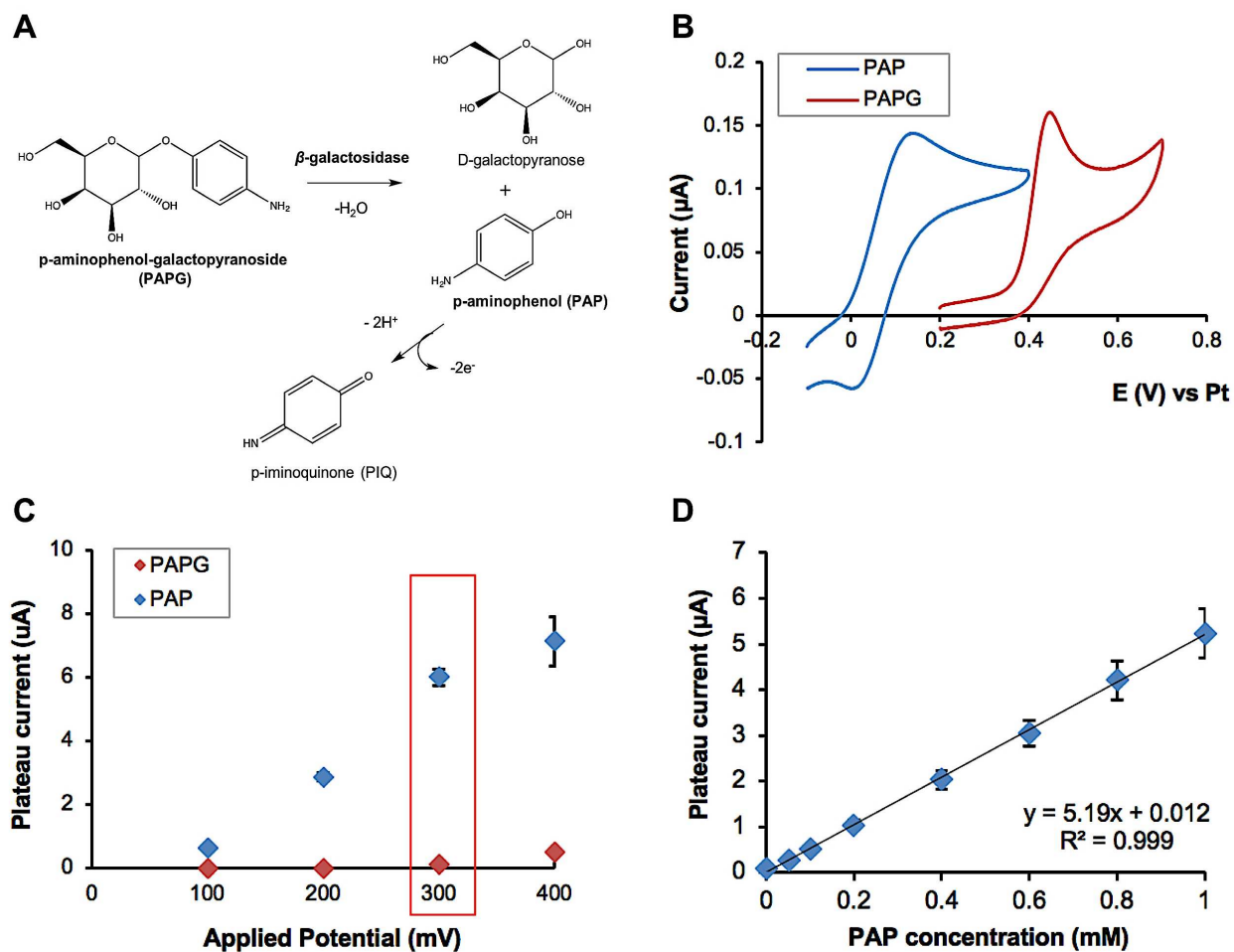


**Figure 2.4:** Detection PAP in the presence of PAPG: (A) an enzymatic conversion of PAPG by  $\beta$ -galactosidase into PAP. (B) Cyclic voltammograms of 1 mM PAP and PAPG in PBS pH 7.4 obtained in separate saturated ePADs. (C) Plateau current as a function of applied potential obtained from amperometric detection of 1 mM PAP and PAPG on the flow ePADs. (D) Calibration curve of PAP detection at 0.3 V vs Pt. Error bars represent standard deviation in 3 separate device measurements.

As proof of concept, the quasi-steady flow device was implemented to continuously monitor the enzymatic activity of  $\beta$ -galactosidase. Enzymatic assays have been employed in analytical detection methods due to their high sensitivity and selectivity to target analytes. The assays typically involve either a reaction between a target analyte and the enzyme to produce a detectable product,<sup>37</sup> a reaction between an enzyme biomarker with a substrate to produce a detectable product,<sup>38</sup> or the use of an enzyme as an antibody tag in enzyme-linked immunosorbent assay (ELISA).<sup>39</sup>  $\beta$ -galactosidase hydrolyzes the  $\beta$ -glycosidic bond between galactose and its organic moiety which is usually colorimetrically or electrochemically detectable. The enzyme has been commonly used as an ELISA's tag and a bacterial indicator for coliform detections.<sup>40,41</sup> The flow ePAD was used to measure the enzymatic conversion of PAPG by  $\beta$ -galactosidase into PAP (Figure 2.4A). PAP is detected electrochemically through a two-electron oxidation reaction. Both the substrate and product (PAPG and PAP) are electrochemically active with peak potential at 0.45 V and 0.15 V vs Pt, respectively (Figure 2.4B). An optimum overpotential for selective detection of PAP was determined at 0.3 V vs Pt (Figure 2.4C) based on the highest signal-to-noise ratio (i.e. ratio of plateau current for PAP to that for PAPG detection). A calibration curve for PAP detection was then established at this selected applied potential as shown in Figure 2.4D. The detection limit for PAP detection was 31  $\mu$ M (blank average + 3 $\times$ standard deviation).

Kinetics of  $\beta$ -galactosidase activity were monitored amperometrically at 0.3 V vs Pt by continuously adding reaction solution with varying PAPG concentrations and 5 U/mL enzyme in PBS pH 7.4 to the ePAD and measuring the changes in plateau current with time. After converting the plateau currents into PAP concentrations using the calibration curve, reaction rates were then extracted from the slope of the concentration vs time plot to establish a Michaelis-Menten plot as shown in Figure 2.5A. The plot revealed the rate of reaction starting to plateau out above 1 mM PAPG concentration, indicating saturation in the catalytic activity of the enzyme. Michaelis-Menten constant ( $K_m$ ) which shows the concentration of the substrate at which the reaction rate is equal to one-half of the maximum rate can be directly extracted from the plot or more easily estimated using a Lineweaver-Burk plot (Figure 2.5B).  $K_m$

is equal to slope/ $y_{\text{intercept}}$  in the Lineweaver-Burk plot and was found to be 0.36 mM. Similar  $K_m$  values were reported by Viratelle and Yon from the detection of PAP using a spectrophotometer at 306 nm ( $K_m = 0.33$  mM) and also by Laczka et al. who employed Au microelectrode array for electrochemical detection of PAP ( $K_m = 0.43$  mM).<sup>42,43</sup> The close agreement between results obtained by the ePADs and the literature reported values demonstrates that the proposed device provides similar viable performance to the more complex and expensive detection methods for monitoring enzyme kinetics in real-time.

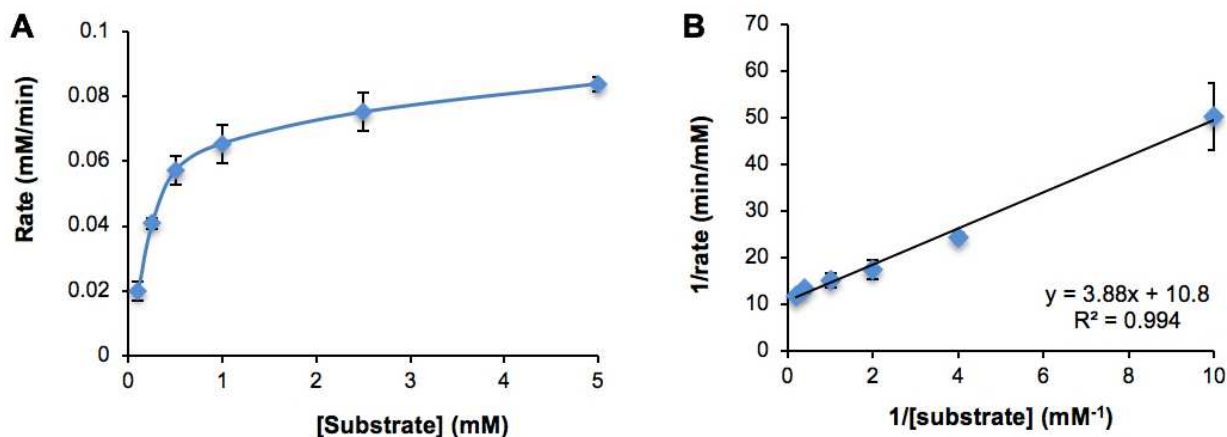


**Figure 2.5:** Enzyme kinetics determination by measuring PAPG conversion into PAP by  $\beta$ -galactosidase shown in Michaelis-Menten (A) and Lineweaver-Burk (B) plots. Error bars represent standard deviation in 3 separate device measurements.

## Conclusions

A simple and inexpensive (USD 1-2) Pt microwire-based ePAD employing an increasing capillary network of paper to generate a steady flow has been developed for semi-automation in bioanalysis. The two-layer paper device demonstrated in this work exhibited an increased flow rate compared with previously reported single-layer paper devices employed for FIA, improving analysis time from typically 10-20 min to only a minute. As a proof-of-concept, the devices were used to monitor the enzymatic activity of  $\beta$ -galactosidase with the kinetic value obtained was similar to those found in the literature. The ePAD could serve as an alternative detection platform to currently available methods, that also enables analysis of multiple samples within a single disposable device. This device shows great promise toward use in

ELISA or other analytical techniques where flow or washing steps are necessary. To perform immunoassays including ELISA, biorecognition elements capable of generating electrochemical signals upon binding to target analytes can be deposited on the surface of the working electrode. This device could use target-binding antibodies, for example, attached to the microwire working electrode or the paper itself. Similar to a lateral flow assay (LFA), reagents can be stored within the device, and upon addition of sample, the analyte can be reacted, captured, and washed of unbound material prior to the detection at the microwire electrodes. Detection of disease biomarkers in electrochemical lateral flow assays has been previously demonstrated.<sup>44</sup> Pt electrodes have also been employed to carry out ELISA in stationary and flow-based systems.<sup>45-47</sup>

## REFERENCES

- (1) Adkins, J. A.; Noviana, E.; Henry, C. S. *Analytical Chemistry* **2016**, *88*, 10639-10647.
- (2) Pradela-Filho, L. A.; Noviana, E.; Araujo, D.; Takeuchi, R.; Santos, A.; Henry, C. S. *ACS Sensors* **2020**.
- (3) Růžička, J.; Hansen, E. *Analytica Chimica Acta* **1975**, *78*, 145-157.
- (4) Ruzicka, J.; Hansen, E. H. *TrAC Trends in Analytical Chemistry* **2008**, *27*, 390-393.
- (5) Trojanowicz, M.; Kołacińska, K. *Analyst* **2016**, *141*, 2085-2139.
- (6) Leach, A. M.; Wheeler, A. R.; Zare, R. N. *Analytical Chemistry* **2003**, *75*, 967-972.
- (7) Iverson, B. D.; Garimella, S. V. *Microfluidics and Nanofluidics* **2008**, *5*, 145-174.
- (8) Opekar, F.; Nesměrák, K.; Tůma, P. *Electrophoresis* **2016**, *37*, 595-600.
- (9) Sheikhlou, M.; Shabani, R.; Reza zadeh, G. *Nonlinear Dynamics* **2016**, *83*, 951-961.
- (10) Saren, A.; Smith, A.; Ullakko, K. *Microfluidics and Nanofluidics* **2018**, *22*, 38.
- (11) Yang, D.; Krasowska, M.; Priest, C.; Popescu, M. N.; Ralston, J. *The Journal of Physical Chemistry C* **2011**, *115*, 18761-18769.
- (12) Juncker, D.; Schmid, H.; Drechsler, U.; Wolf, H.; Wolf, M.; Michel, B.; de Rooij, N.; Delamarche, E. *Analytical Chemistry* **2002**, *74*, 6139-6144.
- (13) Zimmermann, M.; Schmid, H.; Hunziker, P.; Delamarche, E. *Lab on A Chip* **2007**, *7*, 119-125.
- (14) Böhm, A.; Carstens, F.; Trieb, C.; Schabel, S.; Biesalski, M. *Microfluidics and nanofluidics* **2014**, *16*, 789-799.
- (15) Gökçe, O.; Castonguay, S.; Temiz, Y.; Gervais, T.; Delamarche, E. *Nature* **2019**, *574*, 228-232.
- (16) Cate, D. M.; Adkins, J. A.; Mettakoonpitak, J.; Henry, C. S. *Analytical Chemistry* **2014**, *87*, 19-41.
- (17) Elizalde, E.; Urteaga, R.; Berli, C. L. *Lab on A Chip* **2015**, *15*, 2173-2180.
- (18) Lankelma, J.; Nie, Z.; Carrilho, E.; Whitesides, G. M. *Analytical Chemistry* **2012**, *84*, 4147-4152.
- (19) Granica, M.; Fiedoruk-Pogrebniak, M.; Koncki, R.; Tymecki, Ł. *Sensors and Actuators B: Chemical* **2018**, *257*, 16-22.
- (20) WitkowskaNery, E.; Santhiago, M.; Kubota, L. T. *Electroanalysis* **2016**, *28*, 2245-2252.
- (21) Channon, R. B.; Nguyen, M. P.; Scorzelli, A. G.; Henry, E. M.; Volckens, J.; Dandy, D. S.; Henry, C. S. *Lab on A Chip* **2018**, *18*, 793-802.
- (22) Camplisson, C. K.; Schilling, K. M.; Pedrotti, W. L.; Stone, H. A.; Martinez, A. W. *Lab on A Chip* **2015**, *15*, 4461-4466.
- (23) Adkins, J.; Boehle, K.; Henry, C. *Electrophoresis* **2015**, *36*, 1811-1824.
- (24) Rattanarat, P.; Dungchai, W.; Cate, D.; Volckens, J.; Chailapakul, O.; Henry, C. S. *Analytical Chemistry* **2014**, *86*, 3555-3562.
- (25) Siegel, A. C.; Phillips, S. T.; Dickey, M. D.; Lu, N.; Suo, Z.; Whitesides, G. M. *Advanced Functional Materials* **2010**, *20*, 28-35.
- (26) Cunningham, J. C.; Brenes, N. J.; Crooks, R. M. *Analytical Chemistry* **2014**, *86*, 6166-6170.
- (27) Ge, L.; Wang, S.; Yu, J.; Li, N.; Ge, S.; Yan, M. *Advanced Functional Materials* **2013**, *23*, 3115-3123.
- (28) Hu, C.; Bai, X.; Wang, Y.; Jin, W.; Zhang, X.; Hu, S. *Analytical Chemistry* **2012**, *84*, 3745-3750.
- (29) Fosdick, S. E.; Anderson, M. J.; Renault, C.; Degregory, P. R.; Loussaert, J. A.; Crooks, R. M. *Analytical Chemistry* **2014**, *86*, 3659-3666.
- (30) Adkins, J. A.; Henry, C. S. *Analytica Chimica Acta* **2015**, *891*, 247-254.
- (31) Mendez, S.; Fenton, E. M.; Gallegos, G. R.; Petsev, D. N.; Sibbett, S. S.; Stone, H. A.; Zhang, Y.; López, G. P. *Langmuir* **2010**, *26*, 1380-1385.
- (32) Lineweaver, H.; Burk, D. *Journal of the American Chemical Society* **1934**, *56*, 658-666.
- (33) Washburn, E. W. *Physical Review* **1921**, *17*, 273-283.
- (34) Compton, R. G.; Fisher, A. C.; Wellington, R. G.; Dobson, P. J.; Leigh, P. A. *The Journal of Physical Chemistry* **1993**, *97*, 10410-10415.
- (35) Beden, B.; Largeaud, F.; Kokoh, K. B.; Lamy, C. *Electrochimica Acta* **1996**, *41*, 701-709.

- (36) Yan, X.; Ge, X.; Cui, S. *Nanoscale Research Letters* **2011**, *6*, 313-313.
- (37) Wang, J. X.; Sun, X. W.; Wei, A.; Lei, Y.; Cai, X. P.; Li, C. M.; Dong, Z. L. *Applied Physics Letters* **2006**, *88*, 2004-2007.
- (38) Nosrati, R.; Gong, M. M.; Gabriel, M. C. S.; Pedraza, C. E.; Zini, A.; Sinton, D. *Clinical Chemistry* **2016**, *62*, 458-465.
- (39) Lequin, R. M. *Clinical Chemistry* **2005**, *51*, 2415-2418.
- (40) Husain, Q. *Critical Reviews in Biotechnology* **2010**, *30*, 41-62.
- (41) Jokerst, J. C.; Adkins, J. A.; Bisha, B.; Mentele, M. M.; Goodridge, L. D.; Henry, C. S. *Analytical Chemistry* **2012**, *84*, 2900-2907.
- (42) Viratelle, O. M.; Yon, J. M. *European journal of biochemistry / FEBS* **1973**, *116*, 110-116.
- (43) Laczka, O.; Ferraz, R. M.; Ferrer-Miralles, N.; Villaverde, A.; Muñoz, F. X.; Campo, F. J. d. *Analytica Chimica Acta* **2009**, *641*, 1-6.
- (44) Sinawang, Prima D.; Rai, V.; Ionescu, R. E.; Marks, R. S. *Biosensors and Bioelectronics* **2016**, *77*, 400-408.
- (45) Yamaguchi, M.; Matsuda, Y.; Sasaki, S.; Sasaki, M.; Kadoma, Y.; Imai, Y.; Niwa, D.; Shetty, V. *Biosensors and Bioelectronics* **2013**, *41*, 186-191.
- (46) Akanda, M. R.; Joung, H.-A.; Tamilavan, V.; Park, S.; Kim, S.; Hyun, M. H.; Kim, M.-G.; Yang, H. *Analyst* **2014**, *139*, 1420-1425.
- (47) Bhimji, A.; Zaragoza, A. A.; Live, L. S.; Kelley, S. O. *Analytical Chemistry* **2013**, *85*, 6813-6819.

## CHAPTER 3: THERMOPLASTIC ELECTRODE ARRAYS IN FLOW-BASED ELECTROCHEMICAL PAPER DEVICES

### Chapter Overview

Historically, electrochemical paper-based analytical devices (ePADs) have relied almost exclusively on single electrode detection, limiting potential gains in sensitivity and/or selectivity achievable by multiple electrodes. Herein incorporation of thermoplastic electrode (TPE) arrays into flow ePADs is described. Quasi-steady flow was solely generated by capillary action through a fan-shaped paper device. The electrode arrays were fabricated using a simple solvent-assisted method with inexpensive materials (i.e. graphite and thermoplastic binder). These electrodes can be employed as an array of individually addressable detectors or connected as an interdigitated electrode array. The TPEs were characterized through SEM, optical profilometry and cyclic voltammetry. Chronoamperometry was used to characterize the flow-based TPE-ePADs. Trace detection of a ferrocene complex ( $\text{FcTMA}^+$ ) was demonstrated through generation-collection experiments, achieving a limit of detection of 0.32 pmol. These TPE arrays containing ePADs show great promise as a rapid, sensitive and low-cost sensor for point-of-need (PON) applications. This work has been published in *Analytical Chemistry*.<sup>1</sup> Kevin J. Klunder and Robert B. Channon contributed to the published work by providing suggestions during experiments and assistance in manuscript writing.

### Introduction

Microfluidic paper-based analytical devices ( $\mu$ PADs) are low-cost, have a high surface area to volume ratio for chemical reaction and detection, facilitate reagent storage within the fiber network, and can provide fluid transport through capillary action.<sup>2,3</sup>  $\mu$ PADs are also amenable to modifications (e.g. biomolecule attachment, electrode incorporation and coupling with external power source), making assays on paper tunable to achieve a required sensitivity, selectivity and analysis time for different applications.<sup>4</sup>

<sup>6</sup> Various  $\mu$ PADs have been reported to date for point-of-need (PON) applications featuring colorimetric or

electrochemical detection.<sup>6-8</sup> While colorimetric detection provides an easy signal readout, allowing for instrument-free measurements,<sup>9,10</sup> colorimetric  $\mu$ PADs often suffer from poor detection limits – limiting their PON use.<sup>11</sup> Electrochemical detection for  $\mu$ PADs (ePADs) is an attractive alternative due to its high sensitivity and tunable selectivity through choice of the electrode material, technique, potential, and/or incorporation of biomolecules to specifically recognize the target analyte.<sup>12,13</sup> Additionally, while electrochemical detection relies on external instrumentation such as potentiostats, inexpensive hand-held potentiostats have been built for PON applications.<sup>14,15</sup>

There are a variety of approaches for incorporating electrodes into ePADs, with screen or stencil printing carbon and/or metal inks onto the paper substrate as the most common.<sup>6,16,17</sup> Carbon electrodes, especially composite materials, are popular in electrochemistry due to their biocompatibility, low cost and easy fabrication.<sup>18</sup> Compared to metallic electrodes, the wider potential window that is frequently achieved with carbon electrodes provides favorable electrochemical activity for many redox species.<sup>19</sup> Carbon composites typically feature a small exposed fractional area of carbon compared to the geometric electrode area, due to the presence of insulating components. This provides lower electrode capacitance, lower background currents and higher signal-to-noise ratios in carbon composite electrodes compared to conventional solid carbon electrodes such as glassy carbon.<sup>18</sup> Various binders including mineral oil, wax, ionic liquids and Nafion have been reported for carbon composite fabrication.<sup>20-23</sup>

Thermoplastic binders such as polymethylmethacrylate (PMMA) and polyethylene have been largely unexplored, despite their great mechanical stability and ability to pattern electrodes through multiple approaches.<sup>24,25</sup> Thermoplastic electrodes (TPEs) are typically fabricated through radiation-induced polymerization, in-situ polymerization of plastic monomers in the presence of graphite, spray coating using a solvent processed plastic-graphite mixture, or molding/casting the material.<sup>26-28</sup> The TPE fabrication approach used in this work was adapted from a simple solvent-assisted electrode fabrication previously reported by our group.<sup>24</sup> However, instead of using PMMA, cyclic olefin copolymer (COC) was employed

here as the binder to create 160  $\mu\text{m}$  wide TPE bands. COC has a high purity, chemical resistance and excellent biocompatibility, making it a good binder material for electrochemical biosensors.<sup>29</sup>

To date, most ePADs reported in literature employed only a single electrode for detection, limiting potential improvements in detection sensitivity and/or selectivity that can be gained when using multiple electrodes.<sup>16</sup> Zhao and coworkers reported the use of electrode arrays in PADs; however, the electrodes were used separately for multiplexed detection.<sup>15</sup> Interdigitated electrode arrays (IDAs) can enable generation-collection (GC) experiments, where the first electrode in the array oxidizes the analyte, the second reduces it, and the process is repeated across the entire array to provide an enhanced cumulative signal. IDAs are very rarely used as low cost-PON sensors as they are limited by expensive conventional fabrication techniques, such as photolithography and chemical vapor deposition.<sup>30,31</sup> A few studies have adapted IDAs into PADs via chemical deposition and gravure printing.<sup>32,33</sup> However, their use was limited to resistance-based measurements with no redox-based electrochemistry performed. Yamamoto et al. recently reported redox cycling in paper-based device.<sup>34</sup> Yet, the experiment was limited to only a pair of electrodes.

In this work, a new PON detection platform is designed by coupling TPE arrays - consisting of up to 8 electrodes - into a flow-based ePAD. The ePAD design is based on a previous work, where fan-shaped PAD geometries generate quasi-steady flow rates, enabling functions like flow injection analysis.<sup>35,36</sup> The device was tested in both generation-generation (GG) mode - where potential was held constant at all electrodes - and GC mode, where two different potentials were applied to drive redox cycling. Using the TPE-ePAD, gains in sensitivity as well as low detection limits can be achieved in a pump-free flow injection system. This platform represents an important step towards low-cost and highly sensitive sensors for PON requirements.

## Experimental Section

### *Chemicals and materials*

Potassium chloride (KCl) and toluene were purchased from Fisher Scientific (New Jersey, USA). Dopamine HCl and graphite (7-11  $\mu\text{m}$  size particles) were purchased from Alfa Aesar (Massachusetts, USA). Ascorbic acid, potassium hexacyanoferrate (III) ( $\text{K}_3\text{Fe}(\text{CN})_6$ ), potassium hexacyanoferrate (II) trihydrate ( $\text{K}_4\text{Fe}(\text{CN})_6$ ) and hexane were purchased from Sigma-Aldrich. All the reagents were used as received without further purification. Ferrocenylmethyl trimethylammonium hexafluorophosphate ( $\text{FcTMA}^+$ ) was synthesized in-house following published procedures.<sup>37</sup> Whatman 1, 4 and 42 filter papers were purchased from GE Healthcare (Pittsburgh, USA). PMMA ( $\frac{1}{8}$  inch thick sheet) was purchased from Plaskolite Inc. (Ohio, USA). COC film (5013F) was purchased from TOPAS (USA). Conductive silver paint was obtained from SPI Supplies (Pennsylvania, USA). Packing tape, epoxy glue, copper wire, and sand papers (240- and 1500-grit) were purchased from local stores. Water used to prepare reagent solutions was purified using a Milli-Q system ( $\rho \geq 18.2 \text{ M}\Omega\cdot\text{cm}$ ).

### *Fabrication of TPE-ePADs*

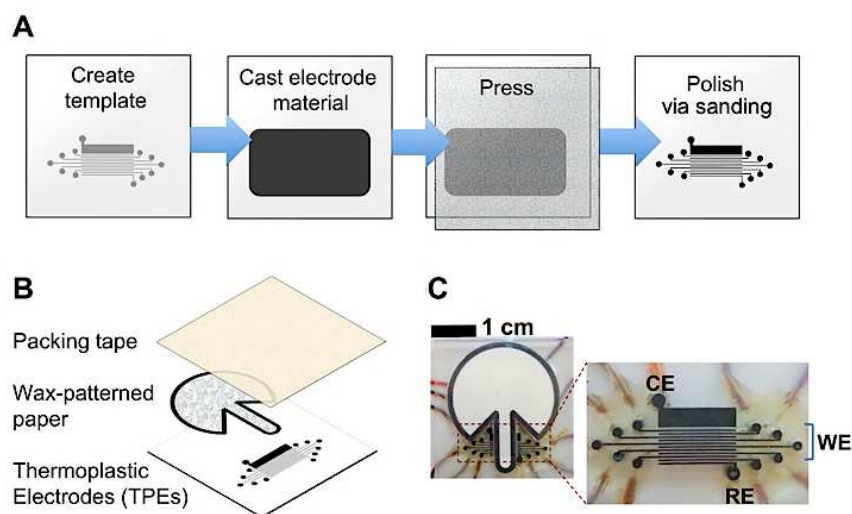


**Figure 3.1:** Schematic illustration of TPE fabrication (A) and assembly into an electrochemical PAD (B). The finished device is shown in C.

The fabrication scheme is shown in Figure 3.1. The electrode pattern was designed using Corel Draw (Corel, Ontario, Canada) and engraved on a PMMA sheet using a Zing CO<sub>2</sub> laser cutter (Epilog, Colorado, USA). The TPE consists of 10 individually addressable band electrodes that can be used separately as working electrodes (WE) or shorted together in generation-generation (GG) or generation-collection (GC) formats. Each WE band electrode is ~160 μm wide, 15-22 mm long, and is separated by ~300 μm from its nearest neighbor. The reference electrode (RE) has the same dimension as the individual WE while the counter electrode (CE) is 1 mm wide and 12 mm long. Thermoplastic electrode was prepared by mixing graphite and cyclic olefin copolymer (COC) at 3:1 w/w in a mixture of toluene-hexane (2:1 v/v). The mixture was left in air (under fume hood) to partially evaporate the solvent before casting onto the electrode mold. The use of COC enables easy dissolution of the binder in aliphatic and/or aromatic hydrocarbon solvents without or with only minimal dissolving of the acrylic mold. The electrode was then covered with a 0.5 cm thick polydimethylsiloxane (PDMS) layer and compressed at 50-100 Psi using a hydraulic press for 4 h at 60°C. After removing the PDMS cover, electrodes were sanded sequentially with 240-grit and 1500-grit paper to create a smooth electrode surface. 3 mm diameter holes were made at one of the working, reference and counter electrodes ends to create connections through the backside of the PMMA plate using plastic-coated copper wire, conducting silver paint and epoxy glue.

The paper device was designed using CorelDRAW and fabricated on Whatman 1 filter paper. To contain the fluid flow, 4-pt line thick wax barrier was created on the filter paper using a ColorQube 8870 wax printer (Xerox, Connecticut, USA), followed by wax melting on a 120°C hot plate for 90 s. The device inlet used a 4 mm inner diameter wax-printed semi-circle well connected to an 18 mm × 4 mm channel. The channel flows into the center of a 37 mm inner diameter circle with ¼ of the section removed to form a 270° wicking fan. TPE-ePAD was constructed by attaching the wax-patterned fan-shaped filter paper onto the TPE bands using packing tape while leaving the sample inlet open to ambient air. Using this approach, the electrodes could be used many times after replacing the disposable paper devices.

### ***Characterization of TPEs***

Prior to ePAD application, the electrode material was optimized by varying the mass ratio of graphite to COC from 1:1 to 5:1. Half cm diameter test electrodes were made on PMMA substrate using these ratios. Through-plane conductivity measurements<sup>24</sup> and cyclic voltammetry (CV) at 0.1 V/s in 0.5 KCl were carried out on the electrodes to compare the electrochemical properties. In addition, CVs of a surface insensitive ( $\text{FcTMA}^+$ ), a surface sensitive ( $\text{Fe}(\text{CN})_6^{3-}/\text{Fe}(\text{CN})_6^{4-}$ ), and two biologically relevant redox species (dopamine and ascorbic acid) were collected on the band electrodes. A saturated calomel electrode (SCE) and TPE were used as the RE and CE, respectively. Scan rate studies were performed by obtaining CVs at 0.01 V/s to 0.5 V/s using 5 mM  $\text{FcTMA}^+$  in 0.5 M KCl. To estimate the charge transfer rate at the electrode surface, CVs of 5 mM  $\text{Fe}(\text{CN})_6^{3-/4-}$  in 0.5 M KCl were acquired at 0.01 V/s to 0.5 V/s and the charge transfer rate ( $k_{ct}$ ) was determined based on Nicholson method (Eq. 2-Appendix). Surface structure and roughness of the electrode were probed using a JSM-6500F field emission scanning electron microscope (JEOL, Tokyo, Japan) at 2 kV acceleration voltage and a ZeScope profilometer (Zemetrics, Arizona, USA), respectively.

### ***Characterization of flow ePADs***

The ePAD was pre-wetted using 10  $\mu\text{L}$  background solution (0.5 M KCl) such that the fluid front reaches the 270° wicking fan, allowing for a quasi-steady flow for the next injections.<sup>36</sup> 5-25  $\mu\text{L}$  of 1 mM  $\text{FcTMA}^+$  solution in 0.5 M KCl was then injected onto the device inlet and hydrodynamic amperometry was performed on one of the WE bands at 0.4 V vs Carbon (C) RE. Carbon electrode was used as a pseudo-reference in the array since adding a separate Ag/AgCl electrode into the flow ePAD would be difficult. Current signals at individual electrodes were monitored by amperometry during injection of 1 mM  $\text{FcTMA}^+$  solution at 0.4 V vs C using an CHI1010A potentiostat (CH Instruments, Texas, USA). Due to the capability of the potentiostat to perform only 8 simultaneous measurements, the study was conducted using up to 8 electrodes. To characterize and optimize the usability of the electrodes to perform redox cycling under a flow condition, several variables including the use of multiple layers of paper and different paper substrates

(Whatman 1, 4 and 42), interelectrode distance and number of electrodes were tested. Conversion and collection efficiency were calculated for each tested variable to compare their performances. Conversion efficiency was calculated as the ratio of total measured charge obtained by integrating current signal over time from an injection of 10  $\mu\text{L}$   $\text{FcTMA}^+$  1 mM to the theoretical total charge if all species injected are detected. Collection efficiency was determined by taking a ratio of total charge at the collector versus the generator during a generation-collection or redox cycling experiment. 0.4 V vs C and -0.2 V vs C were applied to the generator and collector, respectively, using a CHI1242B bipotentiostat (CH Instruments, Texas, USA). To compare sensitivity and limit of detection (LOD) of ePADs operated using a single electrode and multiple electrodes either on GG or GC mode, calibration curves were established using 5  $\mu\text{L}$  of 0.010-5.0  $\mu\text{M}$   $\text{FcTMA}^+$  in 0.5 M KCl. LOD was calculated from the average plus 3 times standard deviations of blank measurements in separate devices ( $n = 5$ ).

## **Results and Discussion**

### ***Characterization of TPEs***

#### ***Morphology of the electrodes***

The TPE IDA was first characterized through light microscopy, profilometry and scanning electron microscopy as shown in Figure 3.2. The average width of the band electrodes was found to be  $162 \pm 11 \mu\text{m}$  ( $n = 10$ ) through light microscopy (Figure 3.2A). While smaller templates are possible based on the spot size of the laser cutter (slightly less than 100  $\mu\text{m}$ ), smaller templates resulted in a poor mechanical stability (during sanding) and increased electrode resistance resulting in poor voltammetry. Smaller features are possible with other approaches, such as a higher resolution laser cutter or focused ion beam milling.<sup>38</sup> In fact, micrometer-sized carbon composite electrodes have been previously reported by creating microcavities using photolithography/metal deposition then filling with a carbon composite, or by coating carbon fiber with polymeric materials through chemical vapor deposition.<sup>39,40</sup> However, these fabrication techniques are more complex, time-consuming and expensive than the approach reported in this study.

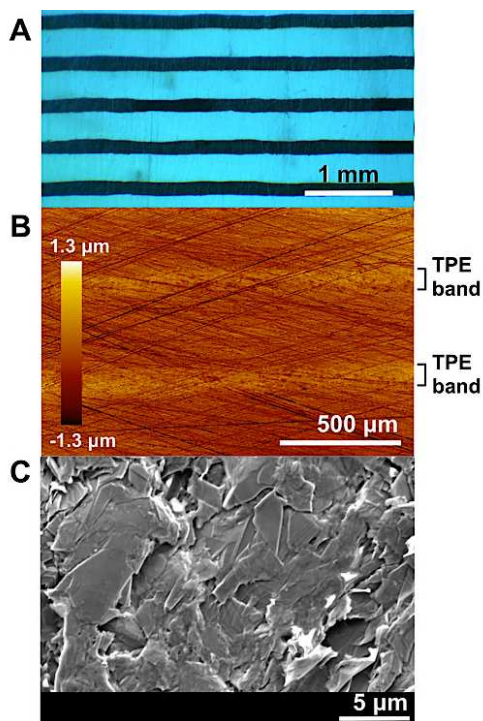


**Figure 3.2:** Surface morphology of the TPE bands imaged using: (A) light microscopy, (B) profilometry and (C) scanning electron microscopy. The electrodes were fabricated using 3:1 graphite-COC (*w/w*).

The wetting properties of a material are often related to the surface roughness. When employed in a flow cell, surface roughness also affects the flow rate and the fluid dynamics (e.g. laminar or turbulent).<sup>41</sup> Surface height ( $S_a$ ) of the TPE bands surface was  $0.24 \pm 0.03 \mu\text{m}$  ( $n = 5$ ). Water contact angles (WCA) were found to be similar between the TPE band and acrylic base surfaces which were  $65.9^\circ \pm 4.9^\circ$  and  $69.0^\circ \pm 4.7^\circ$ , respectively, for freshly sanded materials (Figure S1-Appendix I). This similar wettability was possibly due to mixing of materials on the surface during sanding. Similar contact angles were reported for freshly exfoliated highly-ordered pyrolytic graphite (HOPG).<sup>42</sup> Average static contact angle of the TPEs increased from  $65.9^\circ$  to  $75.7^\circ$  after 1 day exposure. This increase in contact angle was possibly due to adsorption of organic matter from air which could be mitigated by storing the electrodes in a sealed container or re-sanding the surface to remove organic contaminants. The electrode bands were slightly more resistant to abrasion from sanding, as shown by 0.1-0.5  $\mu\text{m}$  higher surfaces than those of the acrylic base

(Figure 3.2B and S2-Appendix), likely due to differences in mechanical strength between the polymeric materials.<sup>43</sup>

Scanning electron microscopy (SEM) was used to understand the surface morphology and graphitic structure (Figure 3.2C). Graphite sheets containing basal and edge planes are clearly visible. Slight charging on the surface was also observed due to the presence of a thin layer insulating plastic binder. Treating the surface with plasma oxidation etched out plastic from the surface, exposing more graphite while reducing surface charging (Figure S3-Appendix). However, this treatment resulted in a significant growth in capacitive current (in addition to the Faradaic current), lowering the signal-to-noise ratio during electrochemical detection.

#### *Electrochemical behavior*

To obtain an optimum electrode material composition, the ratio between graphite and thermoplastic binder was varied and assessed through conductivity measurements. As shown in Figure 3.3A, conductivity of the composite increased with higher graphite mass loading up to 3:1 graphite-COC (*w/w*) where a further increase in graphite mass percentage did not increase conductivity. A similar plateau in conductivity has been previously reported for graphite-PMMA composites above a 3:1 carbon-to-binder ratio.<sup>24</sup> Conductivities of the graphite-COC composites were lower than the previously reported graphite-PMMA composites at similar ratios due to the higher electrical resistivity of the COC material.<sup>24,43</sup> However, the average conductivity for the 3:1 graphite-COC (*w/w*) composite was considerably higher than that of screen-printed carbon electrodes (<10 S/m) typically employed in ePADs.<sup>6,44</sup>

Cyclic voltammetry in 0.5 M KCl solution, as shown in Figure 3.3B, revealed approximately 2.8 V solvent window for the lowest graphite mass loading (1:1 *w/w*). The onset potential for hydrogen evolution and water oxidation decreased as the amount of graphite within the composite increased, narrowing the window significantly. Oxygen reduction peaks were observed at -1.2 V and -1.0 V vs SCE for 4:1 and 5:1 *w/w* of graphite to COC, respectively. This is likely due to trace metals contamination in the graphite powder (purity = 99%), as Fe, Ni and Cu have been detected in graphite bulk material at ppm

levels.<sup>45</sup> It is well reported in literature that trace metals can significantly affect the electrochemical activity.<sup>46</sup>

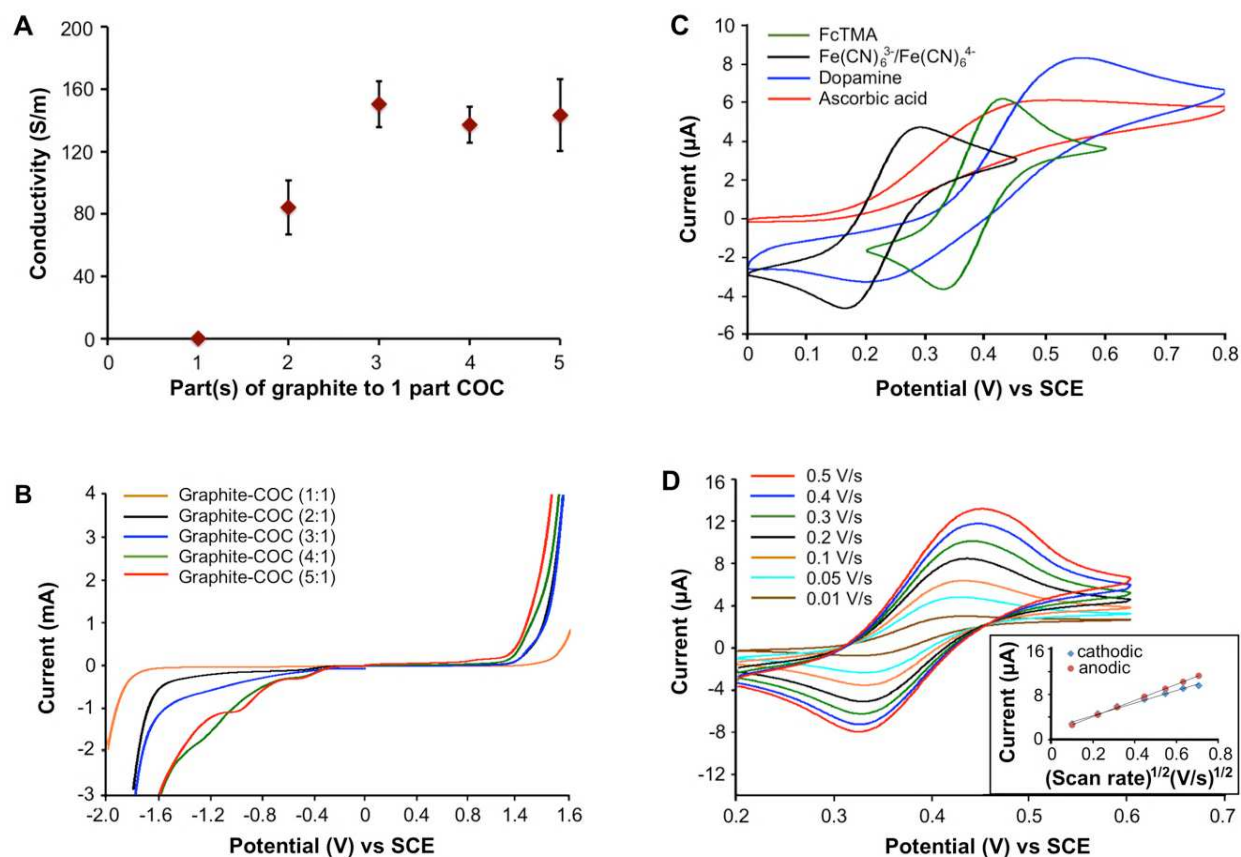


**Figure 3.3:** TPE electrochemical characterization: (A) through-plane conductivity ( $n = 4$ ) and (B) dependence of solvent window on electrode composition, (C) cyclic voltammograms of 5 mM  $\text{FcTMA}^+$ ,  $\text{Fe}(\text{CN})_6^{3-}/\text{Fe}(\text{CN})_6^{4-}$ , dopamine and ascorbic acid in 0.5 M KCl, collected at 0.1 V/s on a  $0.15 \times 3.5$  mm TPE and (D) scan rate study using 5 mM  $\text{FcTMA}^+$  with the resulting Randles-Sevcik plot shown in the bottom right inset.

Band electrodes with  $\sim 160$   $\mu\text{m}$  width were created using 3:1 graphite-COC and characterized before being implemented as detector arrays. Voltammetric responses of 5 mM  $\text{FcTMA}^+$ ,  $\text{Fe}(\text{CN})_6^{3-/4-}$ , dopamine and ascorbic acid on the band electrode are shown in Figure 3.3C. Peak currents of  $\text{FcTMA}^+$  and  $\text{Fe}(\text{CN})_6^{3-/4-}$  were close to that predicted by Randles-Sevcik equation (Eq. 1-Appendix, predicted =  $5.82$   $\mu\text{A}$  experimental =  $6.29 \pm 0.08$   $\mu\text{A}$  and  $5.59 \pm 0.05$   $\mu\text{A}$  for  $\text{FcTMA}^+$  and  $\text{Fe}(\text{CN})_6^{3-/4-}$ , respectively). A scan rate

study performed at 0.01 - 0.5 V/s using 5 mM FcTMA<sup>+</sup> also gave a linear response of peak current vs  $v^{1/2}$ , indicative of a diffusion-controlled reaction (Figure 3.3D). Larger peak separations ( $\Delta E_p$ ) than predicted by theory were observed for these two species ( $\Delta E_p = 91 \pm 2$  mV and  $102 \pm 2$  mV for FcTMA<sup>+</sup> and Fe(CN)<sub>6</sub><sup>3-/4-</sup>, respectively, at 0.1 V/s). Accounting for cell resistance (1.5 k $\Omega$  by electrochemical impedance spectroscopy measurement), an 18 mV gap in peak separation resulted from the  $i$ - $R$  drop while the remaining may be associated with the resistance to charge transfer. The Nicholson method was used to estimate the charge transfer rate ( $k_{ct}$ ) (Eq. 2-Appendix).<sup>47</sup> Calculated  $k_{ct}$  were 0.004 cm/s and 0.006 cm/s for uncorrected and corrected values to cell resistance, respectively (Figure S4-Appendix). These values are between the reported  $k_{ct}$  values of HOPG-basal plane (<10<sup>-7</sup> cm/s) and HOPG-edge plane (0.06-0.1 cm/s).<sup>18</sup> Similar  $k_{ct}$  values (0.004 - 0.05 cm/s for Ru(NH<sub>3</sub>)<sub>6</sub><sup>2+/3+</sup>) were previously reported on a graphene screen printed electrode, although the exact graphene loadings in the inks were not reported.<sup>44</sup> Nonetheless, the charge transfer kinetic of the new composite electrodes is better than those of carbon paste electrodes ( $k_{ct} = 10^{-5} - 10^{-3}$  cm/s).<sup>48</sup>

Sluggish electrode kinetics were observed with dopamine as exhibited by the large  $\Delta E_p$  ( $300 \pm 10$  mV) and overpotential ( $390 \pm 10$  mV) to drive the redox reaction. More favorable electrochemistry has previously been reported for dopamine oxidation on carbon electrodes ( $\sim 150$  mV vs Ag/AgCl for clean HOPG electrodes,<sup>49</sup>  $\sim 180$  mV vs SCE for sanded PMMA-graphite electrodes).<sup>24</sup> As the surface area of the band electrode was much smaller than the overall area of PMMA substrate, polishing the surface using sand paper could potentially contaminate the electrode surface with COC. The COC film could prevent dopamine adsorption on the electrode and potentially affect the electrochemical signal. Although adsorption is not reportedly required for ascorbic acid electrochemical oxidation, the kinetics are extremely sensitive to the cleanliness of the electrode surface.<sup>18</sup>

### ***Electrochemical detection in flow ePADs***

To semi-automate the sample analyses, a fan-shaped paper device was implemented in the ePAD to create quasi-steady state flow, similar to that used in traditional flow injection analyses. The 270° fan

attached to the channel exit provides an expanding wicking area to increase the overall capillary pressure, counterbalancing the increase in viscous drag as the solution travels further down the channel. This results in a constant solution velocity, where straight paper channels normally exhibit decaying flow rates.<sup>35,36,50</sup>

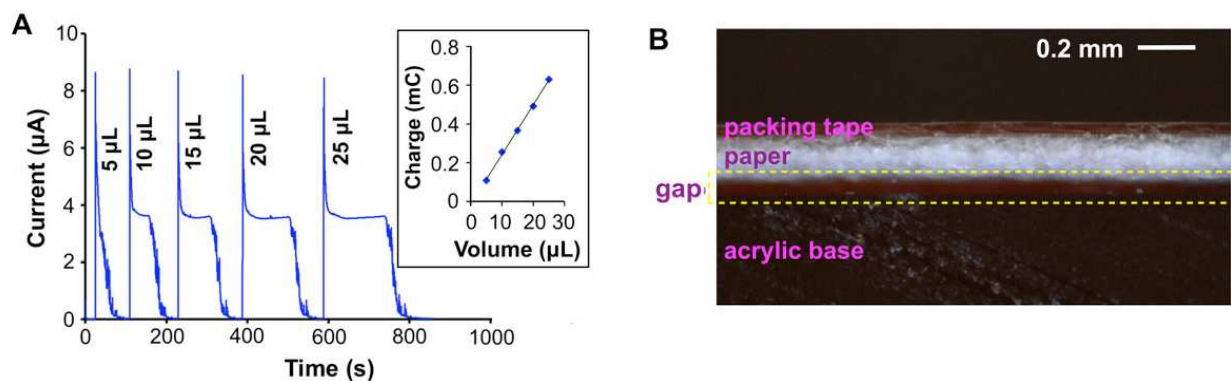


**Figure 3.4:** (A) Hydrodynamic amperogram obtained by injecting 5-25  $\mu\text{L}$  of 1 mM  $\text{FcTMA}^+$  onto an ePAD (channel width ( $w$ ) = 4 mm, TPE band width ( $x_c$ ) = 160  $\mu\text{m}$ ). Inset shows the integrated current for each injection plotted against the solution volume. (B) ePAD channel cross section during flow of a dyed solution.

Figure 3.4A shows the amperometric response of a TPE-ePAD with 5-25  $\mu\text{L}$  injections of  $\text{FcTMA}^+$ . A spike in current is observed immediately after droplet addition due to the high initial velocity of the flow from the small resistance encountered when displacing air with solution. The spike decays as the flow rate stabilizes, giving a current plateau, followed by a decay of current back to the baseline as the flow stops due to liquid depletion at the inlet. The magnitude of the plateau current was independent of the solution volume, suggesting that hydrostatic pressure from the solution droplet was not significant compared to capillary pressure driving the flow. The amount of detected analyte (measured as charge, mC) was linearly proportional to the amount of species of injected (Figure 3.4A inset). Therefore, sample volumes as low as 5  $\mu\text{L}$  are sufficient for analytical measurements, resulting in fast analysis times ( $\sim 1$  min after sample injection for current to decay to baseline). Note, measurement times ranging from 7 to 20 min have been reported in previous  $\mu\text{PADs}$  for sub- $\mu\text{L}$  injection volumes.<sup>51,52</sup> The proposed design can accommodate up to 17 injections of 5  $\mu\text{L}$  before becoming saturated and experiencing a reduction in flow rate as well as

signal (Figure S5-Appendix, 5 mM FcTMA<sup>+</sup> in 0.5 M KCl was used). It is also possible to increase the volume or injection capacity by increasing the size of the fan wicking portion of the device.

To characterize the fluid dynamics, the flow rate within the ePAD was estimated by imaging the flow of a solution of food dye (Figure S6-Appendix). The flow rate from this dye experiment was  $0.13 \pm 0.02 \mu\text{L/s}$ , which is close to the measured flow rate from electrochemical measurements ( $0.11 \pm 0.02 \mu\text{L/s}$  based on the time it took for the current signal to decay for certain injection volumes in Figure 3.4A). Using this experimentally determined flow rate, a theoretical plateau current was then calculated using Levich equation (Eq. 3-Appendix) based on the geometry of the channel (assuming  $150 \mu\text{m}$  paper thickness as the channel height). The theoretical plateau current was estimated to be  $1.4 \mu\text{A}$ , approximately 2.4 times lower than that observed experimentally (Figure 3.4A). This discrepancy could be attributed to the presence of a gap between the TPE-acrylic platform and the paper device, providing a lower resistance flow path compared to that through the porous network of paper.<sup>36,53</sup> Figure 3.4B shows an image of the channel cross-section during solution flow, featuring a  $40 \pm 10 \mu\text{m}$  channel gap. The solution imbibes into this gap and then into the paper substrate above, as shown in Figure S7 (Appendix). Thus, the gap serves as the main microfluidic channel, while the paper substrate sustains laminar fluid flow through capillary action ( $Re < 1$ , Eq. 4-Appendix). The presence of gap between two material interfaces and its contribution to the overall flow has been previously reported.<sup>36,53,54</sup> Assuming a channel height equal to the gap height, theoretical plateau currents are between  $3.0 \mu\text{A}$  for  $50 \mu\text{m}$  gap and  $4.2 \mu\text{A}$  for  $30 \mu\text{m}$  gap which were in agreement to the experimental data.

#### *Signal generation in TPE arrays*

To assess signal generation within the electrode arrays, currents at 8 TPE bands were monitored simultaneously during a  $10 \mu\text{L}$  injection of  $1 \text{ mM FcTMA}^+$  (Figure 3.5AB, potential =  $0.4 \text{ V vs C}$ , GG mode). A reduction in current was observed for each subsequent electrode downstream from the inlet, as expected for consumption of the analyte by upstream electrodes. Figure 3.5C shows the magnitude of plateau current normalized to the electrode area (i.e. current density) for each electrode. The ratios of current

density between two adjacent electrodes ( $i_{g2}/i_{g1}$ ) were approximately  $74 \pm 12\%$  (calculated by averaging ratios of current density in Figure 3.5C). This value was close to the 71% theoretically predicted (i.e. for  $i_{g1} = 2.4 \mu\text{A}$ ,  $V_f = 0.087 \mu\text{L/s}$ ) for a microfluidic device operated under hydrodynamic/Levich condition (Eq. 5-Appendix). The theoretically achievable signal at the electrodes is shown as the dashed yellow line on Figure 3.5C.

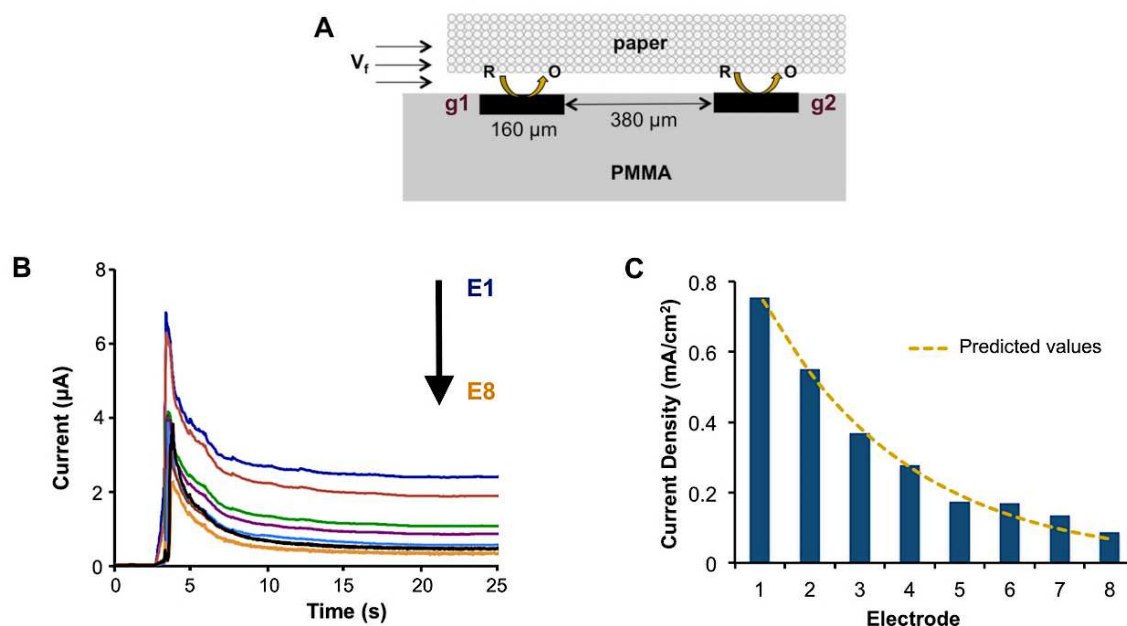


**Figure 3.5:** TPE arrays flow-ePAD under GG mode: **(A)** Schematic illustration of the device and redox reaction that is taking place, **(B)** current signals simultaneously monitored at 8 individually addressable electrodes (E1 was the closest to the inlet (upstream),  $w = 3 \text{ mm}$ ) from the injection of  $10 \mu\text{L}$  of  $1 \text{ mM}$   $\text{FcTMA}^+$ , and **(C)** plateau currents in B plotted against the electrode number and predicted values based on Levich and sequential regime approximation (Eq. 5-Appendix).

Approximately 20% of injected redox species were turned over at the first electrode using a single layer Whatman 1 paper (Figure 3.6B). Under the flow condition and channel geometry, the diffusion layer thicknesses were  $\sim 15 \mu\text{m}$  and  $\sim 19 \mu\text{m}$  at the center and edge of the electrode band, respectively (Eq. 7, Figure S7-Appendix). The collection efficiency between two adjacent electrodes was  $42 \pm 6\%$ , which was higher than predicted by theory (i.e.  $i_{g2}/i_{g1} = 29\%$ , Eq. 6-Appendix). While the theoretical prediction was calculated based on Levich/sequential approximation as previously described,<sup>55</sup> the flow-ePAD may not

fall within the boundary conditions for this equation wherein the predictions accurately depict the experimental results. Sequential regimes are characterized by homogenous flow composition (i.e. no concentration gradient exists) across the microchannel before reaching second electrode. Figure S9 (Appendix) exhibits relationship between interelectrode distance and collection efficiency which indicates that homogenous flow composition was not achieved at electrode gaps  $< 1.2$  mm. Values close to the predicted were reported by Renault and coworkers who obtained approximately 25-30% collection efficiency using screen printed electrodes that were 2.5 mm apart and operated under similar flow velocity.<sup>56</sup>

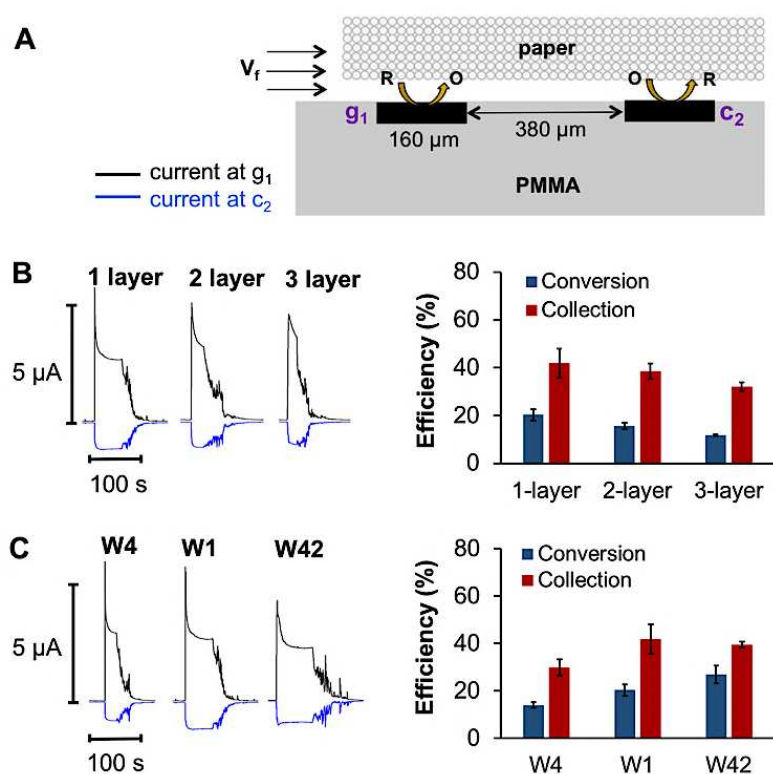


**Figure 3.6:** TPE arrays operated within flow-ePAD under GC mode experiment: schematic illustration of redox reaction that is taking place between generator ( $g_1$ ) and collector ( $c_2$ ) in the device (A), and conversion and collection efficiency for different number of Whatman 1 paper layer (B) and types of paper substrate (C). All these were tested using 10  $\mu$ L of 1 mM FcTMA<sup>+</sup> ( $n = 4$  devices).

#### *Modification of ePADs and GC performance*

To adjust flow rates within the ePAD, the use of multiple layers of paper and different paper substrates as passive pumps was investigated because increases in flow rate have been reported using multiple layers of paper in  $\mu$ PADs.<sup>53,54</sup> The presence of a gap between the two sheets of paper increases the average pore radius and interstitial permeability of the paper channel to fluid flow. A 2 $\times$  increase in flow rate was observed in double layer devices (Table S2), and no significant increase in volumetric flow rate was observed from double to triple layer paper devices, as has been previously observed.<sup>53</sup> This could be attributed to reduction in gap heights within the triple layer device (Figure S10-Appendix) since the paper layers were more tightly packed as the paper swelled.

Increased plateau currents at the generator electrode were observed as the number of paper layers increased (Figure 3.6B). Aside from the higher flow rates, the smaller gaps between paper and acrylic base within double and triple layer devices could reduce the effective channel height as well as the diffusive layer thickness, therefore increasing the flux of species to electrode surface. However, analyte turnover or conversion decreased in multi-layer devices as the solution was distributed into a larger overall channel volume and majority of the species could not diffuse through the paper close enough to the electrode for reacting. Collection efficiency also went down with multiple layers of paper, possibly due to higher flow rates. High flow rate reduces the thickness of diffusive layer and increase concentration gradient of the redox species near electrode surface.<sup>57</sup> This increase in concentration gradient could drive faster diffusion of oxidized species from generator to the bulk solution. Thus, only a small fraction of the species would reach the collector.

Another simple method to adjust the flow rates is to change the pore size of paper substrate. Whatman 1 has an approximate vertical pore diameter of 11  $\mu\text{m}$ .<sup>53</sup> Changing the paper to Whatman 4 (20-25  $\mu\text{m}$  vertical pore diameter) and Whatman 42 (2.5  $\mu\text{m}$  vertical pore diameter) was expected to increase and decrease flow rates, respectively. Compared to flow rates in Whatman 1, an  $\sim$ 33% decrease in flow rates was seen with Whatman 42 while the rates doubled in Whatman 4 (Table S2). These measured flow rates were well correlated to the experimentally observed plateau currents based on the Levich equation

(Figure 3.6C and S11-Appendix). Despite lowering the plateau currents due to reduction in analyte flux, slower flow rates provided longer time for the analyte plug to pass over the electrode. This longer residence time allowed for more analytes to diffuse down to the electrode and increased the conversion efficiency (Fig 6C). The slower flow rates in Whatman 1 and 42 ( $0.12 \pm 0.01 \mu\text{L/s}$  and  $0.08 \pm 0.01 \mu\text{L/s}$ , respectively, compared to  $0.24 \mu\text{L/s}$  in Whatman 4) also improved collection efficiency of the ePAD.

#### Comparison of detection limit and sensitivity

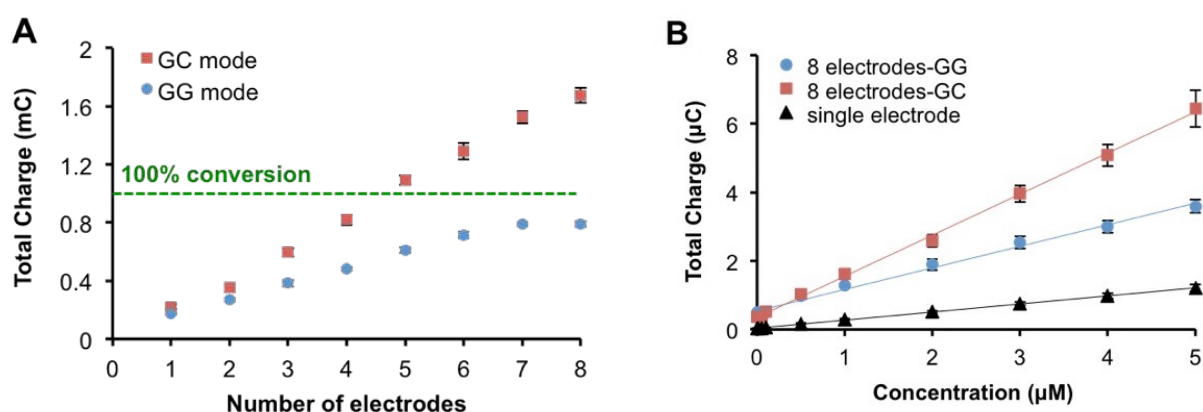


**Figure 3.7.** Signal improvement with TPE arrays: **(A)** total charges measured from ePAD operated with increasing number of electrodes in GG and GC modes using 1 mM FcTMA<sup>+</sup> ( $n = 4$  injections), **(B)** calibration curves of FcTMA<sup>+</sup> using single electrode ( $y = 0.24x + 0.04$ ) and electrode arrays operated in GG ( $y = 0.63x + 0.54$ ) and GC ( $y = 1.20x + 0.36$ ) modes ( $n = 4$  devices). Experiments were performed using 1-layer Whatman 1,  $w = 4$  mm.

Figure 3.7A shows a comparison of generated signal (measured as total charges) as an increasing number of TPE bands were operated together under GG and GC modes. Up to 80% of the total injected species were turned over using an array of 8 TPEs in GG mode. Based on  $i_{g2}/i_{g1}$  that was previously determined above to be  $74 \pm 12\%$ , with approximately 18% analytes were turned over by the first electrode ( $g_1$ ) the predicted total turn-over for 8 electrodes is between 46% to 90%. Thus, the experimental value (80% conversion) falls within the predicted range. By employing GC mode, the achievable signal was higher than that theoretically possible without redox cycling (100% conversion = green dashed line) since

one analyte can be turned over multiple times. Collection efficiency also increased from  $39 \pm 2\%$  with 1 electrode pair to  $62 \pm 1\%$  with 4 electrode pairs possibly due to the overlapping diffusion layer among electrodes (Figure S12-Appendix). The total amount of signal was doubled in GC mode relative to that in GG mode when 8 TPE bands were used. In addition, the trend had not yet shown an indication of signal saturation, suggesting that higher detection sensitivity can be obtained with more electrode pairs operated in GC mode.

Calibrations were established using single TPE band and TPE arrays (eight electrodes) operated in both GG and GC modes using  $0.010 - 5.0 \mu\text{M}$  FcTMA<sup>+</sup> (Figure 3.7B). Detection sensitivities were  $0.24 \mu\text{C}/\mu\text{M}$ ,  $0.63 \mu\text{C}/\mu\text{M}$  and  $1.2 \mu\text{C}/\mu\text{M}$  for single detector, GG arrays and GC arrays, respectively. Limits of detection (LOD) were estimated to be  $90 \text{ nM}$  for single detector,  $130 \text{ nM}$  for GG arrays and  $64 \text{ nM}$  for GC arrays (equivalent to  $0.45 \text{ pmol}$ ,  $0.65 \text{ pmol}$  and  $0.32 \text{ pmol}$ , respectively). Detection of  $100 \text{ nM}$  FcTMA<sup>+</sup> using the 3 detection modes is shown in Figure S13 (Appendix). Signals from the redox analyte are visually discerned from the background signals in all three modes. However, the magnitude of signals from the GG mode-operated device could not significantly be distinguished from the background at  $100 \text{ nM}$  due to the larger noise level (Table S3). Although the detection sensitivity was improved in the electrode arrays due to higher analyte turnover, increase in electrode surface resulted in larger capacitive/background currents which limit the attainable LODs. Nonetheless, detection limits from this TPE-ePADs were considerably lower than those of previously reported direct detection ePADs which were in  $\mu\text{M}$  ranges.<sup>17,36,58</sup> This low LOD of the TPE-ePAD was a huge improvement to make PADs more suitable for future PON applications.

## Conclusions

Incorporation of thermoplastic electrode arrays to improve sensitivity of flow ePADs was demonstrated for the first time here. Fabrication of the electrode arrays was simple and could achieve smaller electrode size and gap compared to conventional screen-printing method. The use of inexpensive graphite and thermoplastic binders allowed for construction of electrochemical devices that cost  $\$1.50$  per device and renewable electrodes through sanding. Increasing capillary network from the fan-shaped paper

in TPE-ePADs generated a quasi-steady flow for semi-automation in analyzing multiple samples without an external pump. In addition to the rate of solution imbibition within paper substrate, the presence of gap between paper and electrode base apparently impacted flow rates within the ePADs. As the solution preferably flows through the gap rather than laterally flow through the porous substrate of the paper, the PAD devices mimic the conventional single channel-microfluidic devices. Analyte turnover was improved from 18% in single electrode detection to 80% in electrode arrays consisting of 8 TPE bands. Up to 62% collection efficiency was achieved in generation-collection experiment using similar number of electrodes. Despite simpler fabrication method, collection efficiency of the TPE-ePADs was comparable to previously reported flow experiment in microfluidic devices using  $\mu\text{m}$ -sized IDA prepared via photolithography.<sup>59</sup>

A low limit of detection (ca. 64 nM) was attainable by the TPE-ePADs operated under GC mode. While the use of the TPE-ePAD is currently limited to analytes that are electrochemically active (electrochemically and chemically reversible for GC mode), coupling immunoassay to the TPE-ePAD will allow for the detection of various analytes ranging from small molecules to organisms such as bacteria. Many antibodies targeting these analytes are commercially available. Suitable enzyme-linked immunosorbent assay (ELISA) substrates can also be employed to generate electrochemically reversible species such as *p*-aminophenol (PAP) and 3,3',5,5'-tetramethylbenzidine (TMB).<sup>33,60</sup> Generation of large number of detectable products from a single analyte binding event in ELISA would also improve LOD of the TPE-ePAD even further for PON applications using saliva or other sample matrices where biomarkers are present at very low concentrations (i.e. sub nM).

## REFERENCES

- (1) Noviana, E.; Klunder, K. J.; Channon, R. B.; Henry, C. S. *Analytical Chemistry* **2019**, *91*, 2431-2438.
- (2) Noh, H.; Phillips, S. T. *Analytical Chemistry* **2010**, *82*, 4181-4187.
- (3) Fridley, G. E.; Le, H. Q.; Fu, E.; Yager, P. *Lab on A chip* **2012**, *12*, 4321-4327.
- (4) Nery, E. W.; Kubota, L. T. *Journal of Pharmaceutical and Biomedical Analysis* **2016**, *117*, 551-559.
- (5) Gong, M. M.; Nosrati, R.; San Gabriel, M. C.; Zini, A.; Sinton, D. *Journal of the American Chemical Society* **2015**, *137*, 13913-13919.
- (6) Dungchai, W.; Chailapakul, O.; Henry, C. S. *Analytical Chemistry* **2009**, *81*, 5821-5826.
- (7) Martinez, A. W.; Phillips, S. T.; Carrilho, E.; Thomas, S. W.; Sindi, H.; Whitesides, G. M. *Analytical Chemistry* **2008**, *80*, 3699-3707.
- (8) Hu, J.; Wang, S. Q.; Wang, L.; Li, F.; Pingguan-Murphy, B.; Lu, T. J.; Xu, F. *Biosensors and Bioelectronics* **2014**, *54*, 585-597.
- (9) Zhang, Y.; Gao, D.; Fan, J.; Nie, J.; Le, S.; Zhu, W.; Yang, J.; Li, J. *Biosensors and Bioelectronics* **2016**, *78*, 538-546.
- (10) Wei, X.; Tian, T.; Jia, S.; Zhu, Z.; Ma, Y.; Sun, J.; Lin, Z.; Yang, C. J. *Analytical Chemistry* **2016**, *88*, 2345-2352.
- (11) Yang, Y.; Noviana, E.; Nguyen, M. P.; Geiss, B. J.; Dandy, D. S.; Henry, C. S. *Analytical Chemistry* **2016**, *89*, 71-91.
- (12) Zang, D.; Ge, L.; Yan, M.; Song, X.; Yu, J. *Chemical Communications* **2012**, *48*, 4683-4685.
- (13) Lu, J.; Ge, S.; Ge, L.; Yan, M.; Yu, J. *Electrochimica Acta* **2012**, *80*, 334-341.
- (14) Nemiroski, A.; Christodouleas, D. C.; Hennek, J. W.; Kumar, A. A.; Maxwell, E. J.; Fernández-Abedul, M. T.; Whitesides, G. M. *Proceedings of the National Academy of Sciences of the United States of America* **2014**, *111*, 11984-11989.
- (15) Zhao, C.; Thuo, M. M.; Liu, X. *Science and Technology of Advanced Materials* **2013**, *14*, 54402-54402.
- (16) Mettakoonpitak, J.; Boehle, K.; Nantaphol, S.; Teengam, P.; Adkins, J. A.; Srisa-Art, M.; Henry, C. S. *Electroanalysis* **2016**, *28*, 1420-1436.
- (17) Nie, Z.; Nijhuis, C. A.; Gong, J.; Chen, X.; Kumachev, A.; Martinez, A. W.; Narovlyansky, M.; Whitesides, G. M. *Lab on A Chip* **2010**, *10*, 477-483.
- (18) McCreery, R. L. *Chemical Reviews* **2008**, *108*, 2646-2687.
- (19) Macpherson, J. V. *Physical Chemistry Chemical Physics* **2015**, *17*, 2935-2949.
- (20) Adams, R. N. *Analytical Chemistry* **1958**, *30*, 1576-1576.
- (21) Wang, J.; Naser, N. *Analytica Chimica Acta* **1995**, *316*, 253-259.
- (22) Wang, J.; Musameh, M. *Analytical chemistry* **2003**, *75*, 2075-2079.
- (23) Liu, H.; He, P.; Li, Z.; Sun, C.; Shi, L.; Liu, Y.; Zhu, G.; Li, J. *Electrochemistry Communications* **2005**, *7*, 1357-1363.
- (24) Klunder, K. J.; Nilsson, Z.; Sambur, J. B.; Henry, C. S. *Journal of the American Chemical Society* **2017**, *139*, 12623-12631.
- (25) Zhong, S.; Kazacos, M.; Burford, R. P.; Skyllas-Kazacos, M. *Journal of Power Sources* **1991**, *36*, 29-43.
- (26) McLaren, K. G.; Batley, G. E. *Journal of Electroanalytical Chemistry and Interfacial Electrochemistry* **1977**, *79*, 169-178.
- (27) Yao, X.; Wu, H.; Wang, J.; Qu, S.; Chen, G. *Chemistry - A European Journal* **2007**, *13*, 846-853.
- (28) Perween, M.; Parmar, D. B.; Bhadu, G. R.; Srivastava, D. N. *Analyst* **2014**, *139*, 5919-5926.
- (29) Nunes, P. S.; Ohlsson, P. D.; Ordeig, O.; Kutter, J. P. *Microfluidics and nanofluidics* **2010**, *9*, 145-161.
- (30) Goluch, E. D.; Wolfrum, B.; Singh, P. S.; Zevenbergen, M. A. G.; Lemay, S. G. *Analytical and Bioanalytical Chemistry* **2009**, *394*, 447-456.

- (31) Lee, G.-Y.; Park, J.-H.; Chang, Y. W.; Cho, S.; Kang, M.-J.; Pyun, J.-C. *ACS Aensors* **2018**, *3*, 106-112.
- (32) Gartia, M. R.; Misra, S. K.; Ye, M.; Schwartz-Duval, A.; Plucinski, L.; Zhou, X.; Kellner, D.; Labriola, L. T.; Pan, D. *Scientific Reports* **2015**, *5*, 16011.
- (33) Zhang, J.; Huang, L.; Lin, Y.; Chen, L.; Zeng, Z.; Shen, L.; Chen, Q.; Shi, W. *Applied Physics Letters* **2015**, *106*, 1-5.
- (34) Yamamoto, S.; Uno, S. *Sensors* **2018**, *18*, 730.
- (35) Mendez, S.; Fenton, E. M.; Gallegos, G. R.; Petsev, D. N.; Sibbett, S. S.; Stone, H. A.; Zhang, Y.; López, G. P. *Langmuir* **2010**, *26*, 1380-1385.
- (36) Adkins, J. A.; Noviana, E.; Henry, C. S. *Analytical Chemistry* **2016**, *88*, 10639-10647.
- (37) Lemay, S. G.; van den Broek, D. M.; Storm, A. J.; Krapf, D.; Smeets, R. M.; Heering, H. A.; Dekker, C. *Analytical Chemistry* **2005**, *77*, 1911-1915.
- (38) Lanyon, Y. H.; De Marzi, G.; Watson, Y. E.; Quinn, A. J.; Gleeson, J. P.; Redmond, G.; Arrigan, D. W. *Analytical Chemistry* **2007**, *79*, 3048-3055.
- (39) Sun, W.; Guo, C. X.; Zhu, Z.; Li, C. M. *Electrochemistry Communications* **2009**, *11*, 2105-2108.
- (40) Yoshida Kozai, T. D.; Langhals, N. B.; Patel, P. R.; Deng, X.; Zhang, H.; Smith, K. L.; Lahann, J.; Kotov, N. A.; Kipke, D. R. *Nature Materials* **2012**, *11*, 1065-1073.
- (41) Taylor, J. B.; Carrano, A. L.; Kandlikar, S. G. *International Journal of Thermal Sciences* **2006**, *45*, 962-968.
- (42) Li, Z.; Wang, Y.; Kozbial, A.; Shenoy, G.; Zhou, F.; McGinley, R.; Ireland, P.; Morganstein, B.; Kunkel, A.; Surwade, S. P.; Li, L.; Liu, H. *Nature Materials* **2013**, *12*, 925-931.
- (43) Lamonte, R. R.; McNally, D. *Advanced Materials and Processes* **2001**, *159*, 33-36.
- (44) Randviir, E. P.; Brownson, D. A. C.; Metters, J. P.; Kadara, R. O.; Banks, C. E. *Physical Chemistry Chemical Physics* **2014**, *16*, 4598-4598.
- (45) Ambrosi, A.; Chua, C. K.; Khezri, B.; Sofer, Z.; Webster, R. D.; Pumera, M. *Proceedings of the National Academy of Sciences* **2012**, *109*, 12899-12904.
- (46) Masa, J.; Zhao, A.; Xia, W.; Sun, Z.; Mei, B.; Muhler, M.; Schuhmann, W. *Electrochemistry Communications* **2013**, *34*, 113-116.
- (47) Nicholson, R. S. *Analytical Chemistry* **1965**, *37*, 1351-1355.
- (48) Rice, M. E.; Galus, Z.; Adams, R. N. *Journal of Electroanalytical Chemistry and Interfacial Electrochemistry* **1983**, *143*, 89-102.
- (49) Patel, A. N.; Tan, S. Y.; Miller, T. S.; MacPherson, J. V.; Unwin, P. R. *Analytical Chemistry* **2013**, *85*, 11755-11764.
- (50) Washburn, E. W. *Physical Review* **1921**, *17*, 273-283.
- (51) Lankelma, J.; Nie, Z.; Carrilho, E.; Whitesides, G. M. *Analytical Chemistry* **2012**, *84*, 4147-4152.
- (52) Dossi, N.; Toniolo, R.; Pizzariello, A.; Impellizzieri, F.; Piccin, E.; Bontempelli, G. *Electrophoresis* **2013**, *34*, 2085-2091.
- (53) Channon, R. B.; Nguyen, M.; Scorzelli, A.; Henry, E.; Volckens, J.; Dandy, D.; Henry, C. *Lab on A Chip* **2018**, *18*, 793-802.
- (54) Camplisson, C. K.; Schilling, K. M.; Pedrotti, W. L.; Stone, H. A.; Martinez, A. W. *Lab on A Chip* **2015**, *15*, 4461-4466.
- (55) Amatore, C.; Da Mota, N.; Lemmer, C.; Pebay, C.; Sella, C.; Thouin, L. *Analytical Chemistry* **2008**, *80*, 9483-9490.
- (56) Renault, C.; Anderson, M. J.; Crooks, R. M. *Journal of the American Chemical Society* **2014**, *136*, 4616-4623.
- (57) Snowden, M. E.; Unwin, P. R.; MacPherson, J. V. *Electrochemistry Communications* **2011**, *13*, 186-189.
- (58) Santhiago, M.; Wydallis, J. B.; Kubota, L. T.; Henry, C. S. *Analytical Chemistry* **2013**, *85*, 5233-5239.
- (59) Bjorefors, F.; Strandman, C.; Nyholm, L. *Electroanalysis* **2000**, *12*, 255-261.

(60) Niwa, O.; Xu, Y.; Halsall, H. B.; Heineman, W. R. *Analytical Chemistry* **1993**, *65*, 1559-1563.

## CHAPTER 4: PAPER-BASED NUCLEASE PROTECTION ASSAY FOR NUCLEIC ACID DETECTION

### Chapter Overview

Pathogen detection is crucial for human, animal, and environmental health. Conventional techniques such as culture-based methods have long turnaround times and lack sensitivity. Nucleic acid amplification tests offer high specificity and sensitivity. However, their cost and complexity remain a significant hurdle to their applications in resource-limited settings. Herein, a paper-based nuclease protection assay (PB-NPA) that can be implemented in field settings is described. The NPA is a nucleic acid hybridization-based technique that does not rely on amplification. In NPA, the hybridization of an antisense probe to the target sequence is followed by single-strand nuclease digestion. The protected double-stranded target-probe hybrids are then captured on a lateral flow device, followed by the addition of a colorimetric enzyme-substrate pair for signal visualization. The nuclease digestion of non-target and mismatched DNA provides high specificity while signal amplification with the reporter enzyme-substrate provides high sensitivity. An on-chip sample pretreatment step utilizing chitosan-modified paper has also been developed to eliminate possible interferents from the reaction and preconcentrate nucleic acids, thereby significantly reducing the need for auxiliary equipment. This work has been published in *Analytical and Bioanalytical Chemistry* as a featured article.<sup>1</sup> Sidhartha Jain (co-1<sup>st</sup> author) contributed to the published work by optimizing the chitosan-based sample pretreatment (optimization data are not shown here) and tested the pretreatment on the PB-NPA. Josephine Hofstetter provided antibody-stripped nitrocellulose strips, suggestions during experiments, and assistance in manuscript writing.

### Introduction

Point-of-need pathogen detection has wide ranging applications in medical diagnostics,<sup>2</sup> food and water safety,<sup>3</sup> agriculture,<sup>4</sup> environmental monitoring,<sup>5</sup> biosafety,<sup>6</sup> and epidemiology.<sup>7</sup> Conventional culture-based methods widely employed in pathogen detection can take days to weeks, have high detection

limits (300-3000 colony-forming units (CFU) per mL) and a prevalence of false-negatives.<sup>2</sup> Moreover, many pathogens cannot be cultured using standard methods or require high-containment culture facilities.<sup>8</sup> Molecular diagnostic methods such nucleic-acid amplifications tests (NAATs) have become very common for pathogen detection in clinical and research labs across the developed world. NAATs include polymerase chain reaction (PCR) and isothermal amplification techniques, both of which are known to offer high sensitivity (~3 CFU/mL) from the exponential amplification of the target of interest. However, PCR is performed at a different temperature requiring a thermocycler which adds significant cost and limits portability. To simplify instrumentation needs, isothermal amplification techniques such as loop-mediated isothermal amplification (LAMP),<sup>9,10</sup> template-mediated amplification (TMA),<sup>11</sup> helicase-dependent amplification (HDA),<sup>12</sup> and rolling circle amplification (RCA)<sup>13</sup> have been used for nucleic-acid analysis. These techniques, however, still require several distinct primers for amplification, significant laboratory infrastructure, and highly trained personnel. In addition, NAATs can produce false negative results due to the presence of inhibitors in complex samples and therefore require extensive sample preparation steps.<sup>14</sup>

Nuclease protection assays (NPAs) have been in used in RNA mapping and determining gene transcription levels for decades.<sup>15</sup> Unlike NAATs, NPAs do not require nucleic acid amplification, which reduces assay time, cost, and complexity. Traditional NPAs involve hybridizing a labeled probe complementary to the target sequence followed by digestion of unhybridized and non-target nucleic acids using a nuclease which selectively cleaves single-stranded oligomers. Thus, only perfectly matched probe-target hybrids remain intact and can be detected using colorimetric or radiological methods.<sup>15-18</sup> NPAs have been integrated with sandwich hybridization (NPA-SH) to detect harmful algae in aqueous samples.<sup>16-19</sup> More recently, a nuclease protection enzyme-linked immunosorbent assay (NP-ELISA) method has also been developed for the detection of Zika and Kunjin virus sequences with colorimetric, chemiluminescent and electrochemical detection motifs.<sup>15</sup> However, these NPA strategies require external readers which are sometimes expensive and not accessible in resource-limited settings.

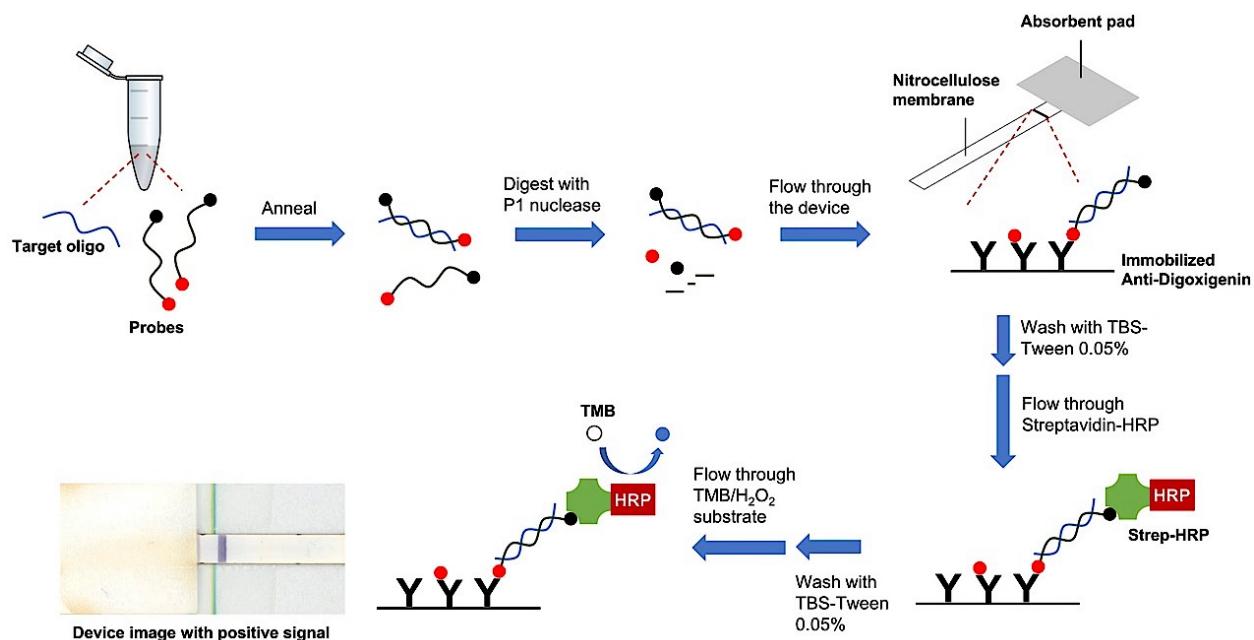


**Figure 4.1:** Schematic representation of paper-based Nuclease Protection Assay

Lateral Flow Assays (LFAs) are frequently used in point-of-care diagnostics, the most ubiquitous of which are the over-the-counter pregnancy tests. LFAs have also been used in direct and indirect detection of pathogens such as *Plasmodium falciparum*<sup>20</sup> and proteins such as Diphtheria Toxin.<sup>21</sup> LFAs can significantly reduce the need for instrumentation and provide user-friendly result readouts, typically with the appearance of a test line when the target is present. This easy-to-read platform offers value as an end-point detection method and has been paired with PCR<sup>22</sup> and isothermal amplification reactions<sup>23-25</sup> to create low-cost nucleic acid sensors. The development of paper-based nuclease protection assay (PB-NPA) for the rapid detection of nucleic acids at the point-of-need is demonstrated here (Figure 4.1). The assay involves hybridization of a 5'-digoxigenin and 3'-biotin-labeled oligonucleotide probe to the target, followed by digestion with P1 nuclease to cleave unhybridized probe, target, and other single-stranded non-target DNA. The protected probe-target hybrids are captured using an anti-digoxigenin antibody immobilized on nitrocellulose membrane and visualized with streptavidin-conjugated horseradish peroxidase (Strep-HRP) and a colorimetric substrate solution (tetramethylbenzidine (TMB) and hydrogen

peroxide). A blue line appears in the detection region to indicate the presence of the target DNA. The use of a reporter enzyme allows for signal amplification from the captured protected probes, providing a sensitive method for detection without performing complex nucleic acid amplification reactions. The assay provides simple yes/no readout with the appearance of a test line when the target sequence is present in the sample above the detectable limit. The assay combines the high specificity of the NPA with the user-friendly lateral flow strip platform for end-point detection.

## Experimental Section

### *Chemicals and materials*

**Table 1.** NPA probe and DNA sequences

Sequence Name	DNA Sequences
NPA Probe	5'biotin/GTGATTGACGATGGGGCCCAA/3'digoxigenin
Complementary Target	5'/TTGGGCCCCATCGTCAATCAC/3'
1-base mismatch	5'/TTGGGTCCCATCGTCAATCAC/3'
2-base mismatch	5'/TTGGGTCCCATGGTCAATCAC/3'
3-base mismatch	5'/TTTGGTCCCATGGTCAATCAC/3'
4-base mismatch	5'/TTTGGTCCCATGGTCAAACAC/3'

Nitrocellulose FF120HP A4-sized sheets, Whatman Grade 1 filter paper and Whatman Grade 4 filter paper were purchased from GE Healthcare (Illinois, USA). Anti-digoxigenin monoclonal antibody was purchased from Abcam (Massachusetts, USA). Trehalose dihydrate and formamide were purchased from EMD Millipore (Massachusetts, USA). StabilGuard® Immunoassay Stabilizer (BSA-free) was purchased from Surmodics, Inc. (Minnesota, USA). P1 Nuclease (from *P. citrinum*) and 10X P1 nuclease reaction buffer were purchased from New England Biolabs, Inc. (Massachusetts, USA). Glycerol was purchased from Mallinkrodt (Staines-upon-Thames, UK). Piperazine-N,N'-bis(2-ethanesulfonic acid) (PIPES), sodium chloride, ethylenediaminetetraacetic disodium salt acid, 2-(N-morpholino)ethanesulfonic acid hydrate (MES), Tris(hydroxymethyl)aminomethane (Tris), Tween® 20 and chitosan oligosaccharide lactate (average  $M_n$  5,000) were purchased from Sigma-Aldrich, Inc. (Missouri, USA). Streptavidin conjugated to horseradish peroxidase (Strep-HRP) was purchased from R&D Systems, Inc. (Minnesota, USA). Pierce™ 1-Step Ultra TMB-Blotting Solution™ was purchased from Thermo Scientific

(Massachusetts, USA). Table 1 gives the NPA probe and DNA oligonucleotide sequences used in the study; all DNA sequences were ordered from Integrated DNA Technologies, Inc. (Iowa, USA).

### ***Device fabrication***

A 100  $\mu\text{L}$  anti-digoxigenin Ab solution (1 mg/mL) was mixed with 2.5  $\mu\text{L}$  of 2 M trehalose and 10  $\mu\text{L}$  of 50% glycerol. The solution was then striped twice onto a nitrocellulose (NC) membrane at 0.036  $\mu\text{L}/\text{mm}$  deposition rate using an Automated Lateral Flow Reagent Dispenser (ALFRD)<sup>TM</sup> from ClaremontBio (California, USA) equipped with a syringe pump (1.5  $\mu\text{L}/\text{s}$  flow rate; 41 mm/s striping rate). The membrane was let dry at 37°C for 1 h. To block the surface of the NC membrane from non-specific binding, StabilGuard® Immunoassay Stabilizer solution was added to fully wet the membrane. The membrane was then air dried at room temperature for 30 min. After that, the membrane can be immediately used to fabricate devices or stored in a closed container for later use.

To construct the device, the Ab-striped NC membrane was cut using a Zing CO<sub>2</sub> laser cutter from Epilog (Colorado, USA) to create 20 mm x 4 mm strips with the deposited antibody located 5 mm from one edge of the strip (i.e. downstream edge). The NC strip was placed on a transparency sheet (as a backing material) using double-sided adhesive. Two pieces of 20 mm x 15 mm laser cut Whatman No. 4 filter paper were stacked together and placed on the downstream edge of the NC strip using a tape such that there was 2 to 3 mm overlapping region between the materials. The Whatman grade 4 qualitative filter paper was used as an absorbent pad.

### ***Paper-based nuclease protection assay***

Nuclease protection assays were performed based on a protocol described by Filer et al.<sup>15</sup> with some modifications. For a triplicate experiment, 3  $\mu\text{L}$  probe oligo solution was mixed with 3  $\mu\text{L}$  target oligo solution, 2.4  $\mu\text{L}$  10X hybridization buffer (0.4 M PIPES pH 6.8, 4 M NaCl, 0.02 M EDTA) and 15.6  $\mu\text{L}$  DI water in a tube. Formamide was added at 0-80% total concentrations by reducing the volume of DI water to accommodate the volume of formamide added without changing the total volume of the solution. The solution was then heated at 95°C for 2 min and at 53°C for 10 min. The solution was subsequently placed

in ice bath and a 6  $\mu\text{L}$  mixture of P1 nuclease 1 U/ $\mu\text{L}$ -10X P1 buffer (1:1 v/v) was added to the solution. To start digestion, the solution was incubated in a water bath at 37°C for the indicated time. A 10  $\mu\text{L}$  aliquot from nuclease digestion was flowed through the device, followed by an addition of 10  $\mu\text{L}$  TBS-Tween 0.05% wash buffer pH 8.6. The following solutions: 10  $\mu\text{L}$  Streptavidin-HRP (1:200 diluted), 10  $\mu\text{L}$  TBS-Tween 0.05% wash buffer, and 2x 10  $\mu\text{L}$  TMB/H<sub>2</sub>O<sub>2</sub> substrate solution were then added subsequently to develop the colorimetric signal.

### ***On-chip sample pretreatment using chitosan-modified paper***

Wax-patterned filter paper was modified with 2  $\mu\text{L}$  of 1% w/v chitosan oligosaccharide lactate prepared in MES buffer pH 5.0, this layer is referred to as the 'chitosan layer'. The chitosan layer was cut and affixed to a laser cut polymethyl methacrylate (PMMA) support layer. Upon completion of the P1 nuclease digestion step, 10  $\mu\text{L}$  each of the sample was applied to the chitosan layer while in contact with an absorbent pad. The chitosan layer was washed in this position with 40  $\mu\text{L}$  of 100 mM MES buffer pH 5.0 to remove the interfering compounds from the sample while retaining DNA from the sample. The membrane was then moved to the lateral flow strip and the DNA retained in the membrane was eluted on the lateral flow strip using three 10  $\mu\text{L}$  volumes of Tris buffer pH 8.6. The sample pretreatment setup was then removed from the lateral flow strip and 10  $\mu\text{L}$  of Tris buffer + 0.05% Tween<sup>®</sup> 20 was applied to the inlet followed by the remaining chromogenic components (Strep-HRP, Tris buffer + 0.05% Tween<sup>®</sup> 20, and the TMB blotting solution).

### ***Image analysis***

After color development, the strips were allowed to dry briefly to enhance the color contrast. These devices were then scanned using a V600 Epson scanner. The resulting image was inverted, and the detection region mean intensity was quantified using ImageJ 1.05i image processing software (open-source software, National Institutes of Health).

## Results and Discussion

### *Nucleic acid detection*

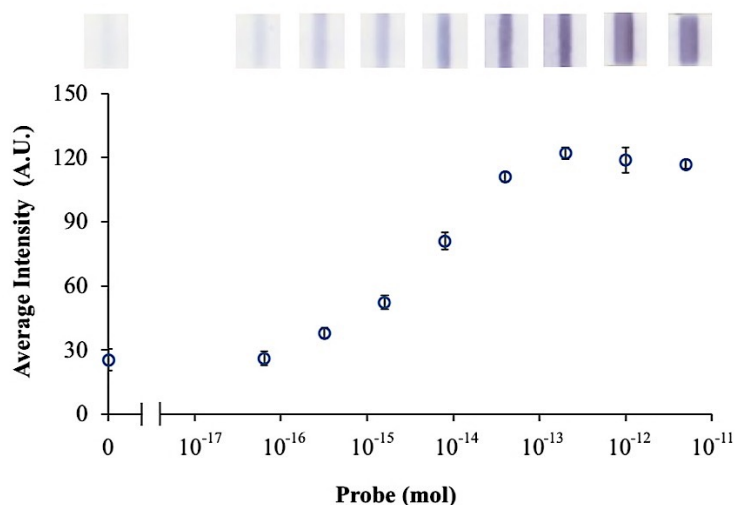


**Figure 4.2:** Dose response of varying amounts of digoxigenin/biotin-labeled oligo probes. Error bars indicate standard deviations ( $n = 4$  devices).

Colorimetric detection in the lateral flow devices was based on enzymatic conversion of TMB by HRP in the presence of  $H_2O_2$ . The use of reporter enzyme allowed for signal amplification to improve detection sensitivity. The binding of digoxigenin/biotin-labeled oligo probe to the capture antibody allowed for accumulation of streptavidin-HRP on the binding sites and subsequent color formation. To assess detection limit of this detection scheme, a series of solutions with varying probe quantities were tested on the flow devices. Colorimetric responses obtained from 64 amol to 5.0 pmol oligo probe are shown in Figure 4.2. The colorimetric signal reached a plateau at around 200 fmol of probe and the detection limit (i.e. mean intensity of blank sample + 3x standard deviation) was approximately 0.57 fmol ( $5.7 \times 10^{-16}$  mol).

### *Nuclease protection assay (NPA)*

Hybridization between the probes and the target oligos and nuclease digestion of the unhybridized oligos are the two major steps in NPA. For nucleic acid hybridization, stringency/specificity can be manipulated by controlling three parameters: temperature, salt concentration and formamide concentration.<sup>26,27</sup> Although cross reaction among related based sequences can be reduced at higher

temperature in aqueous solution, conditions required for specificity are much more easily adjusted by varying ionic strength and formamide concentration.<sup>28</sup> Thus, to optimize hybridization condition for the NPA, formamide concentrations were varied in the presence of 400 mM sodium salt.

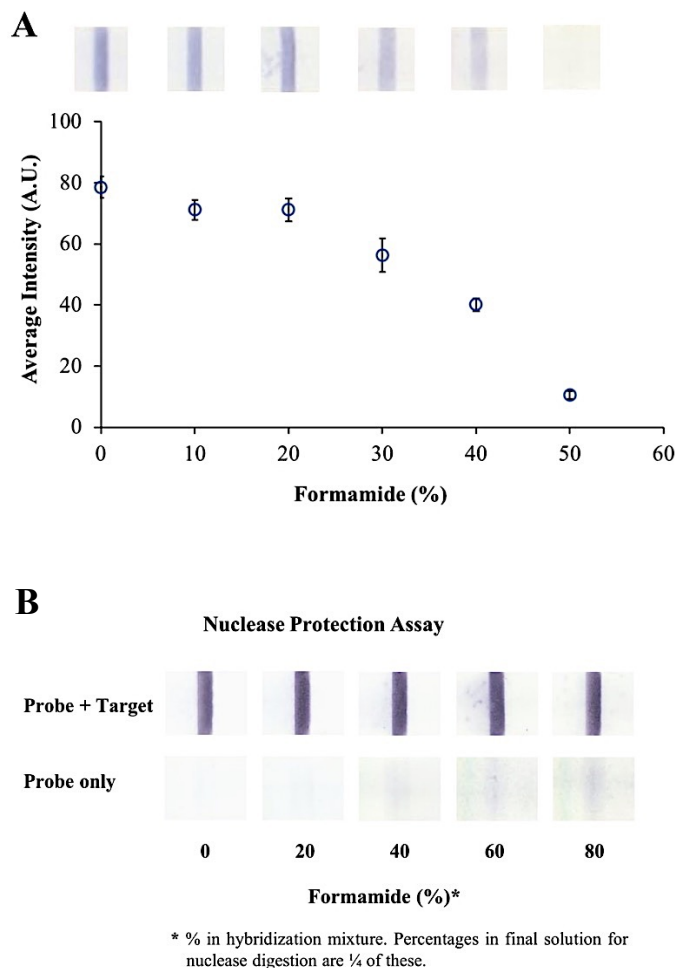


**Figure 4.3:** Effect of formamide concentration on : **(A)** The detection of labeled probe in lateral flow devices and **(B)** nuclease protection assay.

Prior to performing NPA in solutions containing formamide, the effect of formamide on the binding of labeled probes to the detection elements in the lateral flow devices was assessed. This step is important to help distinguish the influence of formamide in different aspects of the PB-NPA including hybridization, nuclease digestion and detection in the flow devices. Formamide concentrations above 20% reduced binding between the probes and the capture antibodies as shown by linear decrease in colorimetric signal

at formamide concentrations ranging from 20-50% (Figure 4.3A). While antigen-antibody binding activity was reported to increase in the presence of several organic-water miscible solvents such as ethanol and methanol,<sup>29</sup> formamide and similar solvents have been shown to disrupt antigen-antibody binding<sup>29,30</sup> potentially by inducing conformation change of the antibodies or lowering the binding affinity by solvating either or both antigen-labeled oligo probes and capture antibodies. Therefore, dilution of test solution to formamide concentrations equal to 20% or lower was required prior to testing using the lateral flow devices.

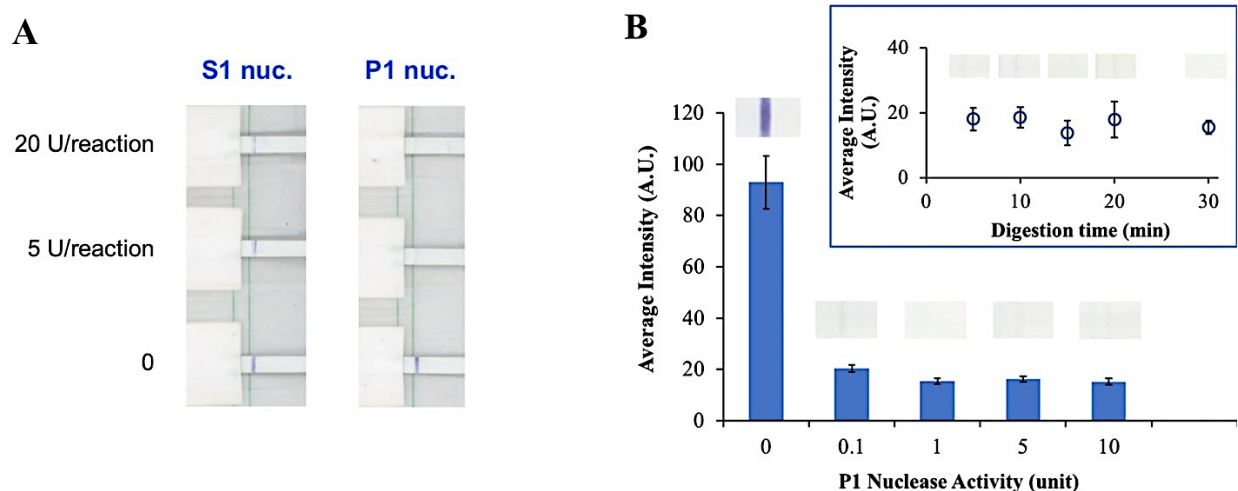


**Figure 4.4:** Optimization of nuclease digestion. **(A)** Comparison between S1 and P1 nuclease activity in degrading 10 pmol single-stranded oligo probe at 37°C for 30 min. **(B)** Effect of P1 nuclease quantity/activity and digestion time (right top inset) in degrading 10 pmol oligo probe. Digestion was carried out for 30 min in experiment shown in the main graph. Error bars indicate standard deviations ( $n = 4$  devices)

The use of a single-strand-specific nuclease is crucial to remove unhybridized labeled probes from the test solution such that any detected signal is only dependent on the quantity of the protected target-probe duplexes. Although more than 30 single-strand-specific nucleases have been identified from various sources, only a few enzymes including S1 nuclease and P1 nuclease have been characterized to a significant extent.<sup>31</sup> S1 nuclease is often employed in NPA<sup>15,32,33</sup> due to the well-characterized nature of the enzyme and high selectivity toward single-stranded DNA in the presence of double-stranded DNA.<sup>31</sup> However, it was later found from the experiment that the catalytic activity of P1 nuclease in digesting the labeled oligo

probes is higher than S1 nuclease, as shown in Figure 4.4A. P1 nuclease was thus selected for the NPA protocol. To optimize digestion conditions, the amount of P1 nuclease and digestion times were varied in the presence of 10 pmol probes and incubation at 37°C. As shown in Figure 4.4B, significant depletion of colorimetric signal was obtained by using 0.1 U P1 nuclease in a 10 µL solution as compared to control experiment in the absence of nuclease. The background signal was further reduced by increasing nuclease activity to 1 U/10 µL, however, no more discernable reduction of signal was observed at higher nuclease activities. The probes were then digested using 1 U P1 nuclease with digestion time varied from 5 to 30 min. No significant difference was observed in measured colorimetric signals from probes digested for 5 to 30 min (Figure 4.4B inset) and thus, digestion with 1 U P1 nuclease for 5 min at 37°C was selected for the NPA.

Formamide is commonly used during hybridization in NPA to increase hybridization stringency. The effect of formamide concentrations on the NPA is shown in Figure 4.3B. No visible difference in colorimetric signals was observed at 0-80% formamide used in hybridization mixtures, suggesting that formamide neither interferes nor improves duplex formation within the experimental conditions described in the method section. However, increased concentration of formamide did affect the P1 nuclease activity in degrading unhybridized probes. Background signals were observed at 10-20% formamide concentrations in digestion mixtures (equivalent to 40-80% formamide concentration in hybridization mixtures due to 1:4 dilution of solution prior to nuclease digestion). Since no signal improvement was obtained by incorporating formamide into the hybridization mixture and the organic solvent has shown some detrimental effects to nuclease digestion and probe binding to the capture antibody, formamide was omitted from the PB-NPA protocol.

Figure 4.5 shows the intensities of colorimetric signal as a function of target oligo quantities in PB-NPA using the optimized protocol. Similar to the probe dose-response shown in Figure 4.2, NPA with target sequence complementary to the probe also reached saturation at approximately 200 fmol of target oligo, suggesting that the hybridization between target oligo and the probe is highly efficient. The background

signal in NPA with target oligo was lower than that in probe only detection, potentially due to the change in pH and ionic strength in assay buffer from addition of P1 buffer to the hybridization buffer that was used solely in probe detection. This lower background signal gave slightly improved detection limit for PB-NPA, which was approximately 0.24 fmol ( $2.4 \times 10^{-16}$  mol).

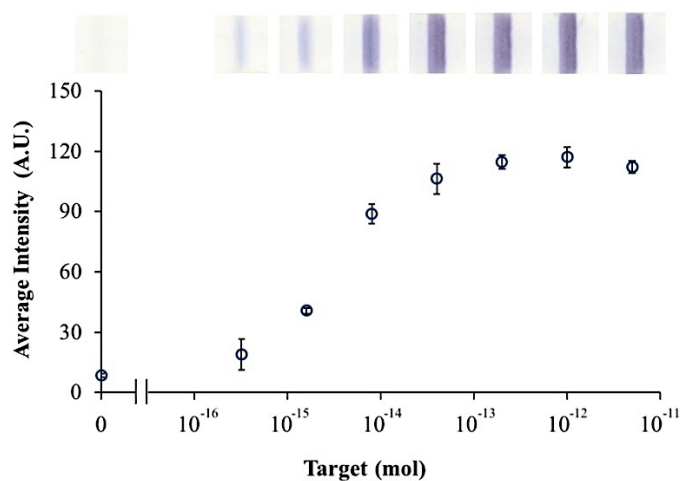


**Figure 4.5:** Dose response of varying amounts of target complementary oligos. Error bars indicate standard deviations ( $n = 4$  devices).

### *Assay specificity*

To investigate the specificity of PB-NPA, target oligos with 1, 2, 3, or 4 base mismatches were designed and tested at 1 to 1 ratio and 125:1 ratio to the quantity of the probes. A completely random sequence was also tested at similar ratios. The results are shown in Figure 4.6A. Significant reduction of signal was observed for the 1 base mismatch compared to that in complementary oligo, indicating sequence selectivity within the assay. However, the considerably high colorimetric responses obtained in various mismatch sequences (in comparison to the baseline level signal obtained from the random sequence) suggested the formation of duplexes or secondary structures between the probe and the mismatch oligos that P1 nuclease was not able to degrade. Increasing quantity of either mismatch or random oligo relative to probe quantity did not affect the observed signals. Single-base mismatches are the least accessible to the single-strand specific nucleases because they present the smallest region for enzyme binding.<sup>34</sup> This

difficulty in accessing single-strand binding sites is possibly the reason why considerable amounts of signal were obtained in all mismatch oligo tested by PB-NPA. Although 4 bases were non-complementary in the 4 bases mismatch oligo, the location of mismatched bases was designed to be single-base mismatch at 4 different locations within the sequence, posing the same difficulty for the nuclease to bind.

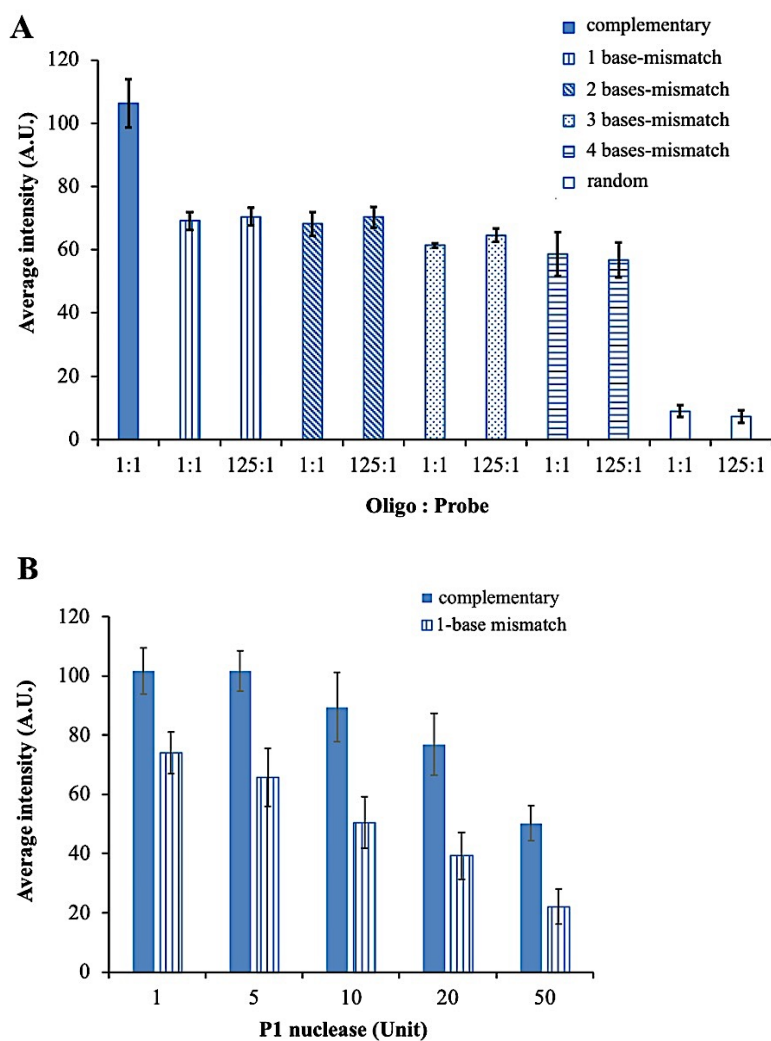


**Figure 4.6:** (A) Colorimetric signals for NPA with complementary, mismatch and random sequences. 1 U P1 nuclease was used for the digestion. Error bars indicate standard deviations (n = 4 devices). (B) NPA signal for complementary and 1-base mismatch at different activities of P1 nuclease. Error bars indicate standard deviations (n = 3 devices)

Increasing the amount of P1 nuclease reduced colorimetric responses from 1 base mismatch oligo (Figure 4.6B). However, the increased nuclease activity also decreased colorimetric signals in complementary oligo, suggesting that P1 nuclease also degrades double-strand DNA at high concentrations. Nevertheless, the signal-to-noise ratio (i.e. ratio of colorimetric signal from complementary oligo to that of 1-base mismatch) was improved by increasing the amount of P1 nuclease from 1 U (S/N = 1.4) to 50 U (S/N = 2.2) despite the lower sensitivity.

#### *Sample pretreatment with chitosan-modified paper*

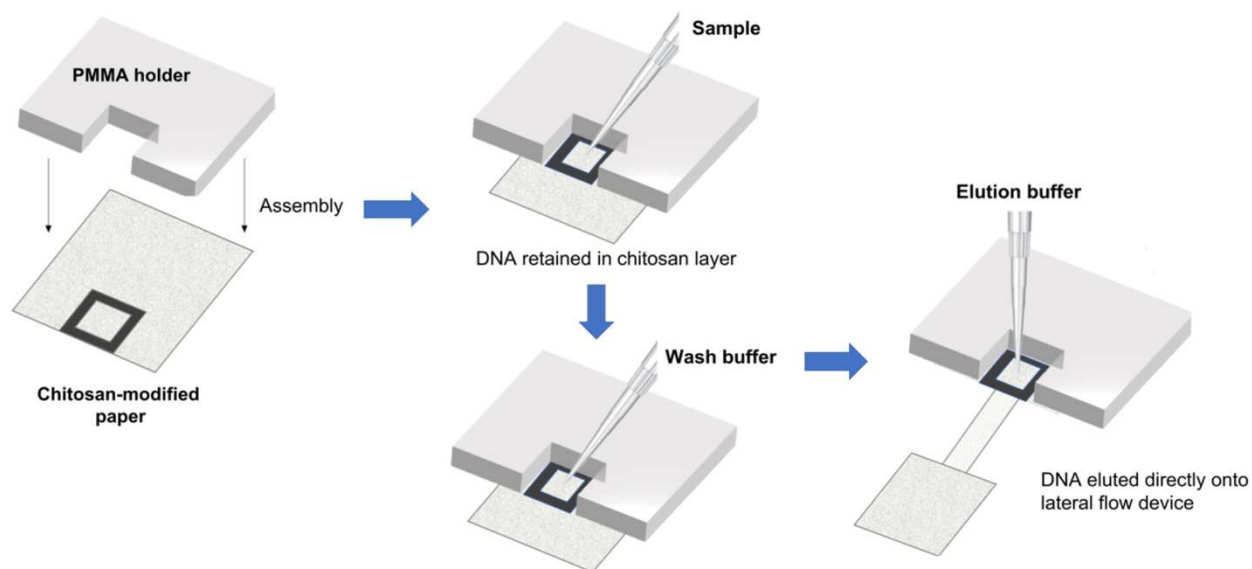


**Figure 4.7:** On-chip sample pretreatment device made of chitosan-modified filter paper affixed to a PMMA template: DNA from nuclease digested samples is captured in the chitosan layer at an acidic pH (pH ~5). The chitosan layer is then washed with a wash buffer (MES pH 5.0), followed by elution of the DNA directly onto the lateral flow device using an alkaline pH buffer (Tris pH 8.6).

In conventional NPA, extensive sample preparation steps are needed in order to perform detection using colorimetric or radiological methods. These steps include inactivation of nuclease enzymes, centrifugation to remove free-label resulting from nuclease digestion and precipitation of protected probe-target hybrids for detection. In the PB-NPA, on-chip sample pretreatment was performed utilizing chitosan-modified filter paper. Chitosan (pKa ~6.4) is a polycationic polymer that exhibits a pH-dependent affinity

for the negatively charged backbone of nucleic acids.<sup>35</sup> This pH-dependent nucleic acid affinity exhibited by chitosan has been exploited to create nanoparticle carriers in gene therapy delivery systems<sup>36,37</sup> and to preconcentrate nucleic acid for point-of-care applications.<sup>38,39</sup> A simple vertical flow device was created using 1% chitosan-modified filter paper affixed to a PMMA support layer (Figure 4.7). This sample pretreatment device was integrated to the PB-NPA to pretreat nuclease-digested samples and remove digoxigenin and other potential interferents from the reaction. Nuclease digested samples were flowed through the chitosan-modified filter paper, the nucleic acids from the sample are retained in the chitosan layer through electrostatic interaction while interfering compounds are washed to the absorbent waste pad. The captured DNA in the chitosan layer can then be eluted directly on to the lateral flow strip for detection using an alkaline pH elution buffer (pH ~8.6). Wax printing provides a hydrophobic barrier and ensures that all sample flows through the chitosan deposition zone.

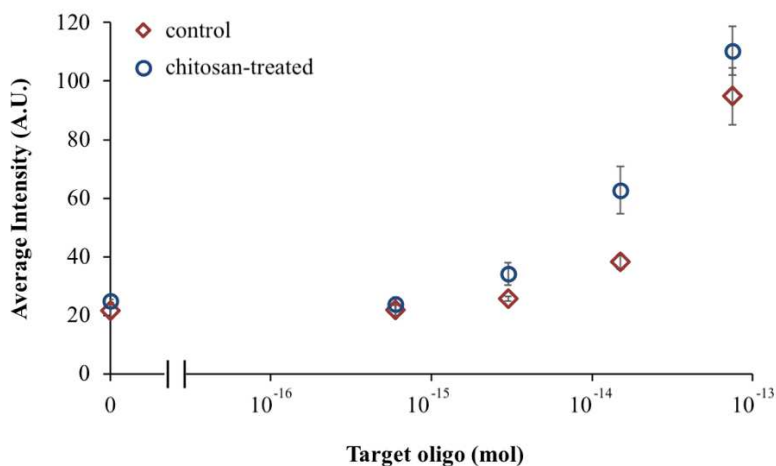


**Figure 4.8:** Colorimetric signals obtained for samples run with chitosan sample pretreatment (blue circle) and untreated controls (red diamond). Error bars indicate standard deviations ( $n = 3$  devices).

Nuclease protection assays were run with varying target oligo amounts and 200 fmol of the NPA probe and then the samples were pretreated using the on-chip sample pretreatment method described above (Figure 4.8). Controls were run in triplicates without sample pretreatment (i.e. samples were applied directly to the inlet of the lateral flow strip). Limit of detection was calculated using mean blank + 3.3 x standard

deviation. The limit of detection obtained for the control condition was  $5.34 \times 10^{-15}$  mol of target oligo DNA whereas with chitosan sample pretreatment, the LOD improved to  $1.16 \times 10^{-15}$  mol. The slope of the linear region (sensitivity) of the assay also improved using chitosan sample pretreatment (Avg. Intensity =  $23.6 \ln(\text{Target}) + 858$ ) compared to the control condition (Avg. Intensity =  $21.5 \ln(\text{Target}) + 737$ ). This on-chip pretreatment allowed for removal of free-label and other potential interferents from the reaction, improved the sensitivity and limit of detection of the PB-NPA, and eliminated the need for a nuclease enzyme inactivation step.

## Conclusions

These results demonstrate the proof-of-concept for the on-chip sample pretreatment capable lateral flow platform for end-point detection in nuclease protection assays. The PB-NPA can detect sub-femtomole of target DNA with high specificity. In addition, the vertical flow on-chip sample pretreatment using chitosan-modified paper eliminated the need for a nuclease inactivation step in the assay and further improved the detection limit by ~5 fold. The paper-based format allows for simplification of the assay compared to the traditional NPA including: (1) easy readout for minimally trained users based on the intensity of the colored lines, (2) lower reagent consumption and less waste generated, and (3) potentially improved assay time for point-of-care applications. The proposed assay only takes around 2-3 h to complete, which is substantially faster than the conventional culture-based method. The assay is also simpler to perform than conventional amplification-based nucleic acid tests, which often require amplification steps, multiple probes, enzymes, and expensive external readers.

While the current format of the assay still relies on multiple manual steps that take a few hours to complete, further optimization by lyophilizing the NPA components for hybridization and nuclease digestion in tubes and storing the detection reagents on the lateral flow strip can provide a rapid, simple, and easy-to-use assay with minimal user interaction. An inexpensive, portable resistive heater can be supplemented to the assay kits to allow for an easy and controlled assay at the point-of-care. To make the PB-NPA suitable for nucleic acid detection in real samples, sample preparation steps need to be

incorporated to the test platform. A lysis/extraction buffer can be provided and combined with the chitosan-based sample pretreatment for the extraction and purification of nucleic acid targets from the sample matrices. Depending on the characteristics of the nucleic acid targets (e.g. the lengths, types, origins, and required specificity), the assay components/steps can be adjusted to meet the detection requirement. For example, a longer probe can be used to improve the assay specificity while targeting a class of pathogens with similar, shared traits may benefit from using a shorter probe sequence. Simultaneous detection of multiple pathogens is also possible with the PB-NPA as probes with different labeling molecules and antibodies to the labels can be obtained from commercial vendors. Despite the higher detection limit compared to other conventional techniques including PCR, PB-NPA can serve a good screening tool for infections in which a high viral load is present in the biological samples such as nasopharyngeal fluids in patients with acute adenovirus infection and patients with chronic infection of hepatitis B virus.<sup>40,41</sup>

## REFERENCES

- (1) Noviana, E.; Jain, S.; Hofstetter, J.; Geiss, B. J.; Dandy, D. S.; Henry, C. S. *Analytical and Bioanalytical Chemistry* **2020**, 1-11.
- (2) Tran, N. K.; Wisner, D.; Albertson, T.; Cohen, S.; Greenhalgh, D.; Galante, J.; Phan, H.; Kost, G. J. *Point of Care* **2008**, 7, 107.
- (3) Vidic, J.; Vizzini, P.; Manzano, M.; Kavanaugh, D.; Ramarao, N.; Zivkovic, M.; Radonic, V.; Knezevic, N.; Giouroudi, I.; Gadjanski, I. *Sensors* **2019**, 19, 1100.
- (4) Neethirajan, S.; Kobayashi, I.; Nakajima, M.; Wu, D.; Nandagopal, S.; Lin, F. *Lab on A Chip* **2011**, 11, 1574-1586.
- (5) Koedrith, P.; Thasiphu, T.; Weon, J.-I.; Boonprasert, R.; Tuitemwong, K.; Tuitemwong, P. *The Scientific World Journal* **2015**, 2015.
- (6) McLeish, C.; Nightingale, P. *Research Policy* **2007**, 36, 1635-1654.
- (7) Woolhouse, M. E.; Haydon, D. T.; Antia, R. *Trends in Ecology and Evolution* **2005**, 20, 238-244.
- (8) Wade, W. *Journal of the Royal Society of Medicine* **2002**, 95, 81-83.
- (9) Rodriguez, N. M.; Wong, W. S.; Liu, L.; Dewar, R.; Klapperich, C. M. *Lab on A Chip* **2016**, 16, 753-763.
- (10) Connelly, J. T.; Rolland, J. P.; Whitesides, G. M. *Analytical Chemistry* **2015**, 87, 7595-7601.
- (11) Systems, B. D., 2013. *510(k) Summary BD ProbeTec™ Trichomonas Vaginalis (TV) Q<sup>x</sup> Amplified DNA Assay*, [https://www.accessdata.fda.gov/cdrh\\_docs/pdf13/K130268.pdf](https://www.accessdata.fda.gov/cdrh_docs/pdf13/K130268.pdf), Accessed on 10 November 2019.
- (12) Kim, H.-J.; Tong, Y.; Tang, W.; Quimson, L.; Cope, V. A.; Pan, X.; Motre, A.; Kong, R.; Hong, J.; Kohn, D. *Journal of Clinical Virology* **2011**, 50, 26-30.
- (13) Chang, C.-C.; Chen, C.-C.; Wei, S.-C.; Lu, H.-H.; Liang, Y.-H.; Lin, C.-W. *Sensors* **2012**, 12, 8319-8337.
- (14) Stults, J. R.; Snoeyenbos-West, O.; Methe, B.; Lovley, D. R.; Chandler, D. P. *Applied Environmental Microbiology* **2001**, 67, 2781-2789.
- (15) Filer, J. E.; Channon, R. B.; Henry, C. S.; Geiss, B. J. *Analytical Methods* **2019**, 11, 1027-1034.
- (16) Cai, Q.; Li, R.; Zhen, Y.; Mi, T.; Yu, Z. *Harmful Algae* **2006**, 5, 300-309.
- (17) Yu, Z.; Tiezhu, M.; Zhigang, Y. *Journal of Environmental Sciences* **2008**, 20, 1481-1486.
- (18) Zhen, Y.; Yu, Z.; Cai, Q.; Mi, T.; Li, R. *Hydrobiologia* **2007**, 575, 1-11.
- (19) Park, M.; Park, S. Y.; Hwang, J.; Jung, S. W.; Lee, J.; Chang, M.; Lee, T.-K. *Acta Oceanologica Sinica* **2018**, 37, 107-112.
- (20) Labbe, A.; Pillai, D.; Hongvathong, B.; Vanisaveth, V.; Pomphida, S.; Inkathone, S.; Hay Burgess, D.; Kain, K. *Annals of Tropical Medicine and Parasitology* **2001**, 95, 671-677.
- (21) Engler, K.; Efstratiou, A.; Norn, D.; Kozlov, R.; Selga, I.; Glushkevich, T.; Tam, M.; Melnikov, V.; Mazurova, I.; Kim, V. *Journal of Clinical Microbiology* **2002**, 40, 80-83.
- (22) Aveyard, J.; Mehrabi, M.; Cossins, A.; Braven, H.; Wilson, R. *Chemical Communications* **2007**, 4251-4253.
- (23) Cordray, M. S.; Richards-Kortum, R. R. *Malaria Journal* **2015**, 14, 472.
- (24) Jaroenram, W.; Kiatpathomchai, W.; Flegel, T. W. *Molecular and Cellular Probes* **2009**, 23, 65-70.
- (25) Kersting, S.; Rausch, V.; Bier, F. F.; von Nickisch-Rosenegk, M. *Malaria Journal* **2014**, 13, 99.
- (26) Bonner, J.; Kung, G.; Bekhor, I. *Biochemistry* **1967**, 6, 3650-3653.
- (27) Zhang, D. Y.; Chen, S. X.; Yin, P. *Nature Chemistry* **2012**, 4, 208.
- (28) McConaughy, B. L.; Laird, C.; McCarthy, B. J. *Biochemistry* **1969**, 8, 3289-3295.
- (29) Rehan, M.; Younus, H. *International Journal of Biological Macromolecules* **2006**, 38, 289-295.
- (30) Caruccio, L.; Byrne, K.; Procter, J.; Stroncek, D. *Vox Sanguinis* **2002**, 83, 63-69.
- (31) Desai, N. A.; Shankar, V. *FEMS Microbiology Reviews* **2003**, 26, 457-491.

- (32) Rimsza, L. M.; Wright, G.; Schwartz, M.; Chan, W. C.; Jaffe, E. S.; Gascoyne, R. D.; Campo, E.; Rosenwald, A.; Ott, G.; Cook, J. R. *Clinical Cancer Research* **2011**, *17*, 3727-3732.
- (33) Martel, R. R.; Botros, I. W.; Rounseville, M. P.; Hinton, J. P.; Staples, R. R.; Morales, D. A.; Farmer, J. B.; Seligmann, B. E. *Assay and Drug Development Technologies* **2002**, *1*, 61-71.
- (34) Till, B. J.; Burtner, C.; Comai, L.; Henikoff, S. *Nucleic Acids Research* **2004**, *32*, 2632-2641.
- (35) Shahidi, F.; Abuzaytoun, R. *Advances in Food and Nutrition Research* **2005**, *49*, 93-137.
- (36) Layek, B.; Singh, J. In *Chitosan Based Biomaterials Volume 2*; Elsevier, 2017, pp 209-244.
- (37) Bozkir, A.; Saka, O. M. *Journal of Drug Targeting* **2004**, *12*, 281-288.
- (38) Byrnes, S.; Bishop, J.; Lafleur, L.; Buser, J.; Lutz, B.; Yager, P. *Lab on A Chip* **2015**, *15*, 2647-2659.
- (39) Schlappi, T. S.; McCalla, S. E.; Schoepp, N. G.; Ismagilov, R. F. *Analytical Chemistry* **2016**, *88*, 7647-7653.
- (40) Kidd-Ljunggren, K.; Holmberg, A.; Bläckberg, J.; Lindqvist, B. *Journal of Hospital Infection* **2006**, *64*, 352-357.
- (41) Shike, H.; Shimizu, C.; Kanegaye, J.; Foley, J. L.; Burns, J. C. *The Pediatric Infectious Disease Journal* **2005**, *24*, 29.

## CHAPTER 5: POLYMERASE CHAIN REACTION-LATERAL FLOW ASSAY FOR DETECTION OF ANTIMICROBIAL RESISTANCE BACTERIA

### Chapter Overview

Antimicrobial resistance (AMR) has emerged as a significant public health threat that incurs an immense economic cost. The current gold standard for detecting AMR bacteria is the Kirby-Bauer diffusion test. However, this test can only be performed in a centralized laboratory by trained personnel and requires overnight to several days' incubation of the bacterial culture, in addition to the time necessary to transport samples to the laboratory. Herein, a lateral flow assay (LFA) motif as described in the previous chapter was coupled with polymerase chain reaction (PCR), a widely used nucleic acid amplification technique, to detect AMR bacteria. Two labeled PCR primers (a biotin-labeled forward primer and a digoxigenin-labeled reverse primer) were used to amplify a DNA fragment target that encodes for ampicillin resistance, one of the major contributors to AMR worldwide. The labeled PCR products were then detected on the lateral flow device to provide a yes/no answer through a simple colored line readout. The proposed PCR-LFA method has been used to detect purified plasmids containing the ampicillin resistance gene and bacterial cultures that expressed the resistance gene. Detection limits of the PCR-LFA were approximately 110 plasmid copies (tested with pUC19 vector) and 54 colony-forming units of bacteria (tested with ampicillin-resistant *E. coli* transformed with pT7CFE vector). A low-cost reagent delivery device made of transparency film and double-sided adhesive has also been prototyped for the LFA to simplify user operation. The proposed method can be applied for rapid detection (less than 3 h) of AMR bacteria in environmental samples and can be adapted for field applications in the future.

### Introduction

Antimicrobial resistance (AMR) is one of the major public health challenges that poses a threat to the effective prevention and treatment of infections caused by bacteria, viruses, fungi, and other parasites. The annual cost of AMR to the US health system has been estimated at USD 21 to 34 billion.<sup>1</sup> AMR has

also been projected to cause 10 million deaths and cost USD 85 trillion globally by 2050 if not properly mitigated.<sup>2</sup> Some major causes of AMR include over-prescription of antibiotics, patients not finishing the entire antibiotic course, overuse of antibiotics in livestock breeding, and poor infection control.<sup>3-6</sup> Contaminated environmental samples including water with antimicrobial agents or AMR bacteria are also a significant source of AMR and propagation media for the horizontal transfer of AMR gene from resistant bacteria to non-resistant ones.<sup>7</sup> Due to the notable role of water in the spread of AMR, various sources of water have been investigated for the presence of AMR bacteria to ensure the safe use for human and animal consumption and providing water supply for industrial uses and agricultural irrigation.<sup>8-11</sup>

The Kirby-Bauer disk diffusion test is the most widely used method to determine the susceptibility or resistance of pathogenic bacteria to antimicrobial compounds.<sup>12</sup> The bacteria are grown on an agar plate in the presence of various antimicrobial impregnated filter disks and resistance/susceptibility is indirectly measured from the presence/absence of growth around the disks.<sup>13</sup> While this method provides reliable results, the test can only be carried out in a centralized laboratory by trained personnel, requiring an additional transport time to the already long plate incubation (i.e. 12-16 h or longer) for the disk diffusion test. Other methods for detecting AMR bacteria have been reported such as DNA microarrays for detecting AMR genes,<sup>14,15</sup> paper devices for detecting enzymes produced by resistant bacteria<sup>16</sup> and AMR bacteria similar to the Kirby-Bauer test,<sup>17</sup> and mass spectrophotometry for detecting nucleic acids and proteins related to AMR.<sup>18</sup> However, these techniques either rely on sophisticated instruments for the analysis or require a long incubation of the bacteria sample to achieve the desired detection limits. Nucleic acid amplification tests (NAATs) are well-known methods for sensitive detection of a very low quantity of pathogenic genes due to the ability to increase the number of detectable analytes in a relatively short time (i.e. a few hours compared to an overnight enrichment or plate incubation).<sup>19</sup> Polymerase chain reaction (PCR) is the most widely used NAAT with a detection limit as low as 3 copies of nucleic acid target.<sup>20</sup> This very low detection limit is achieved by a process called thermocycling where the target DNA is reacted with primers, nucleotides, and a polymerase enzyme at appropriate temperatures that are cycled multiple

times to create millions of copies of a particular section of the target DNA (Figure 5.1A). While PCR instruments are relatively expensive (thousands to ten thousands USD) and used exclusively in centralized laboratories, affordable thermocyclers (USD ~100) using off-the-shelf electronics have been reported for point-of-care and field applications.<sup>21,22</sup> Other low-cost thermocyclers have also been demonstrated in fluidic devices based on the heating of a rotating aluminum-based mask<sup>23</sup> and temperature-induced fluid movement.<sup>24</sup>

PCR products are commonly detected via fluorescence using DNA intercalating dyes. However, some of these fluorescence reporters such as ethidium bromide and acridine orange are toxic and mutagenic,<sup>25,26</sup> requiring a cautious handling by trained personnel. More recently discovered dyes including SYBR® family of dyes, Gel Red™, Gel Green™, Red Safe™ etc. are considered non-mutagenic and less toxic;<sup>27</sup> however, they are more expensive. In addition, a fluorescence reader is required for the measurement. This study aimed to combine the PCR with a lateral flow-based readout for the detection of antimicrobial resistant bacteria. Lateral flow assay (LFA) has been widely used in point-of-care medical diagnostics due to its rapid operation and easy-to-interpret results.<sup>28</sup> The presence of colored lines is typically used to indicate positive results. Two PCR primers, one was biotin-labeled and the other was digoxigenin-labeled, were used to target an ampicillin resistance gene that encodes for the production of  $\beta$ -lactamase (Figure 5.1A).  $\beta$ -lactamase degrades  $\beta$ -lactam antibiotics, the most widely used antibiotics for the treatment of various infectious diseases, and is a major contributor to the worldwide AMR.<sup>29</sup> After the biotin/digoxigenin-labeled amplicons were obtained through the PCR, the sample was flowed through the LFA device where the amplicons were captured by the immobilized anti-digoxigenin antibody on the nitrocellulose membrane (Figure 5.1B). Colorimetric reagents including streptavidin conjugated to horseradish peroxidase (strep-HRP) and 3,3',5,5'-tetramethylbenzidine (TMB), a substrate to the HRP, were then added to the device to develop a blue-colored line. The proposed PCR-LFA method has been applied to detect  $\beta$ -lactamase-resistant bacteria in culture media and will be applied to detect AMR related to these bacteria in wastewater samples.

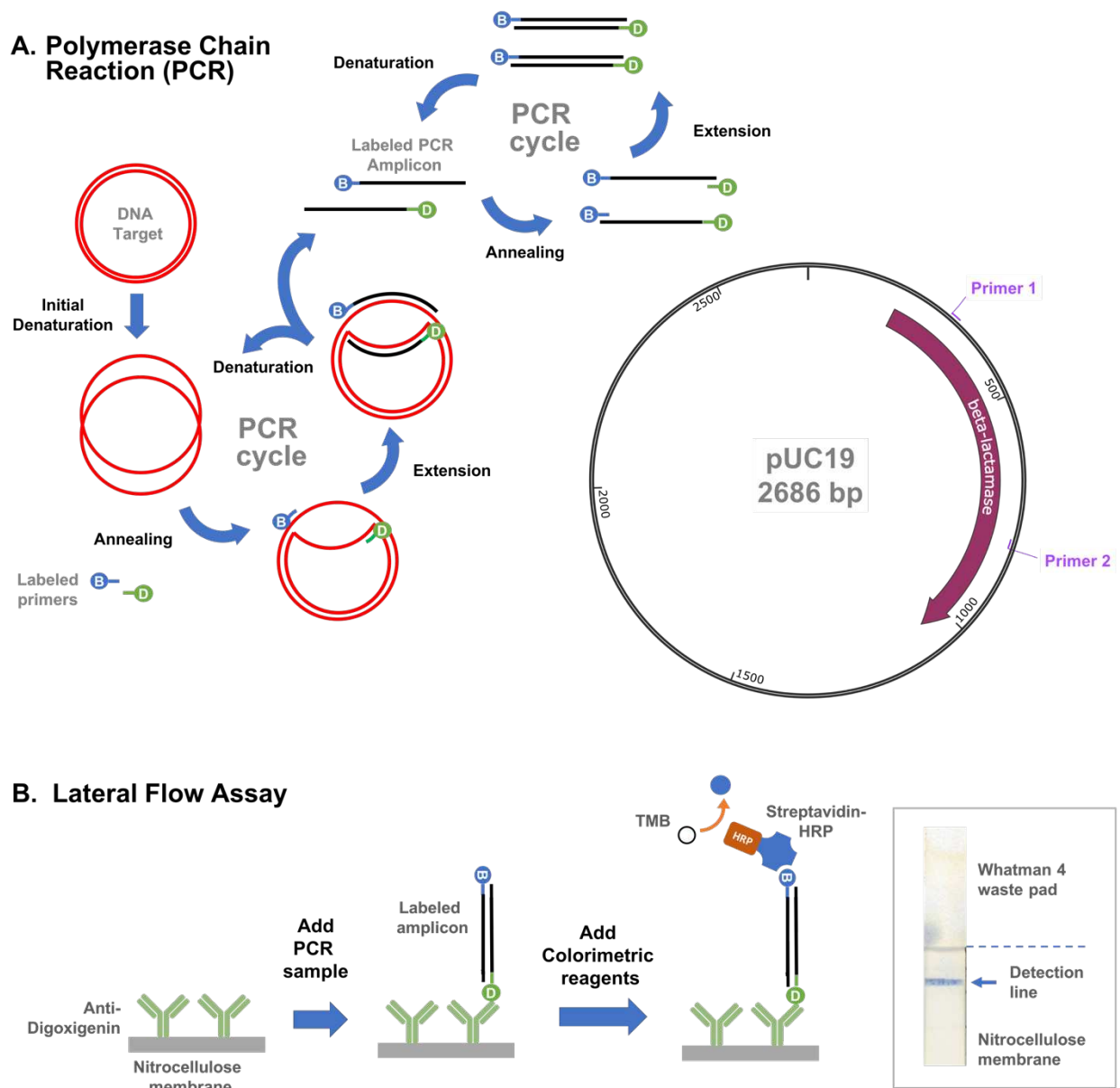


**Figure 5.1:** Schematic representations of: **(A)** PCR cycles with biotin-labeled and digoxigenin-labeled primers to amplify a fragment of beta-lactamase gene in pUC19 **(B)** lateral flow assay to detect PCR amplicons.

## Experimental Section

### *Chemicals and materials*

Nitrocellulose FF120HP A4-sized sheets, Whatman Grade 1 filter paper, and Whatman Grade 4 filter paper were purchased from GE Healthcare (Illinois, USA). Anti-digoxigenin monoclonal antibody was purchased from Abcam (Massachusetts, USA). Trehalose dihydrate and Luria-Bertani (LB) agar were purchased from EMD Millipore (Massachusetts, USA). StabilGuard® Immunoassay Stabilizer (BSA-free) was purchased from Surmodics, Inc. (Minnesota, USA). Q5 polymerase (including 5x buffer and 5x high GC enhancer) and deoxyribonucleotides (dNTPs) were purchased from New England Biolabs, Inc. (Massachusetts, USA). Glycerol was purchased from Mallinkrodt (Staines-upon-Thames, UK). 2-(N-morpholino)ethanesulfonic acid hydrate (MES), Tris(hydroxymethyl)aminomethane (Tris), Tween® 20, Gel Red, and chitosan oligosaccharide lactate (average  $M_n$  5,000) were purchased from Sigma-Aldrich, Inc. (Missouri, USA). Ultrapure agarose was purchased from Invitrogen (California, USA). LB broth/medium was purchased from RPI (Illinois, USA). Strep-HRP was purchased from R&D Systems, Inc. (Minnesota, USA). Ampicillin, chloramphenicol, TAE 50 buffer, Pierce™ 1-Step Ultra TMB-Blotting Solution, and Generuler 1 kb plus DNA ladder were purchased from Thermo Scientific (Massachusetts, USA). Labeled PCR primers were ordered from Integrated DNA Technologies, Inc. (Iowa, USA) with the following sequences: **Primer 1:** 5'biotin/AGATCAGTTGGGTGCACGAG/3'

**Primer 2:** 5'digoxigenin/TTGTTGCCGGGAAGCTAGAG/3'

All reagents were used as received without further purification. Water used to prepare reagent solutions was purified using a Milli-Q system ( $\rho \geq 18.2 \text{ M}\Omega\cdot\text{cm}$ ). pUC19 plasmids were grown in *E. coli* and purified using QIAGEN Plasmid Maxi Kits (Hilden, Germany).

### *Fabrication of lateral flow strips*

A 100  $\mu\text{L}$  anti-digoxigenin Ab solution (1 mg/mL) was mixed with 2.5  $\mu\text{L}$  of 2 M trehalose and 10  $\mu\text{L}$  of 50% glycerol. The solution was then striped twice onto a nitrocellulose (NC) membrane at 0.036  $\mu\text{L}/\text{mm}$  deposition rate using an Automated Lateral Flow Reagent Dispenser (ALFRD)<sup>TM</sup> from

ClaremontBio (California, USA) equipped with a syringe pump (1.5  $\mu\text{L/s}$  flow rate; 41 mm/s stripping rate). The membrane was let dry at 37°C for 1 h. To block the surface of the NC membrane from non-specific binding, StabilGuard® Immunoassay Stabilizer solution was added to fully wet the membrane. The membrane was then air dried at room temperature for 30 min. After that, the membrane can be immediately used to fabricate devices or stored in a closed container for later use.

To construct the device, the Ab-stripped NC membrane was cut using a Zing CO<sub>2</sub> laser cutter from Epilog (Colorado, USA) to create 20 mm x 4 mm strips with the deposited antibody located 5 mm from one edge of the strip (i.e. downstream edge). The NC strip was placed on a transparency sheet (as a backing material) using double-sided adhesive. Two pieces of 20 mm x 15 mm laser cut Whatman No. 4 filter paper were stacked together and placed on the downstream edge of the NC strip using a tape such that there was 2 to 3 mm overlapping region between the materials. The Whatman grade 4 qualitative filter paper was used as an absorbent pad.

### ***PCR-LFA***

PCR was performed based on a previously described protocol.<sup>30</sup> 1  $\mu\text{L}$  pUC19 solution/sample was mixed with 5  $\mu\text{L}$  5x Q5 buffer, 5  $\mu\text{L}$  5x enhancer, 0.25  $\mu\text{L}$  Q5 polymerase, 0.5  $\mu\text{L}$  dNTPs 10 mM, 1.25  $\mu\text{L}$  of 10  $\mu\text{M}$  primer 1, 1.25  $\mu\text{L}$  of 10  $\mu\text{M}$  primer 2 and 10.75  $\mu\text{L}$  water. The solution was then run for thermocycling with the following condition:

	<u>Temperature</u>	<u>Time</u>
<b>Initial denaturation</b>	98°C	30 s
<b>37 cycles of:</b>		
Denaturation	98°C	10 s
Annealing	68°C	30 s
Extension	72°C	20 s
<b>Final extension</b>	72°C	120 s

A 5  $\mu\text{L}$  PCR aliquot was diluted with 10  $\mu\text{L}$  MES buffer pH 5.0, run through the chitosan pretreatment device, and then transferred to the lateral flow device. The following solutions: 10  $\mu\text{L}$  Tris-buffered saline

(TBS) pH 8.6-Tween 0.05% wash buffer, 10  $\mu$ L Streptavidin-HRP (1:200 diluted), 10  $\mu$ L TBS-Tween 0.05% wash buffer, and 4x 10  $\mu$ L TMB/H<sub>2</sub>O<sub>2</sub> substrate solution were then added subsequently to develop the colorimetric signal.

#### ***Sample pretreatment using chitosan-modified paper***

Wax-patterned filter paper was modified with 2  $\mu$ L of 1% w/v chitosan oligosaccharide lactate prepared in MES buffer pH 5.0. This chitosan-modified filter paper was then affixed to a laser-cut polymethyl methacrylate (PMMA) support layer (Figure 4.7). Upon completion of the PCR, 15  $\mu$ L each of the samples (i.e. 1:3 diluted PCR sample in MES buffer pH 5.0) was applied to the chitosan layer while in contact with an absorbent pad. The chitosan layer was washed in this position with 40  $\mu$ L of 100 mM MES buffer pH 5.0 to remove interfering compounds from the sample while retaining DNA. The membrane was then moved to the lateral flow strip and the DNA retained in the membrane was eluted on the lateral flow strip using three 10  $\mu$ L volumes of Tris buffer pH 8.6.

#### ***Gel electrophoresis***

Gel electrophoresis was used to confirm the amplification of the target gene and compare results obtained from the PCR-LFA method. A 5  $\mu$ L PCR aliquot was mixed with 1  $\mu$ L 6x Gel Red DNA staining dye and loaded into 1% agarose gel. The electrophoresis was run in 1x TAE buffer (40 mM Tris, 20 mM acetic acid, 1 mM ethylenediaminetetraacetic acid/EDTA) at 120 V for 30 min. The gel was then imaged using a Bio-Rad Gel Doc EZ Imager (California, USA).

#### ***Testing bacterial cultures***

Two bacterial isolates were tested: an ampicillin-resistant *E. coli* transformed with pT7CFE vector and a chloramphenicol-resistant *E. coli* transformed with pLysS vector as a negative control. To determine the number of bacteria present in the culture media, a series of 10-fold dilutions of the bacteria culture ( $10^{-2}$  to  $10^{-9}$ ) were prepared in LB medium. 25  $\mu$ L of antibiotic solutions (ampicillin 50 mg/mL for pT7CFE-transformed *E. coli* and chloramphenicol 34 mg/mL for pLysS-transformed *E. coli*) were spread on 25 mL

LB agar plates and incubated for 30 min at room temperature. 100  $\mu$ L of each bacterial culture dilution was then spread on the designated plate and incubated for 18 h. The number of colony-forming units (CFU)/bacteria in the two initial cultures were determined by counting bacterial colonies on the dilution plates. To test the bacterial culture using PCR-LFA, 1  $\mu$ L aliquot was pipetted from the culture stock and subjected to the procedure described above. For diluted samples, water was used to dilute the stocks prior to mixing the sample with other PCR reagents.

### ***Image analysis***

After color development, the strips were allowed to dry briefly to enhance the color contrast. These devices were then scanned using a V600 Epson scanner. The resulting image was color-inverted, and the detection region mean intensity was quantified using ImageJ 1.05i image processing software (open-source software, National Institutes of Health).

## **Results and Discussion**

### ***PCR-LFA for $\beta$ -lactamase gene detection***

$\beta$ -lactamases are bacterial enzymes that hydrolyze the amide bond in the  $\beta$ -lactam ring of penicillin, cephalosporin, and carbapenem antibiotics, causing the most common multidrug-resistance in the hospitals.<sup>31</sup> To test the ability of the proposed method to detect the  $\beta$ -lactamase gene, pUC19 plasmid was used as a model target DNA. pUC19 plasmid is a commonly used cloning vector that conveys the resistance toward ampicillin, a penicillin antibiotic. The vector is a double-stranded circular DNA, 2686 base pairs (bp) in length, and has a high copy number. PCR primers used in the experiments were 20-mer oligonucleotide sequences that bound to bases number 104 to 123 of the  $\beta$ -lactamase gene (forward primer/primer 1) and to bases number 592 to 611 of the antisense pair (reverse primer/primer 2) to create an approximately 508 bp-long biotin/digoxigenin-labeled amplicons. To assess DNA amplification through PCR, various amounts of pUC19 plasmid were tested and the results were visualized through gel electrophoresis of Gel Red-stained PCR products.

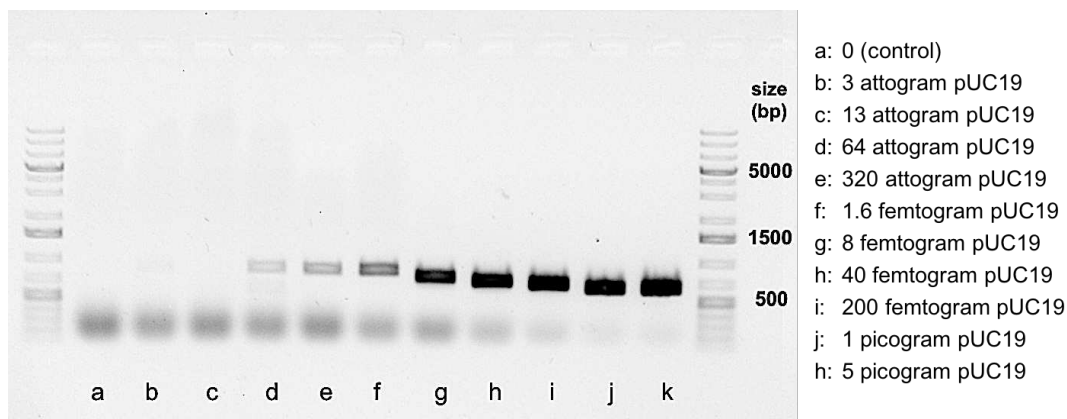


**Figure 5.2:** Image of Gel Red-stained PCR products at different amounts of pUC19 after gel electrophoresis at 120 V for 30 min on 1% agarose

As shown in Figure 5.2, PCR products or amplicons are located between 500 and 1500 bp ladder while the unreacted primers traveled further down the gel due to the small sizes (i.e. diffused bands at the bottom of the gel). Amplicons were observable at as low as 64 attograms of pUC19 (approximately 22 DNA copies) with lengths seeming to vary depending on the plasmid loads. At high amounts/concentrations of pUC19, the amplicon bands were located closer to the 500 bp ruler which is expected based on the locations of the forward and reverse primers. However, larger amplicons whose sizes were between 700 to 1000 bp were seen at low pUC19 loads. A larger amplicon can occur when the primer binds to an incorrect region of the target DNA, for example when a forward primer binds to an upstream region of the targeted fragment or a reverse primer binds to a downstream region of the fragment, resulting in an elongated copied sequence.<sup>32</sup> However, this incorrect priming is unlikely to happen with both primers used in this experiment since only up to 6 bases of the primers can form dimers with pUC19 DNA outside the targeted fragment. These short dimers are usually present at much lower temperatures (i.e. around 10°C or less) than the annealing or extension temperatures used in the PCR. Another possible reason for the larger amplicon is an extension beyond the designated stop regions (i.e. the locations of the primers) due to the pUC19 DNA duplexes not completely renaturing during annealing and/or extension period. Nevertheless, the exact reason for the larger amplicon cannot be confirmed unless the amplicon is sequenced.

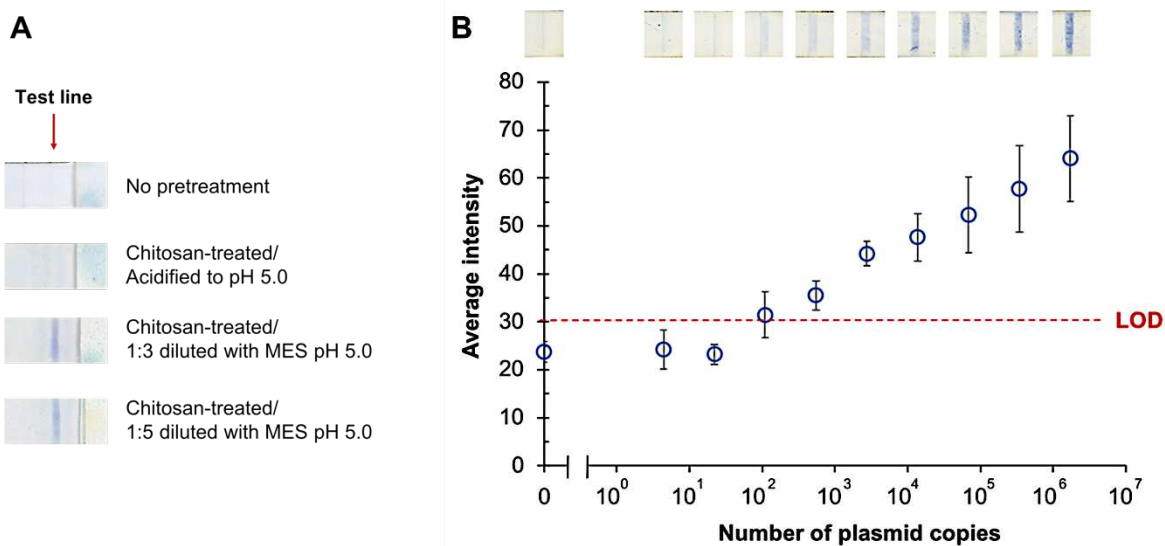


**Figure 5.3:** (A) LFA detection of non-treated and chitosan-treated PCR products (B) PCR-LFA at various amounts of pUC19 plasmid. Error bars indicate standard deviation of triplicate experiments. LOD = limit of detection (blank average + 3x standard deviation)

When the PCR products were tested directly on the lateral flow device, no color signal was observed (Figure 5.3A, top image). The presence of a high GC enhancer in the PCR mixture could be a reason for this binding inhibition. While the composition of this enhancer is unknown due to the proprietary formula, a significantly different viscosity of the enhancer compared to water suggests that it may contain an organic solvent that is water-miscible, potentially dimethyl sulfoxide (DMSO), glycerol, or formamide. DMSO, glycerol, and formamide have been used as PCR additives to reduce secondary structures and are particularly useful for GC rich templates.<sup>33,34</sup> It has been previously reported that formamide inhibited the binding of labeled oligonucleotide on a lateral flow device.<sup>35</sup> To remove the enhancer, PCR products were treated using a chitosan-modified paper device described in the previous chapter (Figure 4.7). Acidified or MES buffer pH 5.0-diluted PCR product was added to the chitosan-modified filter paper where PCR amplicons were retained by the chitosan at a low pH and other small molecules including the enhancer were washed away to the absorbent pad, followed by elution of the retained amplicons to the lateral flow device using Tris buffer pH 8.6. DNA retention by the chitosan-modified paper was apparently affected by the

relatively high concentration of enhancer (i.e. 20% in the PCR mixture) as shown by the absence of signal in the chitosan-treated acidified sample (Figure 5.3A). Dilution with MES buffer to bring this concentration down to 6.7% (in 1:3 diluted sample) and 4% (in 1:5 diluted sample) was able to recover the signal. Thus, 1:3 dilution of PCR products in MES buffer followed by pretreatment using the chitosan-modified paper was carried out prior to the LFA.

Figure 5.3B shows the PCR-LFA dose-response at various amounts of pUC19 ranging from 0 to  $1.7 \times 10^6$  copies. The detection limit was calculated from blank average + 3x standard deviation and found to be approximately 110 copies of pUC19, which was 5 times higher than the visual detection limit from gel electrophoresis with Gel Red staining. However, no external equipment is required for the LFA readout, whereas gel electrophoresis requires an external power supply to perform the DNA separation and a fluorescence imager to visualize the Gel Red-stained DNA.

#### ***Detection of AMR bacteria***

To test the proposed method for detecting resistant bacteria, two bacteria isolates were used: ampicillin-resistant *E. coli* transformed with pT7CFE vector and chloramphenicol-resistant *E. coli* transformed with pLysS vector (negative control). The bacteria cultures (stock concentrations in LB medium:  $2.9 \times 10^5$  CFU/ $\mu$ L for ampicillin-resistant bacteria,  $4.6 \times 10^5$  CFU/ $\mu$ L for chloramphenicol-resistant bacteria) were diluted in water and 1  $\mu$ L of undiluted or diluted culture was subjected to the PCR procedure. The results of gel electrophoresis and LFA detection of the PCR products are shown in Figure 5.4. As seen in Figure 5.4A, a linear relationship was observed between the colorimetric response and the logarithmic of the bacterial count at 4 to  $1.2 \times 10^4$  CFU/ $\mu$ L. A decrease in the colorimetric signal was observed at higher bacterial loads. The detection limit was approximately 54 CFU or CFU/ $\mu$ L (blank average + 3x standard deviation), which is higher than conventional PCR methods that involved DNA extraction from bacterial cells prior to the PCR.<sup>36,37</sup> Yet, this detection limit is lower than those of previously reported paper-based methods for detecting AMR bacteria.<sup>16,17</sup>

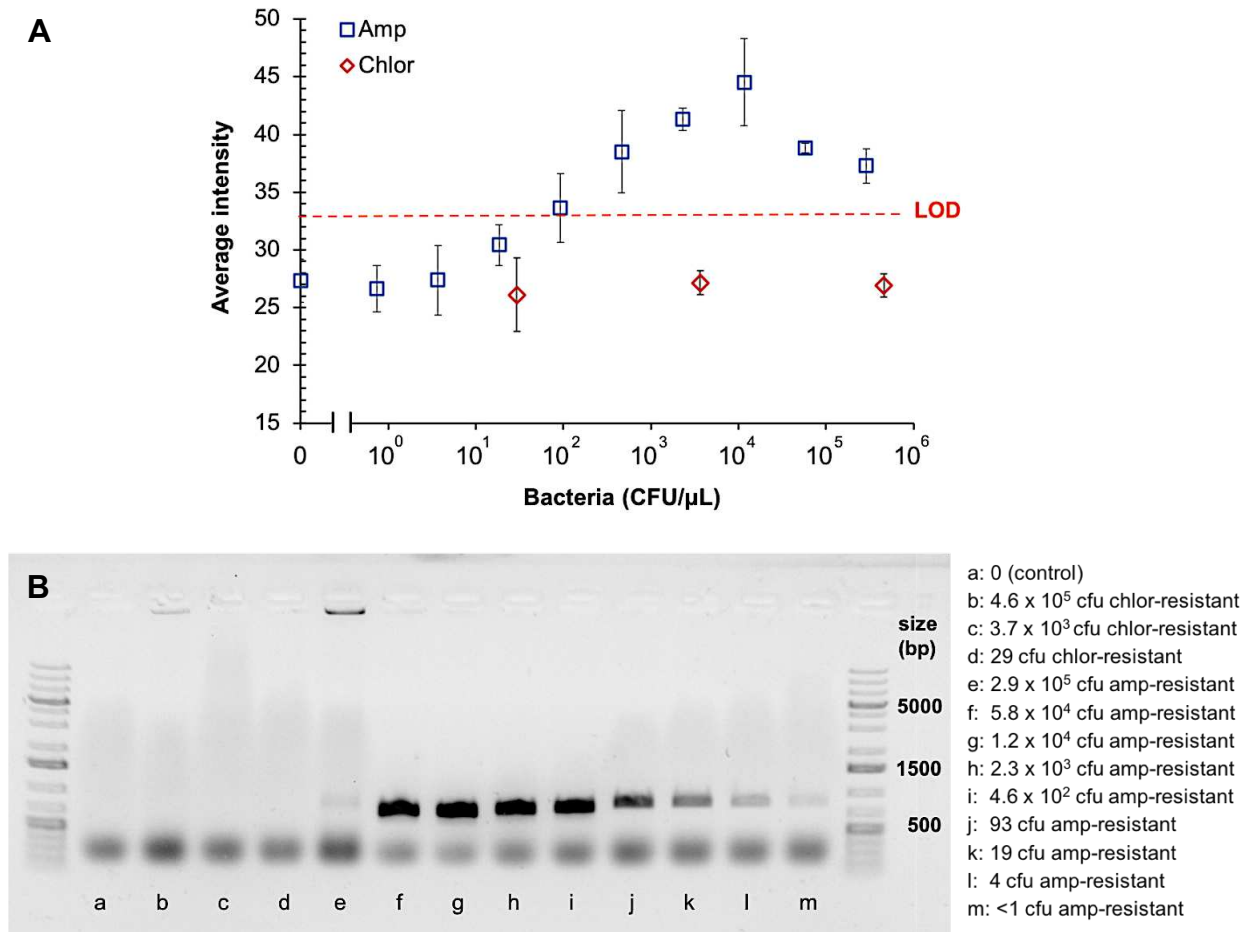


**Figure 5.4:** (A) PCR-LFA detection of ampicillin-resistant (**Amp**) and chloramphenicol-resistant (**Chlor**) *E. coli* at various bacteria concentrations. Error bars indicate standard deviation of triplicate experiments. LOD = limit of detection (blank average + 3x standard deviation). (B) Image of Gel Red-stained PCR products after gel electrophoresis at 120 V for 30 min on 1% agarose

To confirm the effect of the culture media, 2300 CFU of ampicillin-resistant *E. coli* were suspended in four different matrices (1  $\mu$ L 1:100 diluted LB medium in water, 1  $\mu$ L 1:10 diluted LB medium in water, 1  $\mu$ L undiluted LB medium, and 10  $\mu$ L undiluted LB medium), run for PCR, and the results were visualized via gel electrophoresis and Gel Red staining. As shown in Figure 5.5, a very faint amplicon band was observed from the 10  $\mu$ L undiluted LB medium (highest concentration of LB medium), compared with the strong bands obtained at lower concentrations of the culture media. This result suggests that a DNA clean-

up/extraction from the culture media would be necessary to avoid inhibition of the PCR reaction if a larger volume of bacteria culture was used.

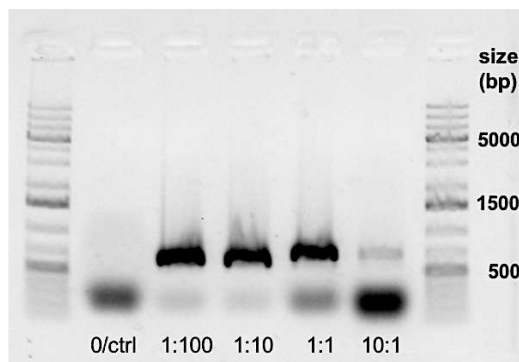


**Figure 5.5:** Image of Gel Red-stained PCR products from 2300 CFU of ampicillin-resistant *E. coli* at different concentrations of LB medium: 1  $\mu$ L 1:100 diluted LB medium in water (**1:100**), 1  $\mu$ L 1:10 diluted LB medium in water (**1:10**), 1  $\mu$ L undiluted LB medium (**1:1**), and 10  $\mu$ L undiluted LB medium (**10:1**)

While the current LFA devices were operated through sequential pipetting of the sample, reagents, and wash buffer which was time-consuming, a colleague in the Henry group, has prototyped a sequential reagent delivery device made of transparency film and double-sided adhesive to simplify the user operation (Figure 5.6). The sequential delivery device consists of 4 separate inlets for the sample, wash buffer, strep-HRP, and TMB substrate. The wash buffer and colorimetric reagents were added to the designated inlets at indicated volumes such that a plug of wash buffer was created between the sample and strep-HRP plugs and between the strep-HRP and TMB plugs. This sequential flow with buffer wash in between allowed for optimized binding of the labeled DNA and strep-HRP to the detection zone and avoided mixing between the colorimetric enzyme and substrate. The addition of the DNA sample to its inlet automatically opened a surface tension-based burst valve between the reagent delivery device and the nitrocellulose membrane, allowing the sample and reagents to flow to the membrane. A color signal was observed approximately 15-20 minutes after the addition of the sample. The intensity of the color signal was comparable to that obtained from the manual, sequential pipetting (Figure 5.6).

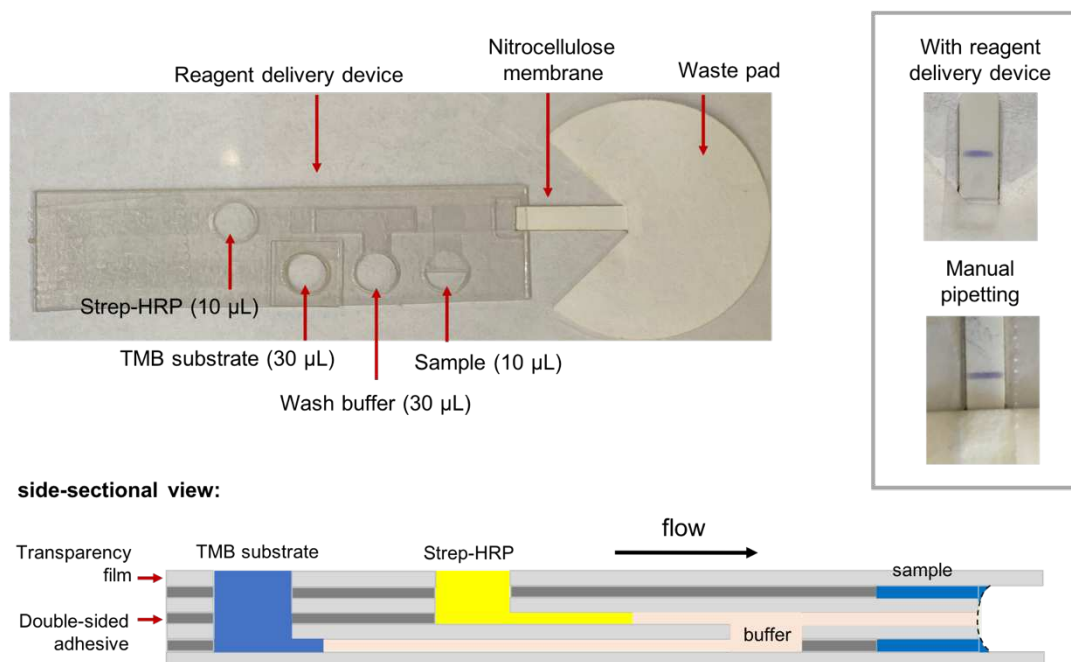


**Figure 5.6:** Sequential reagent delivery device made of transparency film and double-sided adhesive (a courtesy of Ilhoon Jang) coupled to an LFA, tested with a sample containing 280 femtomoles biotin/digoxigenin-labeled oligonucleotide. A result of manual pipetting comparable amounts of sample and reagents to the lateral flow device is also shown for comparison.

The total time required to run the PCR, chitosan-pretreatment, and LFA was approximately 2-3 h, which is substantially shorter than the Kirby-Bauer test. We have planned to test the proposed assay to detect resistant bacteria in water samples collected by our colleagues in Dr. Sheryl Magzaman's laboratory (Environmental and Radiological Health Science, CSU). However, due to the COVID-19 outbreak, the plan has been suspended and will resume once laboratories at CSU are back to normal operation.

## Conclusions

The integration of a simple LFA readout to PCR for detecting AMR bacteria has been demonstrated here with a detection limit of approximately 54 CFU. Amplification of the target sequence through PCR allowed for detection of as low as  $10^2$  target DNA using the lateral flow device, compared with the previous LFA-based nucleic acid detection without amplification procedure (detection limit =  $10^8$  target DNA).<sup>35</sup> The assay does not require an external reader, can be completed in less than 3 h, and potential for

multiplexing by utilization of separate labeled primer sets for different target bacteria. While subjecting the sample directly to PCR without prior DNA extraction apparently hampered the amplification reaction and limited the attainable detection limit, sample pretreatment using chitosan-treated paper, similar to that performed for PCR clean-up, can potentially be employed for the extraction. This chitosan-based extraction would be more cost-effective and amenable for field-based applications than the commercial column-based extraction kits which require a microcentrifuge or a vacuum pump for the operation.

## REFERENCES

- (1) WHO, 2014. *Antimicrobial resistance: global report on surveillance*, [https://apps.who.int/iris/bitstream/handle/10665/112642/9789241564748\\_eng.pdf](https://apps.who.int/iris/bitstream/handle/10665/112642/9789241564748_eng.pdf), Accessed on 18 November 2019
- (2) England, P. H., 2015. *Health Matters: Antimicrobial Resistance*, <https://www.gov.uk/government/publications/health-matters-antimicrobial-resistance/health-matters-antimicrobial-resistance>, Accessed on 18 November 2019
- (3) Llor, C.; Bjerrum, L. *Therapeutic Advances in Drug Safety* **2014**, *5*, 229-241.
- (4) Weinstein, R. A. *Emerging Infectious Diseases* **2001**, *7*, 188.
- (5) Economou, V.; Gousia, P. *Infection and Drug Resistance* **2015**, *8*, 49.
- (6) Woolhouse, M. E.; Ward, M. J. *Science* **2013**, *341*, 1460-1461.
- (7) Lupo, A.; Coyne, S.; Berendonk, T. U. *Frontiers in Microbiology* **2012**, *3*, 18.
- (8) Xi, C.; Zhang, Y.; Marrs, C. F.; Ye, W.; Simon, C.; Foxman, B.; Nriagu, J. *Applied Environmental Microbiology*. **2009**, *75*, 5714-5718.
- (9) Sayah, R. S.; Kaneene, J. B.; Johnson, Y.; Miller, R. *Applied Environmental Microbiology* **2005**, *71*, 1394-1404.
- (10) Da Costa, P. M.; Vaz-Pires, P.; Bernardo, F. *Water Research* **2006**, *40*, 1735-1740.
- (11) Roe, M. T.; Vega, E.; Pillai, S. D. *Emerging Infectious Diseases* **2003**, *9*, 822.
- (12) Biemer, J. J. *Annals of Clinical and Laboratory Science* **1973**, *3*, 135-140.
- (13) Hudzicki, J. *Kirby-Bauer disk diffusion susceptibility test protocol*. **2009**, <https://www.asmscience.org/content/education/protocol/protocol.3189?crawler=true>, Accessed on 9 May 2020.
- (14) Call, D. R.; Bakko, M. K.; Krug, M. J.; Roberts, M. C. *Antimicrobial Agents and Chemotherapy* **2003**, *47*, 3290-3295.
- (15) Frye, J. G.; Jesse, T.; Long, F.; Rondeau, G.; Porwollik, S.; McClelland, M.; Jackson, C. R.; Englen, M.; Fedorka-Cray, P. J. *International Journal of Antimicrobial Agents* **2006**, *27*, 138-151.
- (16) Boehle, K. E.; Gilliland, J.; Wheeldon, C. R.; Holder, A.; Adkins, J. A.; Geiss, B. J.; Ryan, E. P.; Henry, C. S. *Angewandte Chemie International Edition* **2017**, *56*, 6886-6890.
- (17) Deiss, F.; Funes-Huacca, M. E.; Bal, J.; Tjhung, K. F.; Derda, R. *Lab on a Chip* **2014**, *14*, 167-171.
- (18) Vrioni, G.; Tsiamis, C.; Oikonomidis, G.; Theodoridou, K.; Kapsimali, V.; Tsakris, A. *Annals of Translational Medicine* **2018**, *6*, 240.
- (19) Sandle, T. In *Pharmaceutical Microbiology*, Sandle, T., Ed.; Woodhead Publishing: Oxford, 2016, pp 219-231.
- (20) Kralik, P.; Ricchi, M. *Frontiers in Microbiology* **2017**, *8*, 108.
- (21) Mendoza-Gallegos, R. A.; Rios, A.; Garcia-Cordero, J. L. *Analytical Chemistry* **2018**, *90*, 5563-5568.
- (22) Wong, G.; Wong, I.; Chan, K.; Hsieh, Y.; Wong, S. *PLoS One* **2015**, *10*.
- (23) Jiang, L.; Mancuso, M.; Lu, Z.; Akar, G.; Cesarman, E.; Erickson, D. *Scientific Reports* **2014**, *4*, 4137.
- (24) Wheeler, E. K.; Benett, W.; Stratton, P.; Richards, J.; Chen, A.; Christian, A.; Ness, K. D.; Ortega, J.; Li, L. G.; Weisgraber, T. H.; Goodson, K.; Milanovich, F. *Analytical Chemistry* **2004**, *76*, 4011-4016.
- (25) Johnson, I. M.; Kumar, S. B.; Malathi, R. *Journal of Biomolecular Structure and Dynamics* **2003**, *20*, 677-685.
- (26) Sayas, E.; García-López, F.; Serrano, R. *Yeast* **2015**, *32*, 595-606.
- (27) Haines, A. M.; Tobe, S. S.; Kobus, H. J.; Linacre, A. *Electrophoresis* **2015**, *36*, 941-944.
- (28) Bahadır, E. B.; Sezgintürk, M. K. *TrAC Trends in Analytical Chemistry* **2016**, *82*, 286-306.
- (29) Eiamphungporn, W.; Schaduangrat, N.; Malik, A. A.; Nantasenamat, C. *International Journal of Molecular Sciences* **2018**, *19*, 2222.
- (30) Biolabs, N. E. *PCR Using Q5® High-Fidelity DNA Polymerase*, <https://www.neb.com/protocols/2013/12/13/pcr-using-q5-high-fidelity-dna-polymerase-m0491>, Accessed on 5 May 2020
- (31) Nikaido, H. *Annual Review of Biochemistry* **2009**, *78*, 119-146.

- (32) Rothberg, P. G.; Langerak, A. W.; Verhaaf, B.; van Dongen, J. J.; Burack, W. R.; Johnson, M. D.; Slate, D.; Laughlin, T. S.; Payne, K.; Figueiredo, L. *Journal of Hematopathology* **2012**, *5*, 57-67.
- (33) Zhang, D. Y.; Chen, S. X.; Yin, P. *Nature Chemistry* **2012**, *4*, 208.
- (34) Choi, J.-S.; Kim, J.-S.; Joe, C.-O.; Kim, S.; Ha, K.-S.; Park, Y.-M. *Experimental and Molecular Medicine* **1999**, *31*, 20-24.
- (35) Noviana, E.; Jain, S.; Hofstetter, J.; Geiss, B. J.; Dandy, D. S.; Henry, C. S. *Analytical and Bioanalytical Chemistry* **2020**, 1-11.
- (36) Guarddon, M.; Miranda, J.; Rodríguez, J.; Vázquez, B.; Cepeda, A.; Franco, C. *International journal of Food Microbiology* **2011**, *146*, 284-289.
- (37) Hindiyeh, M.; Smollen, G.; Grossman, Z.; Ram, D.; Davidson, Y.; Mileguir, F.; Vax, M.; David, D. B.; Tal, I.; Rahav, G. *Journal of Clinical Microbiology* **2008**, *46*, 2879-2883.

## CHAPTER 6: CONCLUSIONS AND FUTURE DIRECTIONS

Low-cost paper-based sensors offer advantages for performing bioanalytical tasks outside laboratory settings. There has been significant progress in the field exploring paper substrates for point-of-need applications.<sup>1,2</sup> Yet, many challenges remain that need to be overcome to provide robust and viable sensors for the end-users. One of the challenges is automating the system for handling multiple samples and performing continuous monitoring. Steady-rate flow-based paper devices described in Chapters 2 and 3 helped to address this issue by providing a platform where multiple samples can be processed within a single device. In addition, the significantly reduced analysis time allows for an increased throughput (i.e. up to 60 samples per hour) which is suitable for analyzing a large number of samples. The electrochemical flow-based paper devices also have potential for online monitoring of dynamic changes in a reaction vessel or in aquatic environments. Instead of dropping samples onto the paper device, the inlet of the device can be directly dipped into the sample and the electrochemical reader can be programmed to take measurements at designated time points.

While multilayered paper devices provide more tunable flow rates through the selection of membranes and adjustment on the gap height between paper layers,<sup>3,4</sup> swelling of the paper fiber when it is continuously wetted may affect the reproducibility of the testing, especially for an extended, continuous online monitoring. Preliminary studies in our lab showed that a flow device can also be constructed using a plastic/paper hybrid where the main flow channel is entirely made of plastic and paper is solely used as a downstream capillary pump (similar to the device shown in Figure 5.6). This plastic/paper device offers some advantages over the multilayered paper devices including a potentially more reproducible and controlled flow rate from the minimized swelling/expansion of the channel and reduced entrapment or non-specific adsorption of analytes onto the channel wall. Further studies to understand the flow behavior within this hybrid device and how the flow rates can be finely tuned (e.g. by changing the device geometry and

porous materials used as the downstream pump or modifying the surface chemistry of the plastic material) can expand the application of the flow-based paper devices.

Another challenge that is continuously being addressed in the field is how to improve the analytical specifications of the sensors without causing a significant burden to the overall cost. Thermoplastic electrodes (TPEs) used in a work presented in this dissertation are promising sensing materials as they showed comparable performance to more expensive electrodes (i.e. glassy carbon, metal electrodes) at a fraction of the cost. More studies on exploring carbon sources and plastic binders for the electrode fabrication and characterizing the electrodes will provide invaluable knowledge on how to better utilize these electrodes for specific sensing applications such as immunoassays, detecting organic molecules, gas sensing, etc. It has also been demonstrated in Chapter 3 that interdigitated electrode arrays (IDA) can be easily fabricated with the TPEs, compared with the conventional, more cost-prohibited fabrication process via photolithography. However, it is also worth noting that the efficiency of redox cycling/generation-collection is lower in these TPE arrays (i.e. 62%, typically over 90% in IDA fabricated via photolithography)<sup>5</sup> due to the limited attainable electrode width and interelectrode distance. Smaller features can be obtained by creating electrode molds using a higher resolution laser cutter or focused ion beam milling.<sup>6</sup> A more cost-effective approach to increase the redox cycling efficiency is by decreasing the flow rate. The slower flow rate, however, may sacrifice the assay throughput. Thus, it is important to optimize the flow rate to provide both enhanced cycling efficiency/detection sensitivity and reasonable throughput.

Works described in Chapters 4 and 5 combined high selectivity/specificity in nucleic acid-based techniques and a reader-free readout by colorimetric lateral flow assay (LFA) to provide more user-friendly assay platforms that are still high performance. Sub-femtomole ( $\sim 10^8$  copies of target DNA) was achieved using nuclease protection assay (NPA)-LFA. Performing nucleic acid amplification (i.e. polymerase chain reaction (PCR)) provided a lower detection limit ( $10^2$  DNA copies), opening more possibilities to adapt the platform for early disease diagnosis and pathogen detection in environmental samples. Efforts are still

needed to simplify the assay operation for the end-users. More optimization on the reagent delivery device to allow for reagent/buffer storage and release via a simple mechanism can further simplify users' operation. Another strategy that can be pursued is performing NPA or PCR in a fluidic device that can be interfaced with the LFA device. Thermal cycling in fluidic devices has been previously demonstrated<sup>7,8</sup> and can be adapted for the NPA-LFA or PCR-LFA.

## REFERENCES

- (1) Yamada, K.; Shibata, H.; Suzuki, K.; Citterio, D. *Lab on A Chip* **2017**, *17*, 1206-1249.
- (2) Yang, Y.; Noviana, E.; Nguyen, M. P.; Geiss, B. J.; Dandy, D. S.; Henry, C. S. *Analytical Chemistry* **2016**, *89*, 71-91.
- (3) Channon, R. B.; Nguyen, M. P.; Scorzelli, A. G.; Henry, E. M.; Volckens, J.; Dandy, D. S.; Henry, C. S. *Lab on A Chip* **2018**, *18*, 793-802.
- (4) Noviana, E.; Klunder, K. J.; Channon, R. B.; Henry, C. S. *Analytical Chemistry* **2019**, *91*, 2431-2438.
- (5) Bjorefors, F.; Strandman, C.; Nyholm, L. *Electroanalysis* **2000**, *12*, 255-261.
- (6) Lanyon, Y. H.; De Marzi, G.; Watson, Y. E.; Quinn, A. J.; Gleeson, J. P.; Redmond, G.; Arrigan, D. W. *Analytical Chemistry* **2007**, *79*, 3048-3055.
- (7) Jiang, L.; Mancuso, M.; Lu, Z.; Akar, G.; Cesarman, E.; Erickson, D. *Scientific Reports* **2014**, *4*, 4137.
- (8) Wheeler, E. K.; Bennett, W.; Stratton, P.; Richards, J.; Chen, A.; Christian, A.; Ness, K. D.; Ortega, J.; Li, L. G.; Weisgraber, T. H.; Goodson, K.; Milanovich, F. *Analytical Chemistry* **2004**, *76*, 4011-4016.

### Wettability of TPE surface

Wettability of the electrode material was assessed by measuring contact angles between a 0.2  $\mu\text{L}$  water droplet and the surface of the substrate using a DSA10 Drop Shape Goniometer (Kruss, Germany).

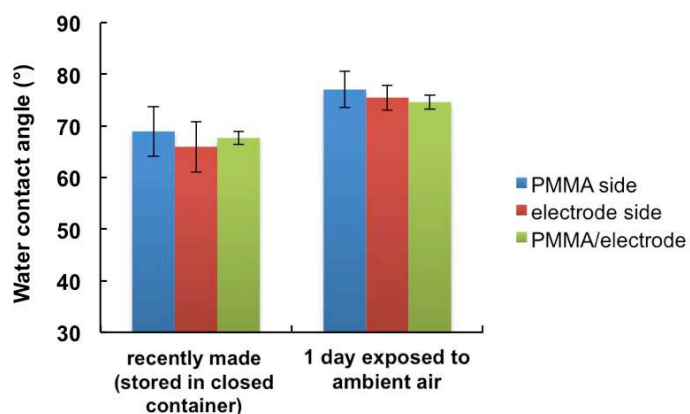


**Figure S1.** Water contact angle measured on TPE bands (n = 5)

### Surface roughness of TPE band

The surface of TPE band was profiled using a ZeScope profilometer (Zemetrics, Arizona, USA) and a line scan was taken for a 514  $\mu\text{m}$  distance covering the full width of the electrode band and PMMA substrate adjacent to the band.

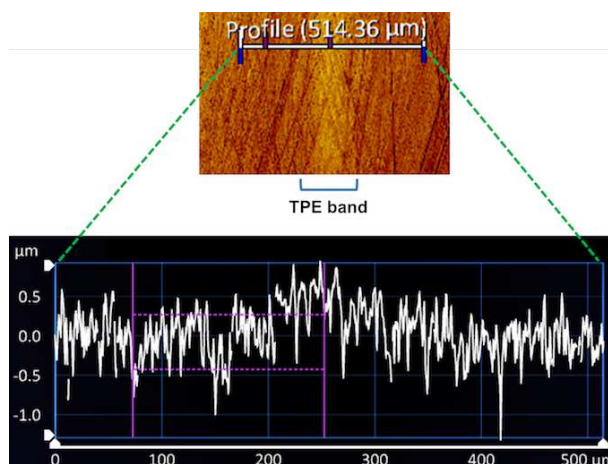


**Figure S2.** Surface roughness of the TPE band

### TPE surface treatment with plasma

TPE was prepared using a solvent-processed method as described in Experimental section. After sanding, the electrode was subjected to plasma oxidation for 5 min in air at 100 W.

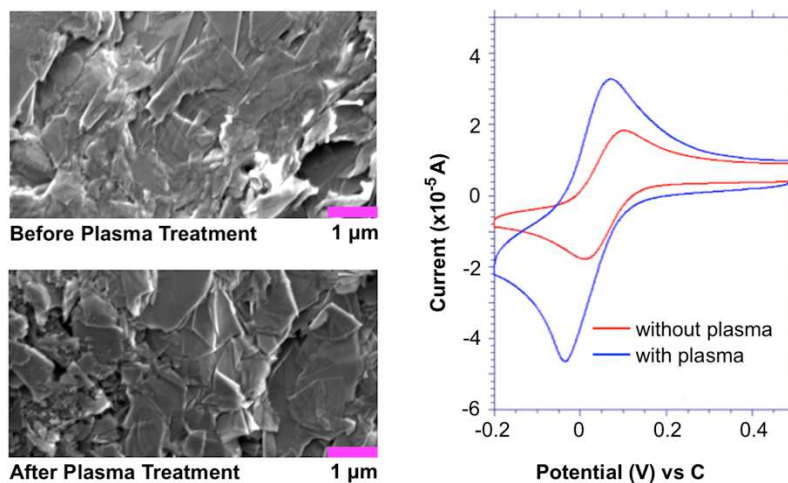


**Figure S3.** Scanning electron microscopy images of TPE surface before and after plasma treatment (left) and cyclic voltammograms at 0.1 V/s using 1 mM Fe(CN)<sub>6</sub><sup>3-/4-</sup> in 0.5 M KCl (right)

### Randles-Sevcik equation

Randles-Sevcik equation predicts the magnitude of peak current ( $i_p$ ) for a Nerstian system where diffusion is one-dimensional semi-infinite.<sup>1</sup>

$$i_p = 0.4463nFAC \left( \frac{nFvD}{RT} \right)^{1/2} \quad (1)$$

where  $i_p$  = peak current (A)

$n$  = number of electrons involved in the redox reaction

$F$  = Faraday's constant (96,485 C/mol)

$A$  = area of the electrode (0.015 × 0.035 cm)

$v$  = scan rate (V/s)

$D$  = analyte diffusion coefficient ( $D_{\text{FeTMA}} = 6.71 \times 10^{-6} \text{ cm}^2/\text{s}$ )<sup>2</sup>

$R$  = gas constant (8.314 J/mol.K)

$T$  = temperature (293 K)

## Nicholson method for estimating charge transfer rate

Heterogenous rate constant of the electron transfer ( $k_{ct}$ ) can be calculated using the following equation:

$$\psi = \frac{\left(\frac{D_O}{D_R}\right)^{\alpha/2} k_{ct}}{\left(\frac{\pi n D_O F v}{RT}\right)^{1/2}} \quad (2)$$

where  $k_{ct}$  = heterogenous rate constant of the electron transfer (cm/s)

$\psi$  = dimensionless kinetic parameter

$D_{O/R}$  = diffusion coefficient of the oxidized/reduced species (cm<sup>2</sup>/s)

$\alpha$  = transfer coefficient ( $\alpha = 0.5$  if cathodic and anodic peaks are symmetrical)

$v$  = scan rate (V/s)

$\psi$  is a kinetic parameter that is a function of peak separation ( $\Delta E_p$ ) of the measured cyclic voltammograms (CVs). For  $\alpha = 0.5$  (i.e. cathodic and anodic peaks are symmetrical),  $\psi$  is given by Nicholson for  $\Delta E_p$  ranging from 61 mV to 212 mV.<sup>3</sup> The following Nicholson plot was obtained from CV measurements of 5.0 mM Fe(CN)<sub>6</sub><sup>3-/4-</sup> in 0.5 M KCl on a TPE band ( $D_{O,Fe(CN)_6} = 7.2 \times 10^{-6}$  cm<sup>2</sup>/s,  $D_{R,Fe(CN)_6} = 6.7 \times 10^{-6}$  cm<sup>2</sup>/s).<sup>4</sup>

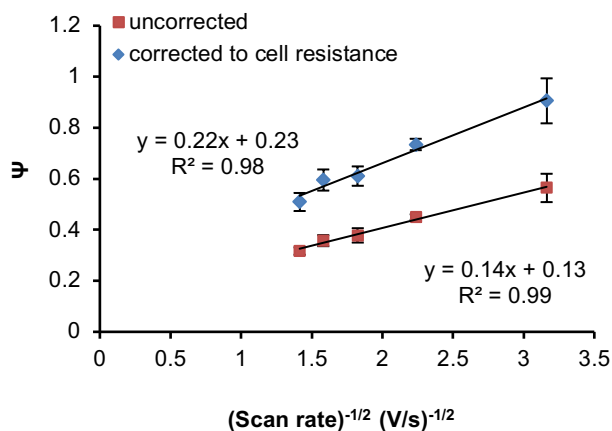


**Figure S4.** Nicholson plot to estimate  $k_{ct}$  of Fe(CN)<sub>6</sub><sup>3-/4-</sup> (n = 4 measurements)

### Hydrodynamic injections on TPE-ePAD

5  $\mu\text{L}$  aliquot of 5 mM  $\text{FcTMA}^+$  in 0.5 M KCl solution was injected onto ePAD multiple times until the wicking portion ( $270^\circ$  fan) was saturated. Potential was hold at 0.4 V vs C during the hydrodynamic amperometry. Single-layer Whatman 1 filter paper was used. The width of ePAD channel was 3 mm and single TPE band was operated as the detector.

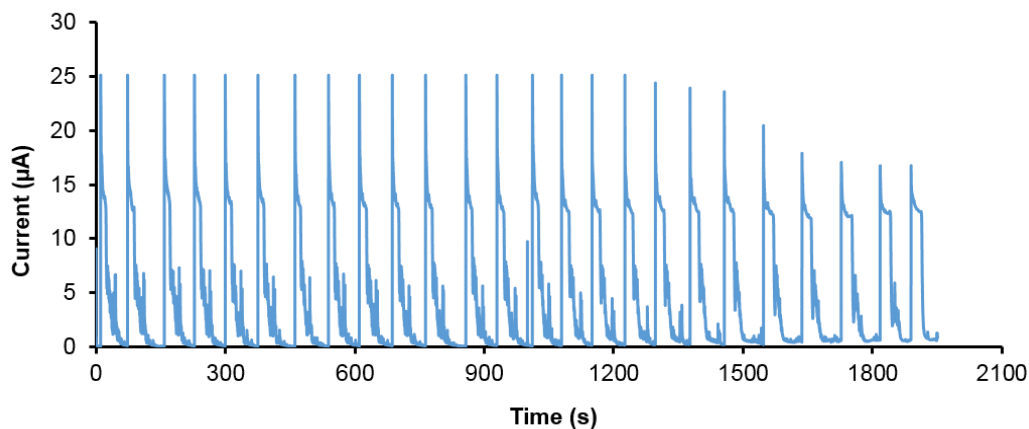


**Figure S5.** Repeated injections of  $\text{FcTMA}^+$  solution on a single-layer TPE-ePAD device

### Flow rates determination using dyed solution

To determine the area of ePAD occupied by certain volumes of solution, 5-30  $\mu\text{L}$  solution containing food coloring were loaded into separate devices. The area-per-volume ratio ( $A/V$ ) was found to be  $14.2 \pm 1.6 \text{ mm}^2/\mu\text{L}$  (Table S1). The rate of dye spread was then monitored by measuring the dyed area every 5 seconds following an injection of 10  $\mu\text{L}$  dye solution. Prior to measurement, 10  $\mu\text{L}$  dye solution was loaded to pre-wet the membrane. Measured areas shown in Figure S6 have been corrected to the area occupied by the dyes during this pre-wetting. The rate of dye spread was  $1.86 \pm 0.17 \text{ mm}^2/\text{s}$  and thus, the volumetric flow rate within ePADs was determined to be  $0.131 \pm 0.019 \mu\text{L}/\text{s}$  based on the previously determined  $A/V$ .

**Table S1.** Measured area from injection of dyed solution into ePADs

Volume ( $\mu\text{L}$ )	Area occupied by dye ( $\text{mm}^2$ )	$A/V$ ( $\text{mm}^2/\mu\text{L}$ )
5	56	11.2
10	158	15.8
15	211	14.1
20	277	13.9
25	382	15.3
30	450	15.0

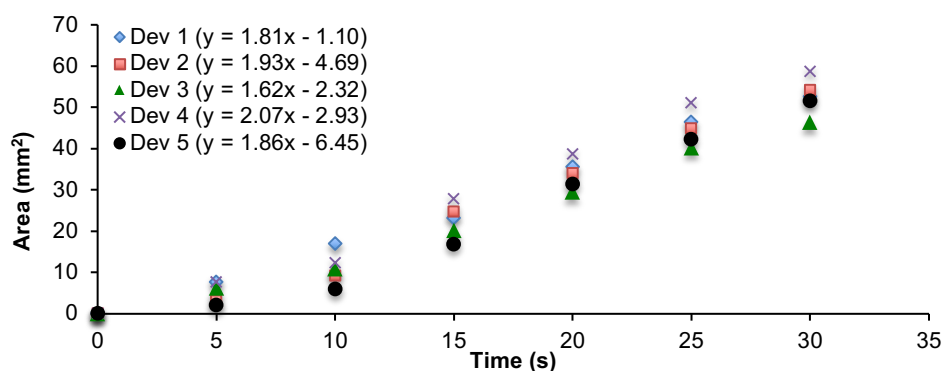


**Figure S6.** Rate of dye solution spread within ePADs

### Levich equation

Levich equation predicts the magnitude of current generated from a hydrodynamic voltammetry experiment. For a band electrode in a flow cell, the current is given by the following equation:<sup>5</sup>

$$i_{\text{lim}} = 0.925nFC_{\infty}w^{2/3}D^{2/3}x_e^{2/3}V_f^{1/3}h^{-2/3} \quad (3)$$

where  $i_{\text{lim}}$  = limiting current (A)

$n$  = number of electron involved ( $n = 1$ )

$F$  = Fadaray's constant (96,485 C/mol)

$C_{\infty}$  = bulk concentration of the analyte ( $\text{mol}/\text{cm}^3$ )

$w$  = channel width (0.4 cm)

$D$  = diffusion coefficient of the analyte ( $D_{\text{FcTMA}} = 6.71 \times 10^{-6} \text{ cm}^2/\text{s}$ )

$x_e$  = electrode length (0.016 cm)

$V_f$  = volumetric flow rate ( $\text{cm}^3/\text{s}$ )

$2h$  = channel height (cm)

The equation is valid under laminar flow condition as long as the diffusion along the direction of flow is negligible and the concentration gradient is confined adjacent to the electrode.

### Solution flow and imbibition in ePAD

The following images were taken using a digital microscope (Dino-Lite, USA) on an ePAD cross-section perpendicular to the direction of the flow.

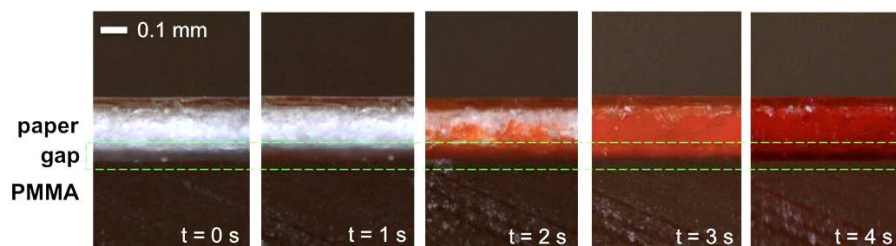


**Figure S7.** Solution flow through gap and imbibition to paper substrate

### Reynolds number

Reynolds number ( $R_e$ ) is used to predict whether the nature of flow within the channel will be laminar or turbulent based on the ratio of inertial and viscous forces.<sup>6</sup>

$$R_e = \frac{\rho v L}{\eta} \quad (4)$$

where  $R_e$  = Reynolds number

$\rho$  = fluid density (1000 kg/m<sup>3</sup>)

$v$  = fluid velocity (0.001 m/s)

$L$  = characteristic length ( $L = \frac{2wh}{w+h}$ ,  $w$  = width (0.004 m),  $h$  = height ( $4 \times 10^{-5}$  m) of the channel)

$\eta$  = dynamic viscosity of the fluid ( $8.9 \times 10^{-4}$  Pa.s)

The equation is valid only for Newtonian/incompressible fluids (i.e. fluids whose viscosity remains constant irrespective of the amount of shear applied at a constant temperature). Fluid flow with Reynolds number less than 1 is considered to be laminar, while  $R_e > 1$  gives a turbulent flow.

### Signal generation in dual band electrodes

Under sequential regime and hydrodynamic/Levich condition, ratio of current generated at two adjacent electrodes ( $WE_1$  and  $WE_2$ ) operated in generation-generation (GG) or generation-collection (GC) mode can be estimated with the following equations:<sup>7</sup>

$$\text{GG mode: } \frac{i_{g2}}{i_{g1}} = 1 - \frac{i_{g1}}{nFC^{\circ}V_f} \quad (5)$$

$$\text{GC mode: } \frac{i_{c2}}{i_{g1}} = \frac{i_{g1}}{nFC^{\circ}V_f} \quad (6)$$

where  $i_{g1}$  = current at first generator (A)

$i_{g2}$  = current at second generator (A)

$i_{c2}$  = current at collector (A)

$C^{\circ}$  = bulk concentration of the analyte (mol/cm<sup>3</sup>)

$V_f$  = volumetric flow rate (cm<sup>3</sup>/s)

$V_f = v_{av}wh$  ( $v_{av}$  = average flow velocity (cm/s),  $w$  = channel width (cm),  $h$  = channel height (cm))

This equation is only valid for same size electrodes operated either in GG or GC mode. Levich condition is achieved when convection prevails over diffusion ( $\frac{WD}{v_{av}h} < 0.4$ ).<sup>8</sup>  $W$  is the electrode length in the direction of the flow.

### Diffusion layer thickness

The size of diffusion layer under a laminar flow, perpendicular to a band electrode is given by:<sup>9</sup>

$$\delta_D = 1.49 \left( \frac{4h^2Dxw}{3V_f} \right)^{1/3} \quad (7)$$

where  $\delta_D$  = diffusion layer thickness (cm)

$2h$  = channel height (cm)

$D$  = diffusion coefficient of the analyte ( $D_{FcTMA} = 6.71 \times 10^{-6}$  cm<sup>2</sup>/s)

$x$  = distance from the upstream edge of the electrode (cm)

$w$  = channel width (cm)

$V_f$  = volumetric flow rate (cm<sup>3</sup>/s)

The following are calculated diffusion layer thicknesses as function of distance ( $x$ ) from electrode upstream edge for a 160  $\mu\text{m}$  TPE band and a 40  $\mu\text{m} \times 4$  mm channel operated under 0.13  $\mu\text{L/s}$  flow rate.

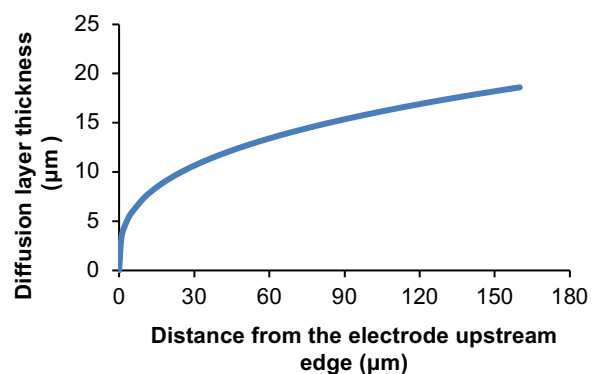


**Figure S8.** Diffusion layer thicknesses at TPE band

#### Dependence of the collection efficiency on electrode distance

TPE dual bands with 160  $\mu\text{m}$  widths and gaps ranging from 380  $\mu\text{m}$  to 1.6 mm were subjected to hydrodynamic amperometric measurements of 1 mM FcTMA<sup>+</sup> in 0.5 M KCl at 0.4 V and -0.2 V vs C for the first and second electrodes, respectively. Collection efficiency was calculated by taking a ratio of integrated current over time (charge) at the second electrode/collector to that of the first electrode/generator.

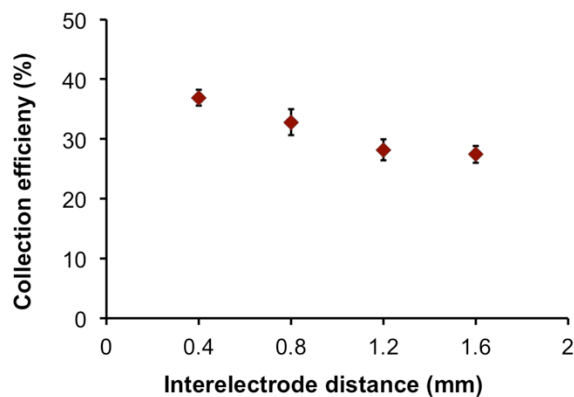


**Figure S9.** Collection efficiency as function of distance between two electrodes ( $n = 4$  injections)

## Multilayered ePADs

The following images were taken using a digital microscope (Dino-Lite, USA) on ePADs cross-section perpendicular to the direction of the flow.

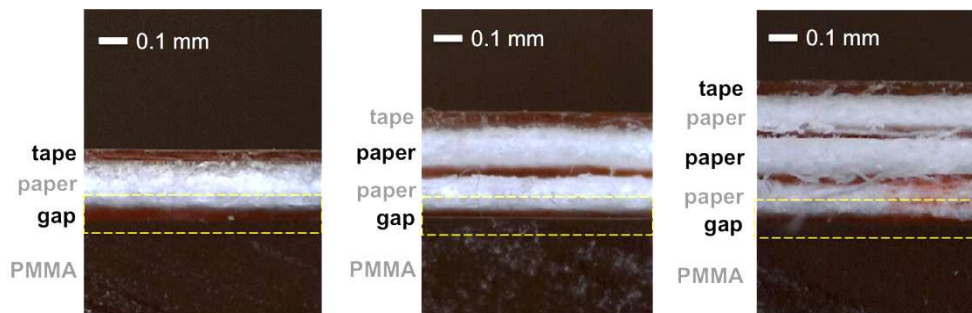


**Figure S10.** Comparison of channel cross-section in single-, double- and triple-layer ePAD

## Flow rates of ePAD

Flow rates were estimated by dividing the injection volume by the time it took for the current signals to reach the baseline level. The following flow rates were obtained from 4 mm-wide ePAD channel.

**Table S2.** Flow rates of several different paper configurations and substrates, \*n = 5 devices

Paper type	Flow rate ( $\mu\text{L/s}$ )*
Whatman 1 – single layer	$0.12 \pm 0.01$
Whatman 1 – double layer	$0.27 \pm 0.04$
Whatman 1 – triple layer	$0.33 \pm 0.02$
Whatman 4 – single layer	$0.24 \pm 0.03$
Whatman 42 – single layer	$0.08 \pm 0.01$

Since the channel sizes were roughly similar for 1-layer devices, the following figure gives the relationship between  $(\text{flow rate})^{1/3}$  generated by different paper substrates and their corresponding plateau currents (Levich plot, Eq. 3).

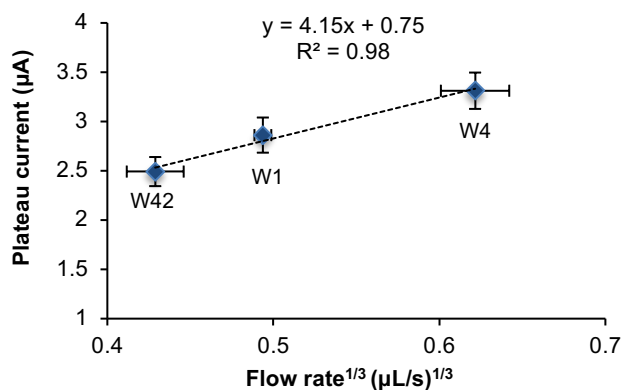


**Figure S11.** Levich plot obtained from single-layer ePAD using Whatman 1, 4 and 42

### Collection efficiency in TPE array

The following figure was obtained by calculating collection efficiency from hydrodynamic amperometry measurements of 1 mM FcTMA<sup>+</sup> in 0.5 M KCl using single- to 4 pair(s) of electrodes at  $V_{\text{gen}} = 0.4$  V vs C and  $V_{\text{col}} = -0.2$  V vs C.

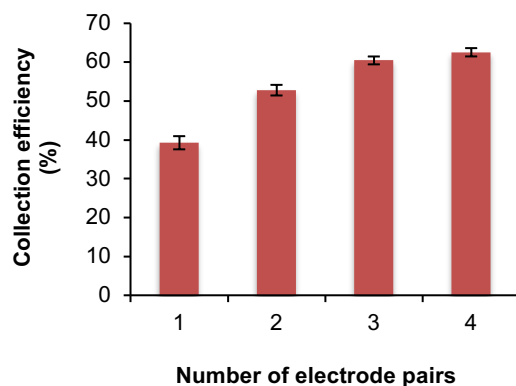
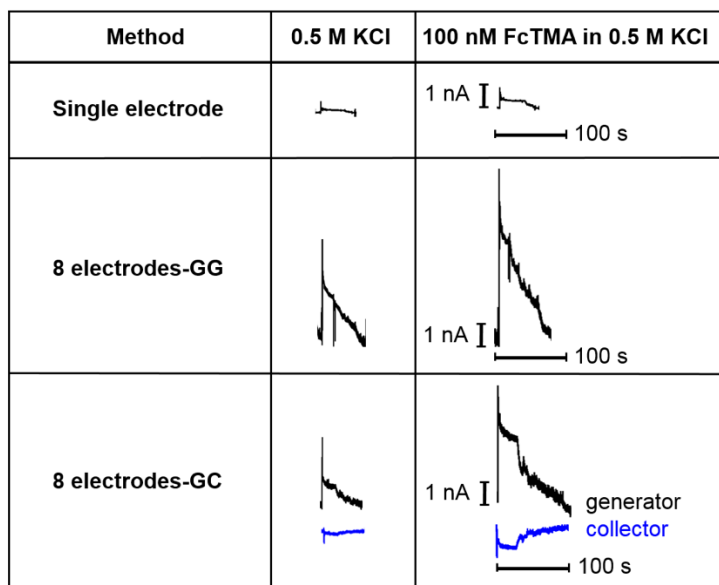


**Figure S12.** Collection efficiency as a function of the number of electrode pairs (n = 3 injections)

### Comparison of signal in single and array of detector

The following figure was obtained from hydrodynamic amperometry measurements of 100 nM FcTMA<sup>+</sup> in 0.5 M KCl using: single electrode at 0.4 V vs C, 8 electrodes in GG mode at 0.4 V vs C and 4 pairs of electrodes in GC mode at  $V_{\text{gen}} = 0.4$  V vs C and  $V_{\text{col}} = -0.2$  V vs C.



\*Signal traces are shown from single device measurements for each detection method.  
Data from replicates are shown in Table S3.

**Figure S13.** Detection comparison between single electrode detector and detector array

**Table S3.** Measurement data of background solution and 100 nM FcTMA<sup>+</sup> solution in 5 separate devices

Detection Methods	Total Charges (nC)		Calibration curve equation (y = Total charge in $\mu\text{C}$ , x = concentration of FcTMA <sup>+</sup> in $\mu\text{M}$ , Calibration range: 0.010-5.0 $\mu\text{M}$ )
	0.5 M KCl (Background)	100 nM FcTMA <sup>+</sup>	
Single electrode	$29.8 \pm 5.3$	$59.0 \pm 9.5$	$y = 0.24x + 0.04$
8 electrodes-GG	$476 \pm 52$	$500 \pm 34$	$y = 0.63x + 0.54$
8 electrodes-GC	$357 \pm 21$	$521 \pm 13$	$y = 1.20x + 0.36$

## REFERENCES

- (1) Gau, V.; Ma, S.-C.; Wang, H.; Tsukuda, J.; Kibler, J.; Haake, D. A. *Methods* **2005**, *37*, 73-83.
- (2) Channon, R. B. *Development of Electrochemical Methods for the Determination of Pharmaceutical Impurities*. 2015.
- (3) Nicholson, R. S. *Analytical Chemistry* **1965**, *37*, 1351-1355.
- (4) Konopka, S. J.; McDuffie, B. *Analytical Chemistry* **1970**, *42*, 1741-1746.
- (5) Compton, R. G.; Fisher, A. C.; Wellington, R. G.; Dobson, P. J.; Leigh, P. A. *The Journal of Physical Chemistry* **1993**, *97*, 10410-10415.
- (6) Squires, T. M.; Quake, S. R. *Reviews of Modern Physics* **2005**, *77*, 977.
- (7) Amatore, C.; Da Mota, N.; Lemmer, C.; Pebay, C.; Sella, C.; Thouin, L. *Analytical Chemistry* **2008**, *80*, 9483-9490.
- (8) Amatore, C.; Da Mota, N.; Sella, C.; Thouin, L. *Analytical Chemistry* **2007**, *79*, 8502-8510.
- (9) Snowden, M. E.; Unwin, P. R.; MacPherson, J. V. *Electrochemistry Communications* **2011**, *13*, 186-189.